



Universidade de Aveiro
2018

Departamento de Engenharia de
Materiais e Cerâmica

**ADRIANA
FERNANDES
MAGUETA**

**Sistemas eletromecânicos (BioMEMs) para
engenharia de tecidos: aplicações em tecidos
duros**

**Biomedical microelectromechanical (BioMEMs)
systems to tissue engineering: applications in
hard tissues**



Universidade de Aveiro
2018

Departamento de Engenharia de
Materiais e Cerâmica

**ADRIANA
FERNANDES
MAGUETA**

**Sistemas electromecânicos (BioMEMs) para
engenharia de tecidos: aplicações em tecidos
duros**

**Biomedical microelectromechanical (BioMEMs)
systems to tissue engineering: applications in
hard tissues**

Dissertação apresentada à Universidade de Aveiro para cumprimento dos requisitos necessários à obtenção do grau de Mestre em Materiais e Dispositivos Biomédicos, realizada sob a orientação científica da Prof. Doutora Paula Maria Lousada Silveirinha Vilarinho e da Prof. Doutora Maria Helena Figueira Vaz Fernandes, Professoras Associadas do Departamento de Engenharia de Materiais e Cerâmica da Universidade de Aveiro.

Dissertation presented to the University of Aveiro to fulfil the necessary requirements for the awarding of the Masters degree in Materials and Biomedical Devices, carried out under the supervision of Prof. Doutora Paula Maria Lousada Silveirinha Vilarinho and Prof. Doutora Maria Helena Figueira Vaz Fernandes, Associate Professors in the Department of Materials and Ceramics Engineering of the University of Aveiro.

“Às vezes precisamos de ir aos vales para depois subir ao cume.” – JJ

Júri

Presidente

Prof. Doutor António Manuel Godinho Completo
Professor Auxiliar C/ Agregação, Universidade de Aveiro

Doutora Maria Ascensão Ferreira da Silva Lopes
Professora Auxiliar, Universidade do Porto

Prof. Doutora Paula Maria Lousada Silveirinha Vilarinho
Professora Associada, Universidade de Aveiro

Agradecimentos

Há pessoas a quem temos o dever de agradecer todos os dias, por todos os ensinamentos, apoio e carinho partilhado ao longo do nosso percurso. E, chegado o final desta etapa, não posso deixar de agradecer a todos eles.

Às minhas orientadoras, Prof. Paula Vilarinho e Prof. Maria Helena Fernandes, agradeço por todo o conhecimento científico, ideias, apoio e orientação ao longo da realização deste trabalho.

Quero agradecer a toda a equipa do DEMaC, pelo apoio técnico prestado durante este trabalho e ao longo de toda a minha formação académica. Agradeço também ao Doutor Gonzalo Otero, pelo apoio prestado na análise dos resultados de XPS.

Aos meus colegas do Electroceramics Group, por se mostrarem sempre disponíveis para apoiar e partilhar ideias e conhecimentos. Quero agradecer em especial ao André, Bernardo, Joana, João, Manuela, Nuno, Duarte, Serrazina e Rui pelo bom acolhimento no grupo e pelo excelente ambiente de trabalho proporcionado.

Aos meus amigos, aos de sempre e aos que foram chegando, quero agradecer por toda a compreensão e apoio, por acreditarem em mim e por sempre me mostrarem o lado bom do dia. Em especial à Balinha, Gonçalo, Hugo, Inês Prata, JJ, Lili, Miguel e Rodrigo.

Aos meus avós, pais e irmão, por todos os valores que me transmitem, por me proporcionarem sempre o melhor e por aceitarem e apoiarem todas as decisões que tomo ao longo do meu percurso. Estou-vos eternamente grata, obrigada!

Palavras-chave

Biomateriais, 316 SS, PLLA, silanização, spin-coating, aderência, ASTM D3359, XPS, FTIR, PBS

Resumo

Os metais e suas ligas são dos materiais mais usados em aplicações médicas para suporte ósseo, devido à sua biocompatibilidade e propriedades mecânicas. No entanto, estes materiais não estimulam a regeneração óssea e, com o decorrer do tempo, libertam íons metálicos para o corpo humano, que em grande quantidade, são nocivos. Uma forma de contornar esta problemática consiste no uso de revestimentos com materiais biocompatíveis, biodegradáveis e capazes de estimular a regeneração óssea. Neste trabalho optou-se pela utilização da liga de aço inox 316, como a componente capaz de suportar as cargas aplicadas ao osso e do ácido poli (L-lático) (PLLA) como revestimento, devido às suas propriedades biocompatíveis, biodegradáveis e piezoelétricas, simulando o colagénio presente no osso. Neste trabalho estudou-se a aderência entre a liga 316 (neste trabalho SS) e o PLLA. Foi feita a funcionalização da liga através de um processo químico, silanização, e realizada a respetiva quantificação dos silanos. Os filmes de PLLA foram depositados por spin-coating, com diferentes espessuras, variando-se as concentrações de solução, o número de camadas depositadas, e o grau de cristalização. Os resultados mostraram que a funcionalização do substrato metálico com silanos é efetiva e eficaz na aderência de filmes de PLLA à liga de aço inox 316. O grau de aderência, medido pelo teste da fita cola, depende para além da funcionalização do substrato, da espessura do filme, da concentração da solução de polímero e do grau de cristalização do filme polimérico. Os melhores resultados foram conseguidos para as menores espessuras de filme. No entanto, para filmes cristalizados, a aderência melhorou para espessuras maiores. Quando imersos em PBS, os filmes não se destacaram, sendo os melhores resultados para os filmes cristalizados. Com este estudo foi possível produzir e caracterizar revestimentos estáveis de PLLA sobre a liga 316, com aderência adequada a aplicações médicas, o que representa um contributo promissor para a exploração da polarização elétrica destas plataformas para regeneração de tecido ósseo e estudo de outras plataformas biomédicas constituídas por dois materiais diferentes.

Keywords

Biomaterials, 316 SS, PLLA, silanization, spin-coating, adhesion, ASTM D3359, XPS, FTIR, PBS

Abstract

Metals and their alloys are the materials most commonly used in medical applications for bone support due to their biocompatibility and mechanical properties. Nevertheless, these materials do not stimulate bone regeneration and, over time, release metallic ions into the human body, which in large numbers is toxic. One way to overcome this problem is to use coatings with biocompatible and biodegradable materials capable of stimulating bone regeneration. In this work, 316 stainless steel alloy was used as the component capable of withstanding the loads applied to bone and poly(L-lactic acid) (PLLA) was chosen as a coating due to its biocompatible, biodegradable and piezoelectric properties, simulating the collagen present in the bone. In this work the adhesion between 316 SS and PLLA was studied. 316 SS functionalization was carried out through a chemical process, silanization, and the respective quantification of silanes was performed. The PLLA films were deposited by spin-coating, with different thicknesses, varying the solution concentrations and the number of deposited layers, and with different degrees of crystallization. The results showed that the functionalization of the metal substrate with silanes is effective and efficient in the adhesion of PLLA films to 316 SS. The degree of adhesion, as measured by the standard tape test depends, besides the functionalization of the substrate, on the film thickness, the concentration of the polymer solution and on the degree of crystallization of the polymeric film. The best results were achieved for the thinner films. However, for crystallized films, adhesion has improved for larger thicknesses. When immersed in PBS, the films did not stand out, being the best results for the crystallized films. With this study it was possible to produce and characterize stable PLLA coatings on 316 SS substrates, with suitable adhesion to medical applications, which represents a promising contribution to the exploitation of the electrical polarization of these platforms for bone tissue regeneration and for the study of other biomedical platforms constituted by two different materials.

CONTENTS

List of Figures.....	iii
List of Tables.....	vii
Abbreviations.....	ix
Chapter I – Context and Objectives	13
1.1. Context.....	13
1.2. Objectives.....	14
Chapter II – State of The Art.....	19
2.1. Bone.....	19
2.1. Piezoelectricity.....	23
2.1.1. General concepts of piezoelectricity	23
2.1.2. Bone piezoelectricity.....	25
2.3. Tissue Engineering.....	26
2.3.1. Strategies and requirements.....	26
2.3.2. Bone Tissue Engineering.....	27
2.4. Polymers in bone tissue engineering	28
2.4.1. Natural polymers	29
2.4.2. Synthetic polymers	29
2.4.3. Poly(L-lactic acid)	30
2.5. Metals in bone tissue engineering.....	33
2.5.1. Magnesium and Titanium based alloys.....	35
2.5.2. Stainless Steel.....	35
2.6. Metal-Polymer interface.....	36
2.6.1. Adhesion	37
2.6.2. Surface treatments	38
2.6.3. Silane coupling agents.....	39

2.6.4. Other metal surface treatments	40
Chapter III – Materials and Methods	45
3.1. Materials	46
3.2. Methodologies	47
3.2.1. Stainless steel substrates	47
3.2.2. Poly(L-lactic acid) solution preparation	48
3.2.3. Poly(L-lactic acid) film deposition	49
3.2.1. Crystallization process of Poly(L-lactic acid)	51
3.3. Characterization	52
3.3.1. Structural properties	52
3.3.2. Morphology	54
3.3.3. Chemical analysis	57
3.3.4. Adhesion measurements	62
3.3.5. Degradability tests in Phosphate buffered saline (PBS) solution	64
Chapter IV – Results and Discussion	69
4.1. Stainless steel substrate characterization	69
4.2. Poly(L-lactic acid) films and platforms characterization	91
4.3. Results in summary	106
Chapter V – Conclusions And Future Work	111
5.1. Conclusions	111
5.2. Future work	113
Bibliography	117

LIST OF FIGURES

Figure 1 - Scheme of final device with three main layers: 316 SS alloy, silanes obtained by the silanization process and PLLA films with different thickness.	15
Figure 2 - Bone structure – compact and spongy bone in a long bone, coated by articular cartilage [21]. Compact bone is constituted by blood vessels, nerves, collagen fibres, apatite crystals, and osteons are their structural unit, while spongy bone is less organized and composed by soft tissues.	20
Figure 3 - Different stages of bone remodelling [25], being the resorption, reversal and formation the main stages. Resorption involves the migration of osteoclasts to areas of needless bone. The reversal phase takes place when osteoblasts receive signals to differentiate and migrate to these areas. The formation stage is when new bone is formed.	21
Figure 4 - Wolff's law. Load of body weight at head of femur, causing compression and tension in femur. Positive and negative charges are formed in this point, leading to bone resorption and growth processes (based on [28-30]).....	22
Figure 5 - Direct and indirect piezoelectric effect on a material - a) original shape; b) direct piezoelectric effect; c) inverse piezoelectric effect (based on [33]), where P is the polarization field, the input is represented in green and the output is represented in orange.	24
Figure 6 - Designation of the axes. 1, 2 and 3 represent the direction, while the respective shear is represented by 4, 5 and 6 (based on [34]).	25
Figure 7 - Different routes to synthesise PLA and produce PLLA and PDLA: (i) condensation, (ii) direct polymerization and (iii) ring opening polymerization (based on [48,49]).	31
Figure 8 - Schematic representation of adhesion mechanisms types: a) adsorption, where the angles are related with the wettability of the surface; b) electrostatic attraction, which are dependent on the surface charges; c) chemical bonding; d) inter-diffusion and e) mechanical interlocking, which is related with the roughness of the surfaces (based on [64]).	37
Figure 9 - Silane treatment of 316 SS substrate a) hydroxyl groups through heat treatments; b.1) (M—O—Si) bonds and b.2) (Si—O—Si) bonds (based on [69]).	40
Figure 10 - Scheme of this work.	46
Figure 11 - Thermal treatment of SS 500C substrate with a heating rate of 5°C/min, dwell of 500°C for 120 min and cooling rate of 10°C/min until room temperature.	48

Figure 12 – Apparatus used in the polymeric dissolution process.....	49
Figure 13 - a) Spin coating of PLLA films on SS and SS 500C substrates. a) Spin-coating procedure that includes the i) dispense stage; ii) substrate spinning at a constant rate and fluid viscous forces dominate fluid thinning behaviour; iii) stage of substrate spinning at a constant rate and solvent evaporation dominates the coating thinning behaviour and iv) final film (based on [78]); b) Spin-coater equipment used in this work. .	51
Figure 14 - Crystallization process to obtain a) semi-crystalline films through a single step for 60 min at 120°C and b) crystalline films through a step at 180°C for 3 min followed by 45 min at 120°C.	52
Figure 15 - Contact angle scheme. A liquid (in blue) contacts with a solid surface (in black). θ_c is the contact angle, γ_{SG} , γ_{SL} and γ_{LG} are the solid/gas, solid/liquid and liquid/gas interface tensions, respectively (based on [89]).	56
Figure 16 - FTIR apparatus and the respective constituents: a spectrometer that allows obtaining an interferogram, that undergoes through a Fourier transformation to get the final FTIR spectrum.....	58
Figure 17 - a) XPS apparatus and b) photoelectric effect principle (based on [92])....	60
Figure 18 - XPS PEAK41 software: example of a decomposition in the different components regarding N 1s peak for SS 500C 30 sil.....	62
Figure 19 - a) 3D printed plastic accessory to help the cutting process and b) the cutting process.....	64
Figure 20 – Scheme of the degradability tests in PBS.	65
Figure 21 – SS substrates (left) and SS 500C (right) under different magnifications and using different equipment. Magnifier glass images (a) and b)), OM images (c) and d)) and SEM micrographs (e), f) and g)). Magnifier glass images display a clear difference in the surface colour while a higher magnification with SEM presents clearly grains and grain boundaries in the heat treated stainless steel substrate.....	71
Figure 22 - SEM micrographs of a) SS, b) SS 500C and c) SS 500C after polishing in different magnification. A clear difference on the polishing marks is evident between SS and SS 500C after polishing and the grain boundaries disappear after the polishing.	72
Figure 23 - <i>In-situ</i> XRD pattern of SS under different temperatures in air atmosphere. The crystallographic phases are identified based on JCPDS-PDF cards ([97-100]). For temperatures lower than 800°C only austenitic phases are identified, while for temperatures above 800°C the formation of iron and chromium oxides phases starts.	74
Figure 24 - Thermal analysis – TG (left) and DTA (right) of SS substrates conducted under three different atmospheres: a) air, b) oxygen and c) argon at three different heating	

rates: 5°C/min (black squares), 10°C/min (red circles) and 20°C/min (green up triangles). The weight gain under air is ~ 14.6%, under oxygen is ~ 5.44% and under argon is ~ 5.24%.77

Figure 25 - XPS overview of SS (black line) and SS 500C (red line) with peaks identification. The major difference is the increase in iron and chromium elements related with the formation of oxides (inside the orange rectangles). Auger electrons are also detected by XPS, although not relevant for this discussion.79

Figure 26 - FTIR spectra of SS (black line) and SS 500C (red line). The peak at 659 cm⁻¹ for SS 500C is attributed to the presence of chromium oxide, Cr₂O₃.80

Figure 27 - Contact angle on SS and SS 500C for different silanization times. For different silanization time, there are no changes for the SS substrates, while for SS 500C substrates as the silanization time increases until 60 sil, so does the contact angle, decreasing to a longer silanization time (90 sil). If the error bars are considered, the contact angle values are almost the same.82

Figure 28 - FTIR spectroscopy results of a) SS (black line) and b) SS 500C (red line) for different silanization times: 30 sil (green line), 60 sil (blue line) and 90 sil (pink line). The presence of vibration modes corresponding to silanes only occur for the SS 500C...84

Figure 29 – XPS of a) O 1s, b) C 1s and c) Si 2p + Fe 3s peaks of SS (black), SS 500C (red) and for different silanization times: 30 sil (green), 60 sil (pink) and 90 sil (blue).86

Figure 30 – XPS decomposition of O 1s and N 1s peaks recorded for different silanization times (30 sil, 60 sil and 90 sil). The N 1s peak is overlapped with a Mo 3p 2/3 contribution. The components are identified in the 30 sil plots.88

Figure 31 – XPS decomposition of C 1s, Si 2p and Fe 3s peaks recorded for different silanization times (30 sil, 60 sil and 90 sil). The components are identified in the 30 sil plots.....89

Figure 32 - C/Si (of silane) ratio (black squares) and Si (of silanes)/M ratio (red circles) for different silanization time. C/Si (of silane) ratio decreases due to the increase of Si concentration, while Si (of silanes)/M increased, suggesting not only that silanes increase, but also that the surface is being covered.91

Figure 33 - Thermal analysis (TG in black and DSC in red) of PLLA 5.0 thick film conducted under air atmosphere from room temperature up to 250°C. T_m is around 180°C.92

Figure 34 - XRD pattern of PLLA 2.5 and 5.0 films for two different crystallization processes: the semi-crystallized films were treated for 60 min at 120°C and the crystallized ones were treated for 3 min at 180°C and followed by 45 min at 120°C.....93

Figure 35 - SEM micrographs of PLLA 2.5 and PLLA 5.0 and with different number of deposited layers (1L, 2L and 3L), for semi-crystalline and crystalline films. For the semi-crystalline films there is no formation of spherulites, while for the crystalline ones the spherulites are not only formed, but also their size increase with the increase of the number of layers.96

Figure 36 - Tape test results for PLLA 2.5 and 5.0 SS 500C 60 sil films with 1, 2 or 3 deposited layers and for semi-crystalline and crystalline films. The solution concentration, number of deposited layers and type of crystallinity influence the adhesion, as seen by the tape test results.99

Figure 37 - a) FTIR spectra for PLLA 2.5 SS 500C 60 sil before (black line) and after (red line) the tape test, and b), c) and d) the respective zoom of the related bands (orange – 2800-3100 cm^{-1} ; green – 1500-1000 cm^{-1} and blue – 970-870 cm^{-1}). The peaks are identified in the graphics and are related to PLLA vibration bonds modes.....101

Figure 38 - FTIR spectra for PLLA 5.0 SS500C 60 sil (red line) and PLLA 2.5 SS 500C 60sil (black line) after the tape test. The peaks are identified in the graphic. PLLA peaks are visible after the tape test for PLLA 2.5, while for PLLA 5.0 only peaks regarding silane layer and substrate are present.102

Figure 39 - PLLA 2.5 3L semi-crystalline and crystalline films in SS 500C 60 sil substrates, for two immersion times (2 and 7 days) in PBS. Semi-crystalline films were almost whole detached, whereas for crystalline films the major part of the film remains on the substrate (green parts), although some small parts of the film are removed (red parts) after 2 days or detached after 7 days.....105

Figure 40 - FTIR results for PLLA 2.5 3L crystalline films in SS 500C 60 sil substrates before immersion PBS solution and for PLLA 2.5 3L semi-crystalline and crystalline films in SS 500C 60 sil substrates after immersion in PBS solution for 2 and 7 days. The present peaks are related to PLLA vibration modes and there are no significant differences between the samples, which indicates that PLLA 2.0 film did not degrade with the immersion in PBS solution.106

LIST OF TABLES

Table I - Applications in TE and respective piezoelectric constants of piezoelectric natural and synthetic polymers [7,36].....	28
Table II - Thermal and mechanical properties of PLLA.	32
Table III - Mechanical properties and medical applications of metallic alloys used in TE.....	34
Table IV - Chemical composition of 316L SS [8,58,59].	35
Table V – Recent studies on metal substrates treatments.	41
Table VI - Relative sensitivity factor for different elements [93].	62
Table VII - Classification of tape test results according to standard ASTM D3359 (based on [67]).....	63
Table VIII - Chemical composition of 304 and 316 stainless steel alloys [8,58,59,96].	70
Table IX - Chemical composition (wt.%) of SS, SS 500C and SS 500C after polishing. There are no significant differences among the samples chemical composition.....	73
Table X - Crystallographic plans and respective compounds for SS under different temperatures in air atmosphere and <i>in situ</i> ([97-100]).	75
Table XI - Contact angles of SS and SS 500C for different silanization times with the respective calculated errors.	82
Table XII - FTIR peak assignment for SS 500C after immersion in a silanized solution with APTES (1 vol.%) [61,110,111].	84
Table XIII - Surface concentrations (atomic %) of the chemical species related with the components of O 1s, N 1s, C 1s and Si 2p, along with C/Si (from silane) ratio, for the different silanization times (30 sil, 60 sil and 90 sil), determined by XPS.....	90
Table XIV - Crystallographic planes for PLLA and respective diffraction angle.	94
Table XV - Results of the tape test for different substrates, silanization times, crystallization and number of layers deposited of PLLA films with different concentrations.	97
Table XVI - FTIR peak assignment of the vibration modes of PLLA films on SS 500C substrates prepared in this work [119,120].....	103

ABBREVIATIONS

APTES –3-(Aminopropyl)triethoxysilane
 β -TCP – β -tricalcium phosphate
BE – Binding energy
BSE – Backscattered electrons
BTE – Bone tissue engineering
CA – Contact angle
CS – Carbon Steel
DSC – Differential scanning calorimetry
DTA – Differential thermal analysis
EDC – 1-ethyl-3-(3-dimethylaminopropyl)carbodiimide
EDS – Energy Dispersive X-ray Spectrometry
ESB – European Society for Biomaterials
FDA – Food and Drug Administration
FFT – Fourier transformation
FTIR – Fourier Transformed Infrared Spectroscopy
HAp – Hydroxyapatite
PBS – Phosphate Buffered Saline
PCL – Polycaprolactone
PDLA – Poly(D-lactic acid)
PEG – Poly(ethylene glycol)
PGA – Poly(glycolic acid)
PLA – Poly(lactic acid)
PLGA – Poly(lactic-co-glycolic acid)
PLLA – Poly(L-lactic acid)
PSI – Phase shift interferometer
PTH – Parathyroid hormone
PVDF – Polyvinylidene fluoride
PVDF-TrFE – Poly((vinylidene fluoride-co-trifluoroethylene)
TBT – tetra-n-butyl titanate
TE – Tissue engineering
T_g – Glass transition temperature
TG – Thermogravimetry
T_m – Melting temperature
SE – Secondary electrons
SEM – Scanning Electron Microscopy
SS – Stainless Steel
UHV – Ultra high vacuum
VSI – White-light vertical scanning interferometer
XPS – X-ray photoelectron spectroscopy
XRD – X-Ray Diffraction

CHAPTER I

CONTEXT AND OBJECTIVES

CHAPTER I – CONTEXT AND OBJECTIVES

1.1. Context

The worldwide incidence of bone disorders and conditions is increasing and it is expected to double by 2020, especially in populations where aging is coupled with increased obesity and poor physical activity [1]. In addition, the musculoskeletal conditions and diseases such as fractures, osteoporosis and bone metastases are also more frequent [2].

Within this context, with life expectancy increasing and owing to the vast functions of bones in the human body, it is of high importance the attempt to mimic the structures of bone tissue; this requires a deep understanding of their composition and mechanisms to promote its regeneration [2]. The ability to mimic bone tissues constitutes a crucial step to maintain and improve people's quality of life. Currently, facing the existing limitation of growing "entire bones", bone implants play a crucial role. The way implants are able to replace bone, accomplish load bearing functions and interacting with bone cells, needs to be considered [2]. The materials to be used in implants should fulfil properties requirements, as being biocompatible, non-toxic and non-inflammatory, bioactive and biodegradable [3-5]. Hence, tissue engineering (TE) has emerged, with the main goal focused on the use of materials and cells to develop biological substitutes that can restore, maintain or improve tissue functions [3,6,7].

Metals and their alloys such as cobalt-chromium, titanium and stainless steel (SS), specifically 316L SS, are nowadays the most used materials in orthopaedic implants, mainly due to their good mechanical properties [2,5,8,9]. However, they have some limitations, that include: the release of toxic metallic ions to the body, the mismatch of Young's modulus between the material and bone, which may lead to stress-shielding, and poor biodegradability and adhesion to the bone tissue [9,10], resulting in a high rate of implant failure and rejection. Thus, implant strategies face numerous difficulties and some adverse effects resulting from poor biological interaction at the implant interface leading to failures and related infection [11]. It is reported that infections associated to orthopaedic fracture and reconstructive devices occur in up to 10% of the implant cases, mainly due to mechanical aseptic loosening of the implant [12].

One way to improve the adhesion between the material and the host tissue is to promote healing process and to have an effective osseointegration [2]. Very recently piezoelectric materials have been considered for this role [13], since it has been proved that piezoelectrics can stimulate osteoblasts activity [14]. We consider that a good candidate for this application might be the poly (L-Lactic acid) (PLLA) [2,15], which in addition to being considered by some authors as a piezoelectric material, is also biocompatible and biodegradable [14,16-20].

PLLA does not have the suitable mechanical properties to be used as a bulk implant structure, but instead it can be used as a coating of a hard implant structures, such as 316L SS and in such a way promote the adhesion to the host tissue (as bone) promoting the biological interaction, and consequently decreasing the implant rejection rate. However, within this scenario another challenge arises related with the adhesion of PLLA to 316L SS and to the integrity of this coating. In a previous work, Marinho *et al.* [10] studied the adhesion of PLLA onto 316L SS, through a mechanical treatment of the steel surface, which consists in increasing the steel surface roughness. PLLA with two different molecular weights were used with three different solution concentrations, being further spin-coated into the steel. The polymer crystallinity degree, the adhesion between both materials as well as the degradation in Phosphate Buffered Saline (PBS) solution were studied. The increase of the steel surface roughness improved the adhesion of PLLA and the thin the film, the higher the adhesion. Even though the mechanical treatment was not efficient and the adhesion of PLLA to the metal was still poor. Alternative solutions are required. In that same work, chemical surface treatment, named silanization, was also initiated, as a possible alternative strategy to be studied. Although very preliminary these silanization approach looked promising. However, a deeper knowledge and understanding of the influence of 316 SS silanization and its effect on the adhesion of PLLA films is indeed required.

1.2. Objectives

Within this framework, the main purpose of this master thesis project was to study an alternative methodology to improve the adhesion of PLLA films onto 316 SS, namely silanization. The following experimental approaches were considered, and a schematic representation of the final structure is shown in Figure 1:

1. Functionalization of 316 SS surface, through a chemical treatment, designated as silanization;
2. Coating functionalized 316 SS with PLLA layers (semi-crystalline and crystalline) and with different thickness;
3. Bioactivity evaluation of the selected platforms (PLLA on 316 SS) by immersion in PBS solution.

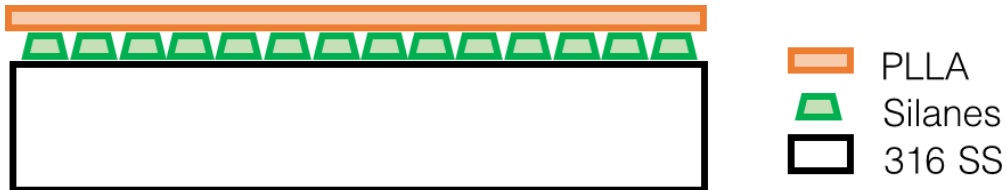


Figure 1 - Scheme of final device with three main layers: 316 SS alloy, silanes obtained by the silanization process and PLLA films with different thickness.

The present report is divided in four main chapters: state of the art, materials and methodologies, results and discussion and conclusions. In the state of the art a brief review of the studies and results already obtained in this field, as well as an explanation of some useful concepts for a thorough understanding of this thesis work are presented. Afterwards, the methodology used to obtain all the results is completely described and explained, along with the techniques used. The follow chapter presents the results in detail, followed by an extensive discussion, where the samples are compared to each other and to other authors work. By the end of the report, the main conclusions and some future work proposal are presented.

CHAPTER II

STATE OF THE ART

CHAPTER II – STATE OF THE ART

2.1. Bone

As the main application of the devices studied in this work is for bone application, an understand of bones, as their functions, structure, chemical composition and remodelling process is necessary.

Bones contribute to the body shape and form, performing several important functions in the human body, such as structural support due to a hard framework, protection of vital internal organs, movement and locomotion by using bones as levers for the muscles, mineral storage and, thus, mineral (calcium, phosphate) homeostasis and blood cell formation (*hematopoiesis*) [21,22].

According to their size and shape, bones are classified as long, short, flat or irregular. Bones have an outer dense layer and an inner soft layer, namely compact (cortical or lamellar) bone and trabecular (spongy or cancellous) bone, respectively [6,21].

At a macroscopic level, compact bone is dense and confers the required strength, while trabecular bone looks like a honeycomb network and contains the bone marrow [6,22]. At a microscopic level, compact bone is constituted by blood vessels, nerves, collagen fibres, apatite crystals, among others, having osteons (Haversian system) as their structural unit, while spongy bone is less organized and composed by soft tissues (Figure 2) [21,23].

Regarding the chemical composition, bone is composed by 65% of inorganic components and 35% of organic components. The inorganic part consists of mineral salts, mainly calcium phosphate and calcium carbonate combined to create hydroxyapatite and the organic part includes cells, glycoproteins and collagen fibres [21].

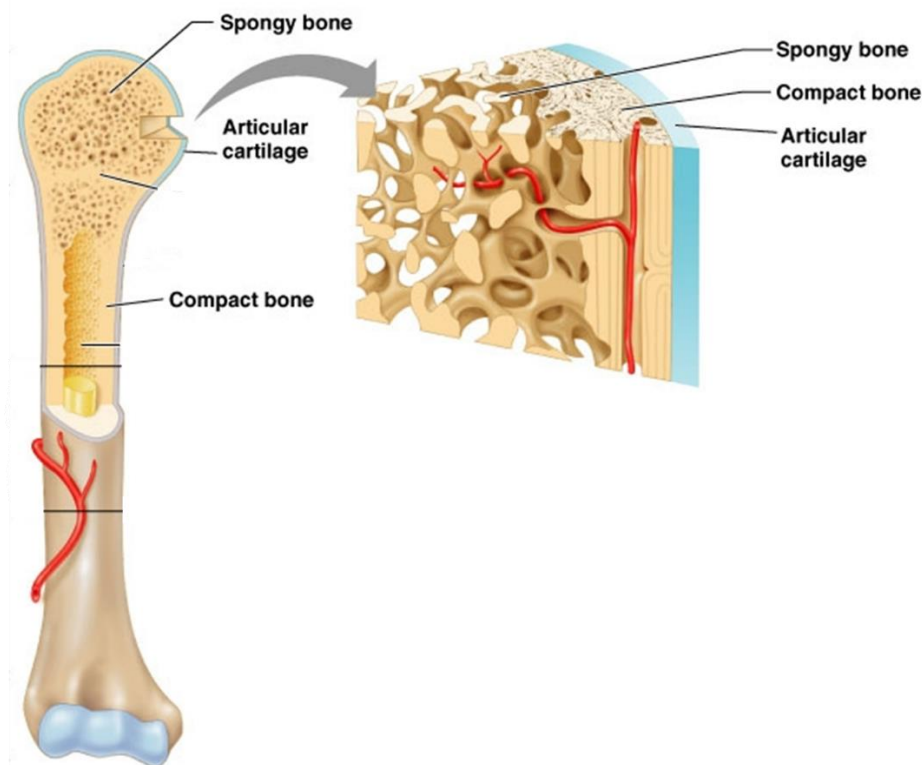


Figure 2 - Bone structure – compact and spongy bone in a long bone, coated by articular cartilage [21]. Compact bone is constituted by blood vessels, nerves, collagen fibres, apatite crystals, and osteons are their structural unit, while spongy bone is less organized and composed by soft tissues.

As mentioned, bones play several important roles in the human body, and they need to be very active, being continually removed and replaced during life, due to the need to respond to changes and adjustments of the skeleton. In fact, new bone formation takes from 4 to 6 months to be complete [22,24]. The bone tissue cells involved in the remodelling process are osteogenic cells, osteoblasts, osteocytes and osteoclasts and they have different shapes, functions and locations [22]:

- Osteogenic cells are undifferentiated and have as main function to develop into osteoblasts. These cells are found in deep layers of the marrow;
- Osteoblasts are responsible for new bone formation and, thus, secretion of collagen matrix and calcium salts. These cells are entrapped within calcified matrix;
- Osteocytes are the primary cell of mature bone, responsible for maintaining mineral concentration, via secretion of enzymes, and are entrapped in the matrix as well;
- Osteoclasts are responsible for bone resorption being, therefore, in bone surface and at sites of old, injured, or unnecessary bone.

This undergoing remodelling is necessary to maintain bone strength and mineral homeostasis and to prevent microdamaged bone accumulation [2,21,22]. This remodelling process, schematically displayed in Figure 3 [25], is coordinated by a “packet” of osteoblasts and osteoclasts, also named remodelling units. Remodelling process is divided in three main stages, namely resorption, reversal and formation. Firstly, migration of osteoclasts occurs to areas of old, damaged or needless bone. The reversal phase takes place when osteoblasts receive signals to differentiate and migrate to these areas, forming new bone in the resorbed area. Finally, a resting period occurs, until the next new remodelling cycle [24].

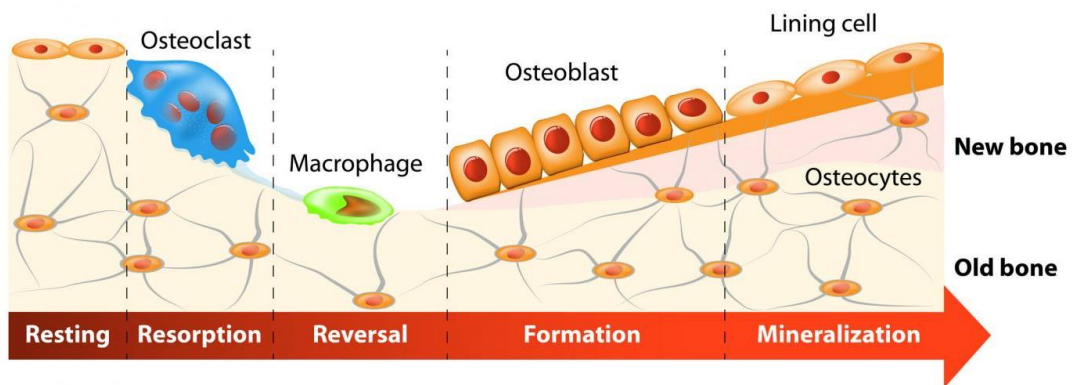


Figure 3 - Different stages of bone remodelling [25], being the resorption, reversal and formation the main stages. Resorption involves the migration of osteoclasts to areas of needless bone. The reversal phase takes place when osteoblasts receive signals to differentiate and migrate to these areas. The formation stage is when new bone is formed.

Bone remodelling is regulated by two different factors: a hormonal mechanism that maintains calcium homeostasis in the blood and a mechanical response to stress (muscle pull) combined with gravity [21]. The first mechanism is dependent on the amount of calcium present in the bloodstream, since it influences the parathyroid hormone (PTH) and the calcitonin hormone. When calcium levels are low, PTH is released into the bloodstream, stimulating osteoclasts to resorb the bone and, therefore, releasing calcium into the blood. Conversely, whenever the calcium levels rise, the calcitonin hormone is released, inhibiting bone resorption and reducing calcium levels [26].

The second mechanism can be explained by the Wolff's Law [21,27]. According to this author, bone remodelling (bone deposition and resorption) occurs in a way to achieve an optimal balance between strength and weight. For this, the trabeculae in cancellous bone tend to align with the directions of the main stresses applied to the bone [27]. In addition,

osteoclasts (responsible for bone resorption) are triggered by a reduction in stress applied to the bone and osteoblasts (responsible for bone formation), on the other hand, are triggered by an increase of stress [22]. This phenomenon is considered a mechanism of self-regulation and consists in the response to the mechanical forces acting upon bone tissues [27]. A scheme of Wolff's law is presented in Figure 4 [28-30].

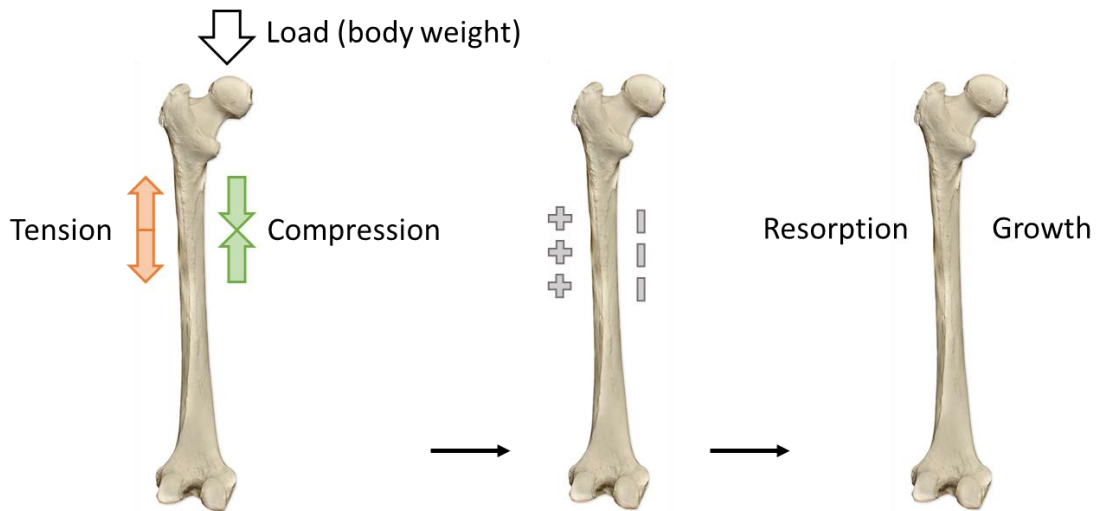


Figure 4 - Wolff's law. Load of body weight at head of femur, causing compression and tension in femur. Positive and negative charges are formed in this point, leading to bone resorption and growth processes (based on [28-30]).

This dependence on the applied stresses is also related to the electromechanical behaviour of the bone, firstly proposed to be piezoelectric by Fukada *et al.* [23] in 1957 [23]. In their work, they conclude that the piezoelectricity in bone is attributed to the symmetry of the collagen fibres in the bone and not related with the biologic part of the bone [23].

To discuss the role of piezoelectricity in the bone formation process, basic concepts of piezoelectricity will be introduced.

2.1. Piezoelectricity

2.1.1. General concepts of piezoelectricity

Some materials are considered as smart or active materials, that is, materials capable of adapting and changing due to an external stimulus [7,31]. This group of materials includes electroactive materials, as piezoelectrics, pyroelectrics and ferroelectrics, with the possibility to use in medical, automotive and chemical fields [31].

Piezoelectricity was discovered by the Curie brothers, Jacques Curie and Pierre Curie, in 1880 [31] and it is the ability of some crystalline materials to generate an electrical charge (polarization) proportional to a mechanical stress [31]. This effect is also known as direct piezoelectric effect. The polarity of the charges at the surface depend on the direction of the applied stress (compressive or tensile). Contrarily, inverse (or converse) piezoelectric effect is displayed when an external applied electric field gives rise to mechanical strain, occurring changes the material dimensions. The material either contracts or expands, depending on the direction of the field [14,31,32]. Piezoelectricity is then considered as a reversible phenomenon. A scheme of direct and inverse piezoelectric effect is presented in Figure 5 [33].

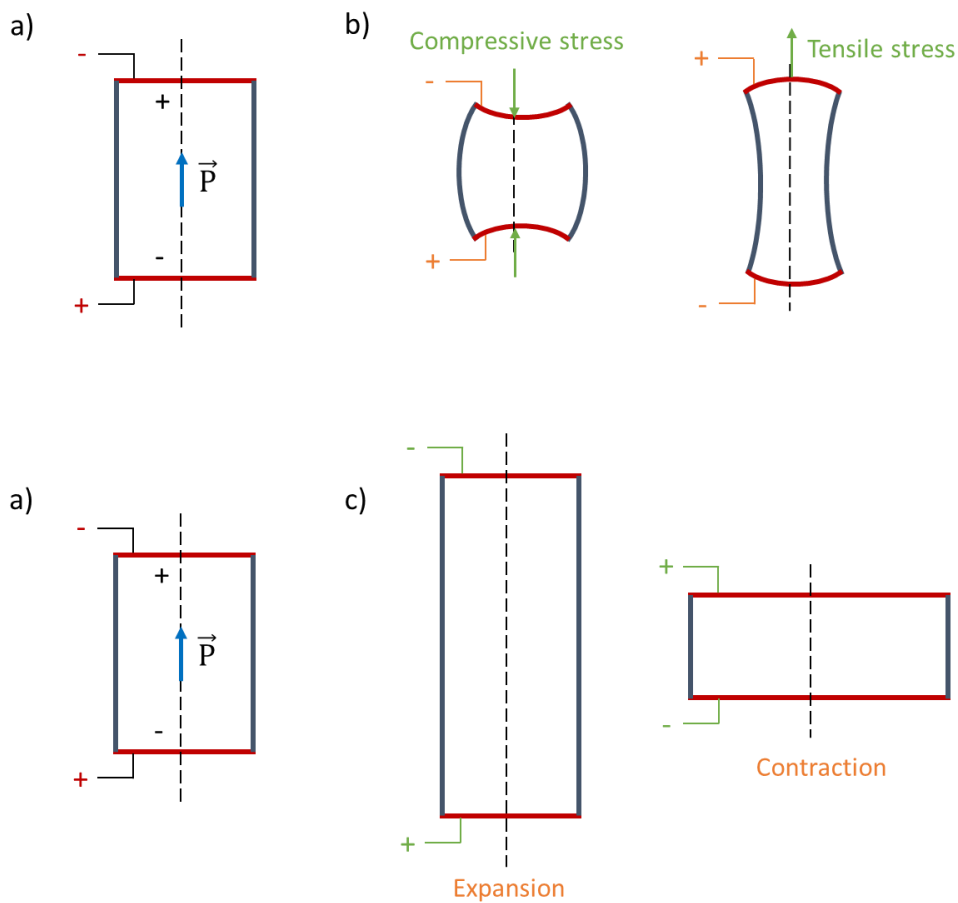


Figure 5 - Direct and indirect piezoelectric effect on a material - a) original shape; b) direct piezoelectric effect; c) inverse piezoelectric effect (based on [33]), where \vec{P} is the polarization field, the input is represented in green and the output is represented in orange.

On the other hand, pyroelectric materials are non-symmetric and can exhibit spontaneous electrical charge in response to temperature changes. Among pyroelectric materials, there are ferroelectric materials that have spontaneous polarization at the absence of an external electric field and polarization can be reversible upon an applied electric field [20,31].

Regarding piezoelectric materials, it is important to know that magnitude of P depends on the magnitude of the mechanical stress and the sign of the produced charges depends on the type of applied stress (compressive or tensile, as seen in Figure 5 c)). The relationship between polarization and stress is given in equation 1 (Eq. 1), whilst the relationship between strain and electric field strength is given in equation 2 (Eq. 2):

$$P = d\sigma \quad \text{Eq. 1}$$

$$x = dE \quad \text{Eq. 2}$$

where P is the polarization field, d is the piezoelectric coefficient, σ is the stress, x is the strain and E is the electric field strength. Piezoelectric coefficient can also be defined as d_{ij} (Coulomb per Newton, C/N), where the field has the i direction and the strain has j direction [31]. This constant is related with the direction of the applied stress, applied field and polarization, as presented in Figure 6 [34]. Usually, the direction of positive polarization coincides with Z axis. The direction of X , Y and Z are represented by 1, 2 and 3, while the respective shear is represented by 4, 5 and 6. In case of d_{33} , the induced polarization in direction 3 per unit stress applied in direction 3; or induced strain in direction 3 per unit electric field applied in direction 3 [34].

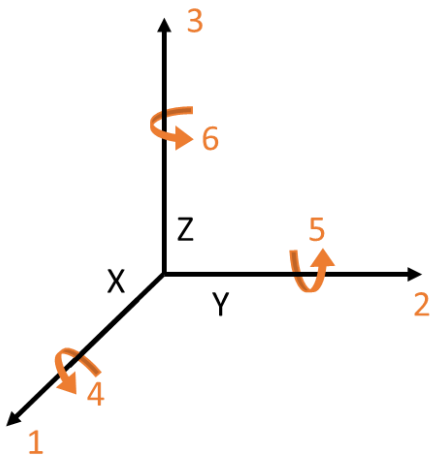


Figure 6 - Designation of the axes. 1, 2 and 3 represent the direction, while the respective shear is represented by 4, 5 and 6 (based on [34]).

2.1.2. Bone piezoelectricity

Piezoelectric studies in bone started in the 20th century by Fukada *et al.* [23], as mentioned, in which they found that bone is piezoelectric [23]. In case of bone, it is known that this piezoelectric response is due to collagen fibrils. When submitted to internal stress, collagen can generate electric signals. These signals are, in turn, transmitted through the extracellular matrix to the voltage-gated channels present in the cell

membrane. Consequently, the channels are activated and intracellular signals are transmitted, attracting osteoblasts and bone repair and growth start on the stressed side [14,35-37]. Besides collagen presented in the bone [38], piezoelectricity can be found in different parts of the human body, such in cartilage and cell membranes [7].

2.3. Tissue Engineering

2.3.1. *Strategies and requirements*

Owing to the vast functions of bones in the human body and the need to improve people's quality of life, it is of high importance to attempt to mimic the bone tissue structures, promoting bone regeneration. To achieve this, different strategies can be undertaken, being one of them the use of biomaterials.

According to the European Society for Biomaterials (ESB) [3], biomaterials are intended to interact with biological systems in order to evaluate, treat, increase or replace tissues, organs, or functions of the human body [3]. Therefore, biomaterials should follow some specifications, as being [3-5]:

- Biocompatible – non-toxic and non-inflammatory;
- Bioactive – capable of integrate with biological molecules or cells and regenerate tissues. For this, cells must migrate and adhere onto the surface and eventually through the scaffold and begin to proliferate before forming a new matrix;
- Biodegradable – absorbable and degradable by host enzymes or biological processes. Moreover, the degradation of the materials' components should not interfere with the organism, while the host cells are producing their own extracellular matrix;
- Scaffold architecture – Tailored porosity (micro or macro) in such a way that allows diffusion and cell migration;
- Mechanical properties – Compressive, elastic and fatigue strength comparable to host tissue.

Tissue engineering (TE) is an inter and multi-disciplinary field concerned with the development of biological substitutes capable of restore, maintain or improve diseased or damaged tissues or even whole organs [39-41]. To achieve TE main goal, the principles and methods of engineering and the life sciences are applied [3,6,7] and thus TE consists

of three major areas: cells and growth factors, biologically active molecules and engineering principles and synthetic materials [3,40].

2.3.2. Bone Tissue Engineering

In case of bone tissue engineering (BTE), osseointegration should be taken into consideration. Osseointegration is the bonding of living bone tissue with implants, in such a way that these implants are able to replace the bone and accomplish load bearing functions [2] without any relative motion between the implant and bone. For this to occur without any major problems new tissue should be dynamic and responsive to the host environment. Tissue restoration may occur in two different ways – cell-based and cell-free. The first one intends to increase the number of cells at the local needed area to promote both the healing response and the healing process. This can be achieved using scaffolds as carrier to deliver cells to the defect or through a generation of tissue using cells *in vitro* [42]. On the other hand, cell-free approach consists on stimulation of local cells and, consequently, enhancement of the body's inherent capacity for healing. To accomplish this, scaffolds with an optimal size and the shape of new tissue are used [4], being these scaffolds capable of delivering specific signals that will stimulate the cells [42].

In addition, it is an advantage if the material used for bone implants is Osteoinductive and Osteoconductive. The first characteristic will promote the differentiation of the progenitor cells in an osteoblastic lineage, whereas the second supports bone growth, besides stimulating the growth of the surrounding bone [4].

Some materials are considered as smart or active materials, that is, materials capable of adapting and changing due to an external stimulus [7]. Piezoelectric materials are one example of smart materials and they are used in the biomedical field, since they can generate electrical signals when subjected to an applied stress [37], without the need of an external source to apply electric stimulation [36,37]. Particularly, piezoelectric materials have been employed for different tissue repair, as bone and neural repair. In case of bone, these materials are able to mimic collagen behaviour present in the bone, generating charges in response to applied stress, promoting bone repair. On the other hand, in case of neural repair, the electric pulses stimulate neurite direction outgrowth [36].

2.4. Polymers in bone tissue engineering

Polymers present attractive properties for bone tissue engineering, since they are light weight, inexpensive, mechanically and electrically resistant and easy to conform. These properties can be relevant when compared to inorganic materials. Moreover, polymers show excellent compatibility with other organic and inorganic materials, being possible the development of multifunctional hybrid systems. Among all these properties, some biocompatible polymers are biodegradable [2,5,7]. Nevertheless, the mechanical properties of polymers may not be adequate for certain tissue substitution applications, however, they can be enhanced by cross-linking the polymer with other polymers [2,5].

Polymers, either natural or synthetic, have many applications in TE, as resumed in Table I [7,36]. The piezoelectric constants are also presented to compare with the piezoelectric constant of bone, $d_{15} = (0.1-0.3) \text{ pC/N}$ [7,36]. Furthermore, properties, benefits and limitations of natural and synthetic polymers will be pointed in the next sections.

Table I - Applications in TE and respective piezoelectric constants of piezoelectric natural and synthetic polymers [7,36].

Polymer	Application in TE	Piezoelectric constant (pC/N)
Collagen	Bone regeneration	$d_{15} = 2.0$
	Neural regeneration	
PVDF	Neural growth in vitro	$d_{15} = - 25$
	Bone formation in vitro	
	Muscle regeneration	
PVDF-TrFE	Neural differentiation and growth in vitro	$d_{15} = - 25.2$
	Bone growth in vivo	
PLLA	Neural differentiation and growth in vitro	$d_{14} = - 9.82$
	PLLA blends for vascular differentiation in vitro	
PVDF – Polyvinylidene fluoride		
PVDF-TrFE – Poly((vinylidene fluoride-co-trifluoroethylene)		
PLLA – Poly(L-lactic) acid		

2.4.1. *Natural polymers*

Natural polymers for biomedical applications are obtained from natural sources, such as silk, collagen, chitosan, hyaluronic acid, fibrin and alginate. These natural polymers display similar properties as the tissues they are replacing, are biocompatible and bioactive, stimulating specific cues for cell attachment, integration and differentiation on implant. Nevertheless, they may have pathogenic impurities, increasing the risk of disease transmission, and exhibit poor mechanical and electrical properties [4].

Studies with natural polymers have been made to identify which properties are crucial for good osseointegration, and how to improve them, being the main ones: porosity, structural stability and mechanical properties [5,43].

Collagen is a biologic protein present in bone, cartilage, teeth, among others, being responsible for structural and mechanical support [37]. As it makes part of human bone, it is one of the most used natural polymer in BTE due to its excellent biocompatibility, biodegradability and piezoelectric properties. Thus, collagen has been used as a scaffold for bone healing. However, this polymer has low mechanical strength and low osteointegration capacity, being therefore, incorporated with other materials, such as ceramics (hydroxyapatite (HAp), β -tricalcium phosphate (β -TCP), bioglass), carbon and natural and synthetic polymer materials [37,43].

2.4.2. *Synthetic polymers*

Synthetic polymers, such as poly(lactic acid) (PLA), poly(glycolic acid) (PGA), poly(caprolactone) (PCL) and poly(ethylene glycol) (PEG), as well as co-polymers as poly(lactic-co-glycolic acid) (PLGA) and poly((vinylidene fluoride-co-trifluoroethylene) (PVDF-TrFE) have also been used in TE. These polymers have many advantages when compared to natural polymers, since they have a defined chemistry and formulations along with their easy processing. Though, unlike natural polymers, some of these synthetic materials are generally hydrophobic, making the adhesion process difficult for cells and leading to undesirable inflammatory responses [2,5,7,44].

Polyvinylidene fluoride (PVDF) and poly(L-lactic acid) (PLLA) are piezoelectric, flexible and non-toxic, ideal candidates for a variety of biomedical applications as BTE scaffolds or even neural regeneration [14,36]. PVDF is biocompatible and non-toxic, has high flexibility as well as high chemical and physical resistance, and can be linked with other materials, forming PVDF-TrFE, per example. However, PVDF is non-biodegradable.

Nevertheless, from a TE point of view, PVDF and PVDF-TrFE can be used in bone regeneration, scaffolds in skeletal muscle regeneration and neural tissue regeneration. Moreover, these materials are also able to be poled by corona in order to promote cell adhesion and proliferation [36,37]. In turn, PLLA is biodegradable, biocompatible and due to its chemical structure, PLLA does not require poling to generate piezoelectricity. Furthermore, PLLA is degraded by hydrolytic degradation, being PLA the final product, a non-toxic and water soluble material [36,37]. As mentioned before, studies demonstrated that PLLA promote bone regeneration [23] and this in one of the reasons PLLA is used in orthopaedics, such as screws and pins [37].

The most usual in the literature are studies on the PLLA in TE, focusing in its biodegradability and biocompatibility, with no focus on the piezoelectric aspect [36]. Because of that PLLA has been the object of investigation in this group to exploit the piezoelectric properties of PLLA for tissue engineering [10,17-19,26,45,46]. Within this context PLLA was elected in this project as coatings of 316 SS substrates for bone implants. PLLA will be presented with more detail in the next sections.

2.4.3. *Poly(L-lactic acid)*

Poly(lactic acid), PLA, is a biodegradable, bioactive thermoplastic polyester that has been used to make several medical implants including bone screws, fixation devices and vascular grafts [36,37]. PLA can be obtained by different routes, as condensation, direct polymerization or ring opening polymerization. Moreover, PLA has two enantiomeric isomers, poly(L-lactic acid) (PLLA) and poly(D-lactic acid) (PDLA) [5,16,47]. Both routes to obtain PLA, as well as their enantiomeric isomers are schematically presented in Figure 7 [48,49].

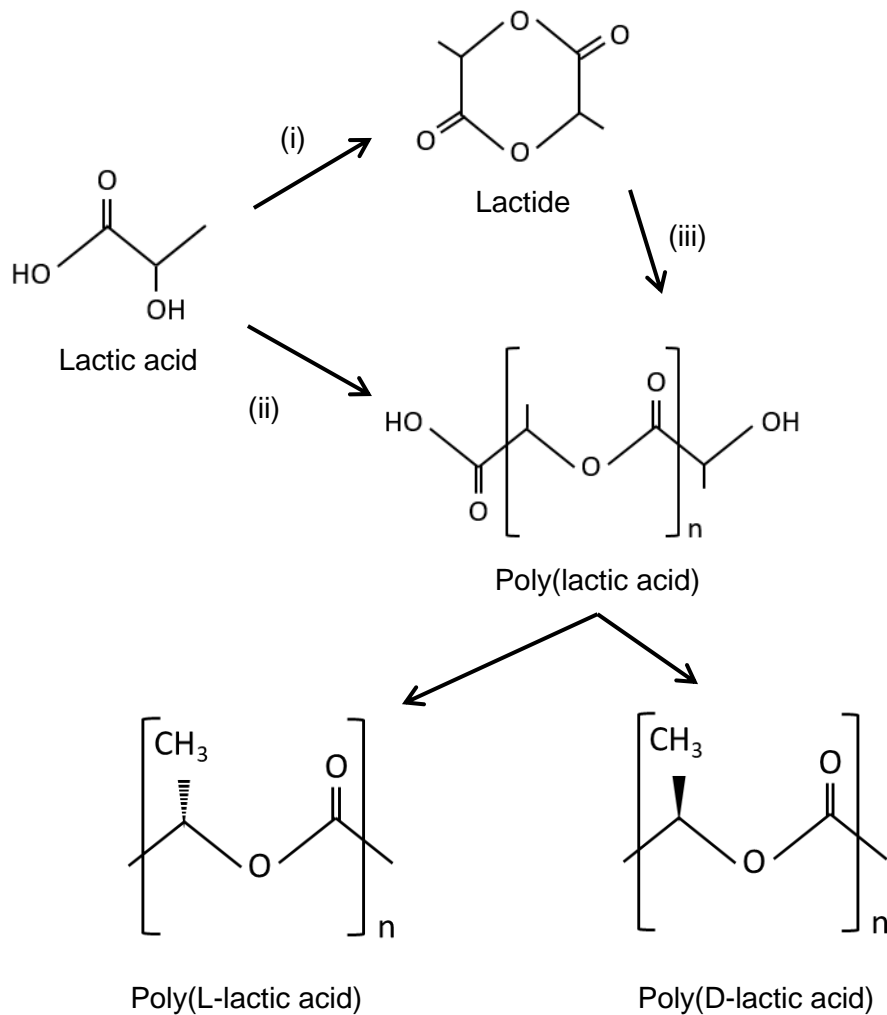


Figure 7 - Different routes to synthesise PLA and produce PLLA and PDLA: (i) condensation, (ii) direct polymerization and (iii) ring opening polymerization (based on [48,49]).

The discovery of the piezoelectricity of PLLA by Fukada *et al.* [14] inspired attempts to use this polymer as a bone substitute. Lately, PLLA was approved by the U.S. Food and Drug Administration (FDA) as a bone implant device [20,36], once it is biocompatible and biodegradable [16,18].

PLLA is a better candidate to use as a bone implant when compared to PDLA. PLLA has slow degradation rate and piezoelectric properties being, therefore, capable to mimic the natural bone [16,18,36]. Furthermore, PLLA is a crystalline polymer (approx. 37% crystallinity [50]) and has a high Young's modulus (Table II) and hence, has been

considered an ideal biomaterial for load bearing applications, such as orthopaedic fixation devices [50]. Other relevant properties of PLLA are presented in Table II [7,36,47,51,52].

Table II - Thermal and mechanical properties of PLLA.

Properties	References	
Melting temperature T_m (°C)	168 - 178	[47,50-52]
Glass transition temperature T_g (°C)	55 - 88	[47,50-52]
Decomposition temperature (°C)	200	[52]
Piezoelectric constant, d_{14} (pC/N)	- 9.82	[7,36]
Young's modulus (GPa)	2.7 - 3.5	[50,51]

The first studies with PLLA started with Ikada *et al.* in 1995 [53]. In their study, they implanted PLLA rods in the tibia and fibula of a cat and concluded that PLLA induced the bones growth. This finding was attributed to the ionic currents caused by the piezoelectric polarization that stimulated the activity of bone cells [14], mimicking the piezoelectricity of natural bone [54].

Jaiswl *et al.* [55] studied two composites of PLLA/HAp and PLLA/Gelatin/HAp scaffolds prepared by electrospinning of PLLA or PLLA/Gel, followed by HAp mineralization via alternate soaking in calcium and phosphate solutions. HAp precipitated on scaffold after each soaking cycle, being the hydroxyapatite binding favoured by the functional groups of gelatin. For the *in vitro* tests, human osteosarcoma cells (MG-63) were used and the main conclusion was that PLLA/Gelatin/HAp scaffold increased osseointegration [55].

More recently, Barroca *et al.* [18] studied two crystalline forms of PLLA and how crystallization influences polarization, being polarization an important characteristic for protein and cell adhesion. The samples were electrically poled at different temperatures (room and above glass transition) and the authors have concluded that above glass transition temperature, the polarization was stable up to 10 days for both forms, and that such time was enough to trigger and maintain proteins adhesion and cells proliferation, if intended to use as platform for tissue growth [18].

Biodegradability, biocompatibility, the piezoelectric properties of PLLA and the fact that it is approved by FDA to medical applications, make this material a great option to use in this thesis work. Moreover, as mentioned, in the literature the studies focus only in some properties [36], leaving aside the piezoelectricity of this material.

2.5. Metals in bone tissue engineering

Metallic materials are inorganic substances and are by far the oldest materials used in surgical procedures [8], mainly due to their good mechanical properties.

Metals and its alloys such as cobalt-chromium, titanium and stainless steel are the most used materials in orthopaedic implants, namely in joint replacement and fracture fixation implants, due to their good yield strength, ductility, fatigue strength, and fracture toughness and hence can offer support during the bone healing [2,5,8,9]. Mechanical properties as well as medical application of metallic alloys are summarized in Table III. For further information on medical applications, [15,56,57] should be consulted.

Table III - Mechanical properties and medical applications of metallic alloys used in TE.

Material	Young module (GPa)	Yield strength (MPa)	Compression strength (MPa)	Tensile strength (MPa)	Fatigue strength (MPa, 10⁷ cycles)	Applications	References
Cortical bone	7-30	NA	100-230	164-240	27-35	Not applicable	[9,56]
Ti6Al4V	114	760-880	NA	895-930	600-700	Pacemakers, ventricular devices, screws, dental implants and craniofacial devices	[56,57]
CoCrMo alloys	240	500-1500	NA	900-1540	500-900	Total hip arthroplasty, aneurysm clips, dental implants, vascular stents	[15,56]
Magnesium alloys	41	21	40	87	NA	Screws, micro clips for laryngeal microsurgery, orthopaedic and cardiovascular systems	[56,57]
316L SS	193	170-310	480-620	540-1000	240-480	Femoral prosthesis, aneurysm clips, orthodontic wire leads, cardiovascular and coronary stents, heart valves parts	[15,56]

NA – not available

2.5.1. Magnesium and Titanium based alloys

Magnesium alloys have adequate mechanical properties and biodegradation and are non-toxic. However, they are difficult to manufacture since they are prone to form hydrogen on the surface. Magnesium-based alloys are used as micro clips for laryngeal microsurgery, screws for orthopaedic and cardiovascular systems [57].

Titanium, on the other hand, and its alloys (Ti-6Al-4V, for example) have good biocompatibility, corrosion resistance and lower modulus and form easy bonding with bone, however require surface modifications to increase their wear resistance and they are more expensive compared to stainless steel (SS). Titanium alloys are used in pacemakers, ventricular devices, screws, dental implants and craniofacial devices [57].

2.5.2. Stainless Steel

The most widely used SS in medical applications is 316L SS, an austenitic alloy with a chemical composition presented in Table IV [8,58,59]. The ideal composition for an implant is the austenitic single phase, since this steel has high content of chromium and nickel, being thus more resistance to corrosion [10,15].

Table IV - Chemical composition of 316L SS [8,58,59].

Component	C	Si	Mn	P	S	Cr	Ni	Mo	N	Fe
Min. (wt.%)	-	-	-	-	-	16.0	10.0	2.00	-	Balance
Max. (wt.%)	0.030	0.75	2.00	0.045	0.030	18.0	14.0	3.00	0.10	

Ideally a bone implant material should have a Young's modulus close to the bone Young's modulus [9,56] to ensure a more uniform distribution of stress, minimizing the stress shielding effect. Moreover, an implant should have:

- High tensile and compressive strength to prevent fractures and improve functional stability (Table III);
- High yield strength and fatigue strength to prevent brittle fracture under cyclic loading;
- Adequate hardness to minimize the incidence of wear of material and high toughness to prevent fracture of the implants [9,57].

316L SS have all these advantages, although there are also some limitations as well, release of toxic metallic ions from metal surface that may cause local and distal toxicity, superior Young's modulus that may lead to stress-shielding¹ [60] and poor biodegradability, are some of the drawbacks. All these aspects may result in the need for further surgery or even in tissue loss [9,10]. It is reported that infections associated to orthopaedic fracture and reconstructive devices occur in up to 10% of the implant cases, mainly due to mechanical aseptic loosening of the implant [12].

Hence, it is important that implants have strong adhesion with the host tissue occurring as fast as possible, to promote the healing process and, consequently, have an effective osseointegration [2]. Metals usually behave as inert materials which makes implant integration and recognition by the host tissue very difficult. To achieve this osseointegration a possible strategy is to use a coating layer, per example, of a biocompatible, biodegradable and approved by FDA material, such as PLLA [2,15].

2.6. Metal-Polymer interface

Inorganic-organic materials composed of layers and aiming to “mimic” the nature of a real bone should combine the toughness and low weight density of a polymer with the stiffness and compressive strength of an inorganic metal. This will allow to generate a device with improved mechanical properties, while increasing the impact resistance and osseointegration [4,15,61].

However, the adhesion between metals and polymers is still a tricky procedure, due to the large difference in physical and chemical characteristics of these materials, as wettability, roughness and optical properties [61,62]. Thus, it is necessary to develop routes to improve the interfacial strength between 316L SS and PLLA.

¹ Stress shielding – result of removal of normal stress from the bone by an implant.

2.6.1. Adhesion

“Adhesion is the interatomic and intermolecular interaction at the interface of two surfaces” [63]. At a macroscopic level, adhesion is the state in which an interface is formed between two different materials such that mechanical work is transferred between both. At a microscopic level, adhesion is the state in which an interface is formed between two different materials such that the molecular forces are strong enough to resist to the two materials separation [64].

Depending on the type of mechanism occurring at the interface, adhesion can be considered as:

- Physical bonding, explained by adsorption principles (Figure 8 a)) and electrostatic attraction forces (Figure 8 b));
- Chemical or covalent bonding (Figure 8 c));
- Inter-diffusion (Figure 8 d)) and;
- Mechanical bonding or interlocking (Figure 8 e)) [64].

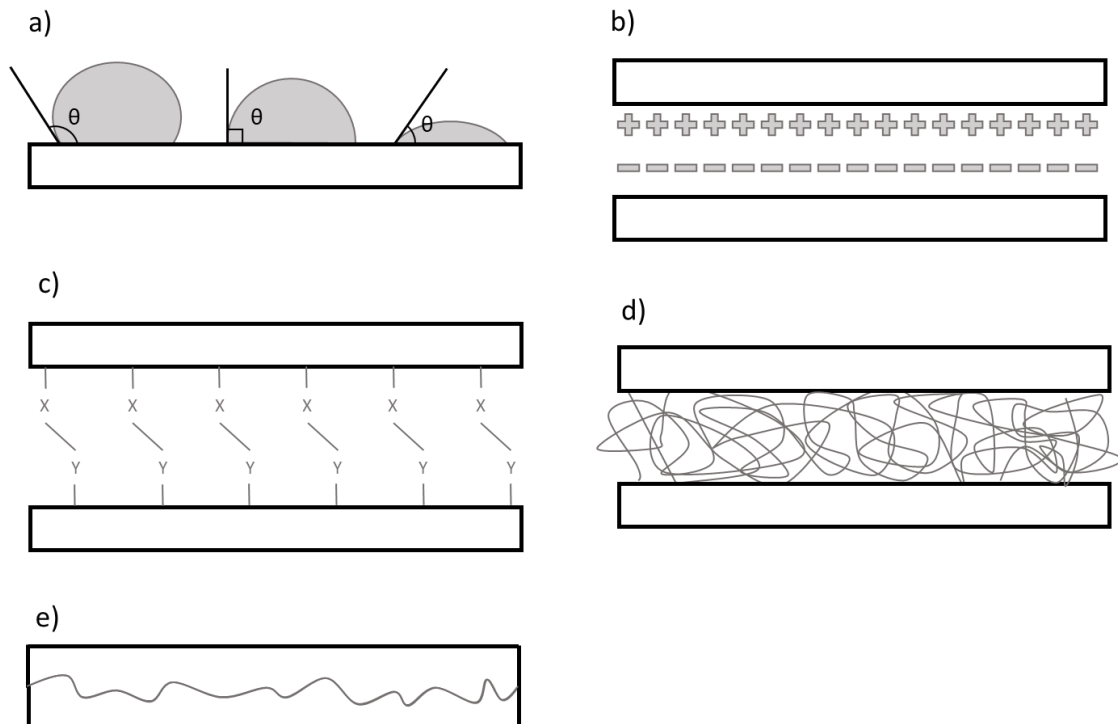


Figure 8 - Schematic representation of adhesion mechanisms types: a) adsorption, where the angles are related with the wettability of the surface; b) electrostatic attraction, which are dependent on the surface charges; c) chemical bonding; d) inter-diffusion and e) mechanical interlocking, which is related with the roughness of the surfaces (based on [64]).

The adsorption theory states that an adhesive must wet the surface to be bonded. It will then adhere to the substrates due to the interatomic and intermolecular forces established at the interface, as long as intimate contact is achieved. The theory of electrostatic interaction, on the other hand, states that the interaction between adhesive and adherent results from the double layer of ions formed at interfaces, charged electrostatically with opposite charges, provoking the attraction of Coulomb [64]. Chemical bonding involves the formation of bonds between compatible groups of the materials joined together, such as ionic, metallic or covalent bonds. The inter-diffusion adhesion theory states that adhesion of two materials is due to the mutual diffusion of molecules through the joined surface, leading to their entanglement. For last, interlocking theory is related to the roughness of the surface, in such a way that the adherent will mechanically bind to the pores and irregularities of the adhesive [63,64].

The adhesion of two materials depends mainly on the mechanical, physical and chemical bonds established between them. And while the pre-treatments have a high influence on the mechanical and physical bonds, the coupling agents have a greater effect on the chemical bonds [64].

2.6.2. Surface treatments

From the TE point of view, adhesion has been mainly considered between polymer matrices and cells. Nevertheless, as the main objective of this work is to coat a 316 SS substrate with PLLA films, it is necessary to study different ways of treating the materials to be used and, consequently, improve the adhesion between them.

Thus, treatment of the substrate surface is one of the most important procedures prior to adhesion since the state of the surface determines the linkage between the substrate and the coating. The treatment of the substrate surface can be divided in different stages: i) surface preparation; ii) surface pre-treatment and iii) surface post-treatment. Surface preparation consists in the removal of oil, grease and other contaminants through cleaning, degreasing and alignment processes. The second stage, surface pre-treatment, is the removal of strongly absorbed surface layers and the activation of the surface, through physical bonding, electrostatic attraction, chemical bonding, inter-diffusion or mechanical bonding. The last one, surface post-treatment, is the application of adhesion promoters, primers or activators to improve adhesion to the substrate and/or protect the surface [64,65]. Still regarding the pre-treatments, the surface can be treated in such a

way that the surface tension or the surface roughness increase or even change the surface chemistry. Increasing roughness implies an increase in the surface area which allows the polymer to flow through the irregularities on the surface, promoting mechanical bonding, while the chemical changes on the surface results in the formation of chemical bonding [66].

Within a previous work conducted in this group, Marinho *et al.* [10] studied ways to improve adhesion between 316L SS and PLLA films with different molecular weights. Mechanical treatment of the steel was used to create substrate roughness and promote polymer adhesion. The tape test was used to study the adhesion of PLLA to 316L SS. This is a qualitative test that consists in stripping the polymer and observing the amount of polymer pulled out, following the ASTM D3359 standard [67]. The best results of tape test were obtained with the lower molecular weight PLLA solution (with the lower solution concentration) with the substrates with higher roughness. Even though it was considered that these results were not sufficient to full adhere the PLLA films to 316L SS substrate. Within that work and based on the results obtained very preliminary tests using a chemical treatment, silanization were also referred. The results obtained seemed promising but because they were at the very initial stage, conclusions could not be drawn. There is the need to deepen this route, as a way to improve PLLA film adhesion on the surface of 316 SS, being this the main objective of this work.

2.6.3. Silane coupling agents

Silanization is a chemical method, which consists in the adhesion of silanes to a surface, particularly organosilanes. Organosilanes are the coupling agents most used to bond organic and inorganic materials [68], forming molecular bridges at the interface of the two materials.

The chemical structure of an organosilane is $X_3-Si(CH_2)_n-Y$, where X is a hydrolysable/inorganic group (e.g. alkoxy, methoxy, ethoxy or acetoxy), Y is an organofunctional group (e.g. amino, methacryloxy or epoxy) and the n value is generally 3 [61,64,68]. In the case of (3-Aminopropyl)trimethoxysilane (APTES), X is OC_2H_5 and Y is NH_2 . The organofunctional group is important to improve reactivity with the polymer matrix, while the hydrolysable group is an intermediate in the formation of silanol groups for bonding to inorganic surfaces [64].

During silane treatment of the substrates via a wet deposition method, there are three significant steps that should be undertaken: i) hydrolysis of silane, ii) silanization of the substrate, and iii) thermal curing of the silanized substrate [68]. First, silane solutions should be diluted (0.01-2%) to decrease molecules reactivity and to promote adsorption of silanol (Si–OH) groups into the substrate (Figure 9 a), by hydrogen bonds. Only during the last step, drying or curing processes, two condensation reactions occur in the silane/metal interface: Si–OH groups and metal hydroxyls (M–OH) form a stable and covalent oxane bond (Si–O–M) (Figure 9 b.1) and Si–OH groups react with each other on the metal surface, resulting in a siloxane network structure (Si–O–Si) (Figure 9 b.2) leaving the Y group available for the polymeric matrix [61,64,68].

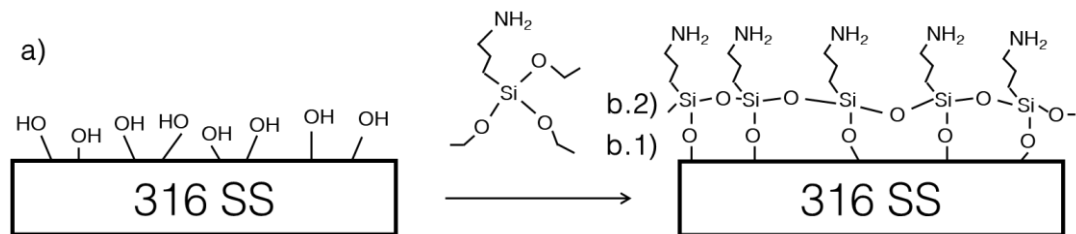


Figure 9 - Silane treatment of 316 SS substrate a) hydroxyl groups through heat treatments; b.1) (M–O–Si) bonds and b.2) (Si–O–Si) bonds (based on [69]).

2.6.4. Other metal surface treatments

The most commonly used methods to modify metal surfaces include acid etching, thermal treatments and scratching the substrates with SiC papers. Other treatments of the metal surfaces are possible and reported in the literature and a resume of recent studies on 316L SS substrates treatments is presented in Table V. In Table V is represented the reagent used on the substrate treatment as well as a small description of the procedure used. The results in summary and respective applications are presented, being the application mainly for TE and BTE. It should be noted that most of the layers that are used after the metal surface treatment are ceramics and oxides, rare are the cases in which polymers are used.

Table V – Recent studies on metal substrates treatments.

Substrate	a. Reagents b. Procedure c. Results	Application	Reference
304L SS	a. Solution of sulfuric/orthophosphoric acids electrolytes ($H_3PO_4:H_2SO_4 = 1:4$ and 4:1 by volume)	Biomaterials	[70]
316L SS	b. Electrochemical treatments, standard (EP50) and a high-current density electropolishing (EP1000). c. EP1000 allows to obtain the reduced Young's modulus of the SS (high importance regarding the use of these steels as biomaterials)		
316L SS	a. APTES b. Firstly, 316L SS was coated with Titania (prepared by sol-gel method) to increase hydroxyl (OH) groups at the surface; secondly, Silanization was performed varying concentrations (0.001 M – 0.04 M), reactions time (15 min, 1 h) and temperatures (25°C, 60°C, 120°C). The maximum density of amine groups on the surface was reached after reaction taking place in ethanol for 1 h at 60°C and 0.04 M APTES. c. Titania-coated SS 316L substrates were successfully silanized.	Cardiovascular	[71]
316L SS	a. Forsterite (Mg_2SiO_4) b. 316L SS ground with SiC papers until 1200 grit; sol-gel dip coating technique c. Crack-free and homogeneous forsterite coating with the crystallite size of around 40 nm was successfully achieved on the surface of 316L SS substrate. Better corrosion resistance compared to the uncoated substrates and <i>in vitro</i> bioactive.	BTE	[72]
316L SS	a. TiO_2 b. TiO_2 sol was prepared from TBT; followed by a dip coating. Afterwards, samples were thermally treated at 450°C for 30 min. c. A uniform, dense and crack free TiO_2 coating on the 316L SS was successfully prepared by sol-gel method.	BTE	[73]

316L SS	a. EDC	Biomedical	[74]
	b. Thermal treatment of 316L SS for 2 h at 500°C in air. Afterwards, they were soaked in a 1 vol.% toluene solution of APTES for 1 h in air and kept at 105°C for 10 min	applications	
	c. Amino groups from APTES improve immobilization of alginic acid and in turn there is an improvement of platelet adhesion.		

APTES – 3-(Aminopropyl)triethoxysilane

TBT – tetra-n-butyl titanate

EDC – 1-ethyl-3-(3-dimethylaminopropyl)carbodiimide

CHAPTER III

MATERIALS AND METHODS

CHAPTER III – MATERIALS AND METHODS

Herein, the experimental procedure and the characterization techniques used in this work are described. The experimental procedure is schematically represented in Figure 10 and detailed in the next sections.

To achieve the aim of this work, i.e. to study alternative methodologies to improve the adhesion of PLLA films onto 316 SS through a chemical treatment, named silanization, several procedures were performed. The approach used consists in firstly thermally treat the metallic substrate and secondly immerse it in a 1 vol.% of APTES in toluene for different immersion times: 0, 30, 60 and 90 min (hereafter designated as 30 sil, 60 sil, 90 sil, respectively). The importance of the pre-thermal treatment step was studied, for that two types of substrates were used, 316 SS as received (in this work named as SS) to which no thermal treatment was applied, and 316 SS subjected to a treatment at 500°C for 2 h (hereafter named as SS 500C).

The polymeric film was deposited by spin-coating on the different substrates (SS and SS 500C). Two different solution concentrations, 2.5 and 5.0 wt.%, of PLLA in 1,4 dioxane (PLLA 2.5 and PLLA 5.0, respectively) were prepared and afterwards spin-coated onto the substrates, SS and SS 500C. The number of deposited layers varied from 1, 2 and 3 layers (1L, 2L and 3L, respectively). After the deposition the polymeric films were submitted to two different thermal treatments (120°C for 60 min or 180°C for 3 min, followed by a 45 min period at 120°C) to induce different degrees of film crystallinity, named as semi-crystalline and crystalline films.

All the platforms were then submitted to a tape test, adapted from the ASTM D3359 standard [67], in order to study the adhesion between the polymeric film and the metal substrate.

The platforms in which the PLLA films adhered were submitted to a degradability study, by immersing them in phosphate buffered solution (PBS) for different periods of time (0, 2, 7 and 60 days), being this process adapted from the standard BS EN ISO 10993-13:1999 “Biological evaluation of medical devices — Part 13: Identification and quantification of degradation products from polymeric medical devices” [75].

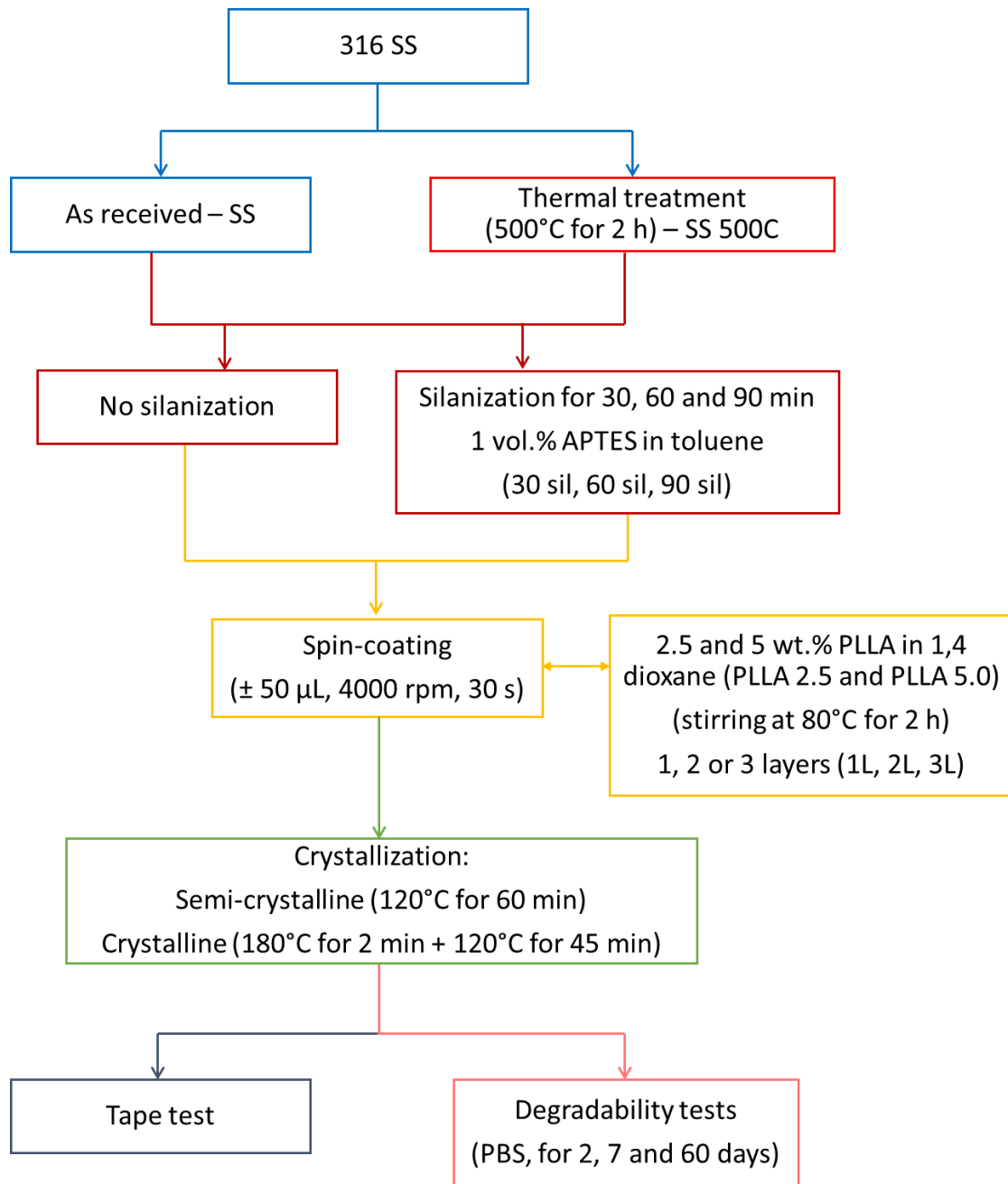


Figure 10 - Scheme of this work.

3.1. Materials

To prepare the platforms under study in this work the materials used include: i) the substrates FE240310 Stainless Steel – AISI 316 Fe/Cr18/Ni10/Mo3 (Goodfellow Cambridge Limited); ii) the films of Poly(L-lactic acid) from Purasorb® PL 38, Purac, The

Netherlands and iii) to functionalize the substrate surface (3-Aminopropyl)trimethoxysilane 97% (APTES, Aldrich) was used.

1,4-Dioxane anhydrous 99.8% (Sigma-Aldrich) and Toluol zur analyse C₇H₈ (Merck) were used to dissolve the PLLA pellets and the APTES, respectively. The tape tests were performed with an Elcometer 99 adhesive tape. For the degradability tests, a phosphate buffered saline (PBS) solution (Sigma-Aldrich) was used.

3.2. Methodologies

3.2.1. *Stainless steel substrates*

The metallic substrates were cut in (10 x 10) mm from sheets of FE240310 Stainless Steel – AISI 316 Fe/Cr18/Ni10/Mo3 (Goodfellow Cambridge Limited) and some of the substrates were functionalised using a silanization process [74].

Silanization is a chemical surface treatment (as explained in Chapter II – 2.6.2.) and it was used in this work to functionalize/activate the SS substrates. The silanization procedure was adapted from Yoshioka *et al.* [74] work, and the SS substrates were submitted to the following steps:

1. Sonication in acetone for 5-10 min three times;
2. Drying by blowing air;
3. Heating at 500°C for 2 h in air (Termolab, Fornos Elétricos), using a heating rate of 5 °C/min and cooling rate of 10 °C/min until room temperature (Figure 11);
4. Soaking in a 1 vol.% toluene solution of APTES for 30, 60 and 90 min in air (pH = 7);
5. Rinsing with toluene and ethanol;
6. Sonication in ethanol for 5 min;
7. Drying in air;
8. Drying at 100°C for 10 min.

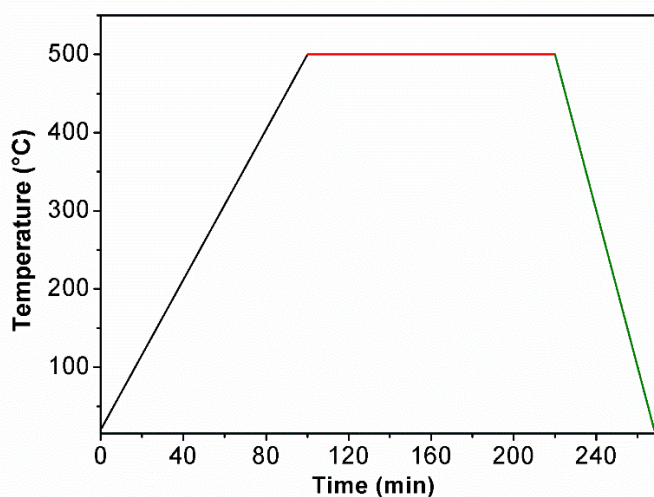


Figure 11 - Thermal treatment of SS 500C substrate with a heating rate of 5°C/min, dwell of 500°C for 120 min and cooling rate of 10°C/min until room temperature.

It is known that the adhesion strength of silanes depends on the material surface to which they are adhered. It is reported that materials such as silica and quartz are the ones exhibiting the strongest adhesion with silanes, due to the formation of siloxane linkages through the condensation with surface hydroxyl groups on the substrate (Si–O–Si) [76]. In metals and their alloys, adhesion is weaker and is formed by Si–O–M linkages, being M the metal. Other materials, such as graphite and carbon are poor in hydroxyl groups (–OH), making difficult the bonding with silane [76].

For this reason, the thermal treatment (step 3) was performed, to create more hydroxyl groups at the metal surface. Moreover, for the functionalization success it is important that APTES only react with –OH groups and not with the solvent (toluene, water, ethanol or acetone) [77]. For example, if water or ethanol were used, hydrolysis or self-condensation reactions will occur. That is the main reason for using toluene (step 4) instead of any other solvent [77].

3.2.2. Poly(L-lactic acid) solution preparation

PLLA solution was prepared dissolving PLLA pellets at 80°C for 2 h in 1,4 dioxane² in air atmosphere without the fume hood turned-on to avoid premature solvent evaporation. To mix these two reagents, a thermal stirrer plate was used, and the temperature was controlled by a thermocouple. The solution was afterwards deposited on the substrate by

² 1,4 dioxane reagent has a sceptre, being therefore, mandatory to use a syringe full of nitrogen (N₂) to take the liquid, in order to maintain an inert atmosphere inside the flask.

spin-coating and kept at room temperature inside a desiccator. The apparatus used in the PLLA dissolution process is presented in Figure 12.

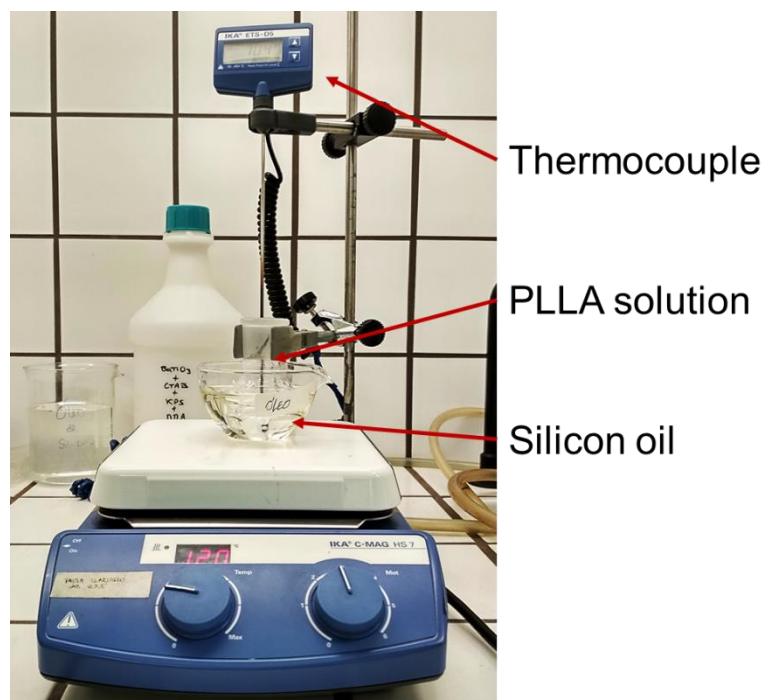


Figure 12 – Apparatus used in the polymeric dissolution process.

Two different polymer solution concentrations, 2.5 and 5.0 wt.% (PLLA 2.5 and PLLA 5.0) were used, in order to achieve homogeneous films with different thickness and, hence study the thickness influence on the adhesion. These solution concentrations were chosen based on previous work by Marinho *et al.* [10]. In addition, the lowest concentration was used since the 5.0 wt.% solution concentration has high viscosity. The temperature of 80°C was chosen, once it is above the glass transition temperature (T_g) (Table II) [47], facilitating crosslinking between PLLA and dioxane. The solution pH was 6.0.

3.2.3. Poly(L-lactic acid) film deposition

To get a uniform and homogeneous thin film of PLLA onto SS and SS 500C substrates, spin coating of the previously prepared PLLA solution was used. The procedure is schematically represented in Figure 13 a) and consists in four principal steps [78,79]:

i) Dispense stage (Figure 13 a) i)): several droplets of the coating solution are dispensed onto the substrate surface, via static or dynamic dispense. The static dispense consists on depositing a small droplet of fluid near the centre of the substrate, while dynamic dispense is the deposition of this droplet while substrate is turning at low speed [79]. In this work we used the static dispense method.

ii) Substrate acceleration stage: substrate starts rotating at high speed and there is a fluid expulsion from the substrate surface due to rotational motion. Eventually, the fluid is thin enough to be completely spun over the substrate. Lastly, the substrate reaches the desired speed. Generally, higher spin speeds and longer spin times create thinner films, being this stage preponderant one to determine the final film thickness [79].

iii) Substrate spinning at a constant rate – stage I (Figure 13 a) ii)): in this stage the fluid viscous forces dominate fluid thinning behaviour. The fluid is gradually thinning in a uniform way, however, surface tension, viscosity and rotation rate can negatively influence it [79].

iv) Substrate spinning at a constant rate – stage II (Figure 13 a) iii)): in this stage the solvent evaporation dominates the coating thinning behaviour. Moreover, the substrate is spinning at a constant rate favouring solution removal [79].

To finish, the airflow dries the solvent and the film is prepared (Figure 13 a) iv)) [78].

In this study, a Chemat Technology, Inc. Spin Coater KW-4A model was used (Figure 13 b)). The PLLA solution drop was approx. 0.5 μL and was spin-coated for 30 s at 4000 rounds per minute (rpm) on the substrates. Both SS and SS 500C substrates were coated and both PLLA 2.5 and PLLA 5.0 were used and different deposition layers for PLLA 2.5 (1, 2 and 3 layers) were spin-coated.

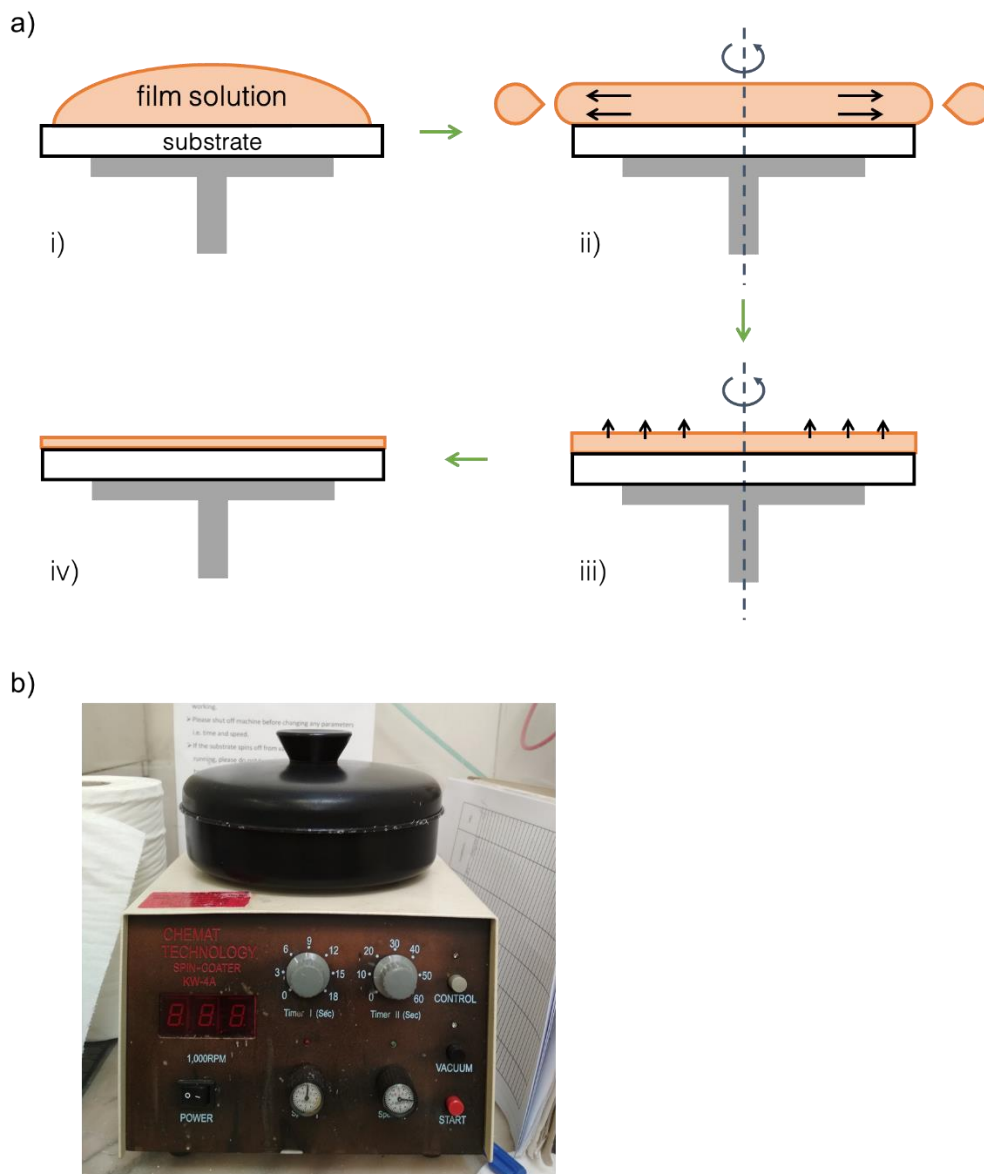


Figure 13 - a) Spin coating of PLLA films on SS and SS 500C substrates. a) Spin-coating procedure that includes the i) dispense stage; ii) substrate spinning at a constant rate and fluid viscous forces dominate fluid thinning behaviour; iii) stage of substrate spinning at a constant rate and solvent evaporation dominates the coating thinning behaviour and iv) final film (based on [78]); b) Spin-coater equipment used in this work.

3.2.1. Crystallization process of Poly(L-lactic acid)

For films that responded in a positive way to adhesion test (the tape test), namely PLLA 2.5 films on SS 500C with 3 layers, further studies were conducted, as investigating the role of the film crystallization on the adhesion process. Hence, these films were

thermally treated following two thermal schedules to obtain different degrees of crystallization.

Half of these films were treated at 120°C for 60 min (Figure 14 a)) to obtain semi-crystalline films, while the other half was subjected to a heat treatment consisting of two parts: first the films were at 180°C for 3 min, followed by a 45 min period at 120°C (Figure 14 b)) to obtain crystalline films. This process was performed in a thermal stirrer plate and based on previous work by Barroca *et al.* [17,18].

The temperature of 120°C was used once it is above PLLA glass transition temperature (T_g), while 180°C was used since it is above melting temperature (T_m) (Table II), promoting PLLA film crystallization since above T_m the nuclei formation is promoted [80].

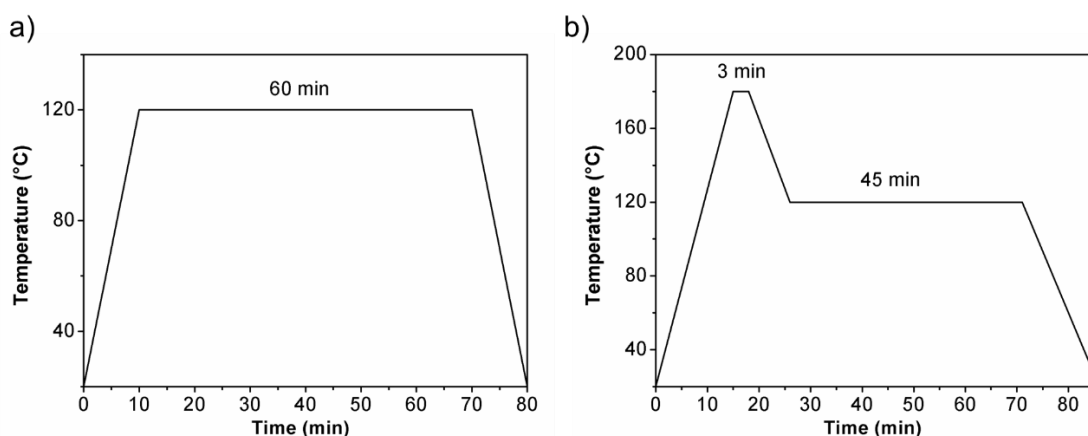


Figure 14 - Crystallization process to obtain a) semi-crystalline films through a single step for 60 min at 120°C and b) crystalline films through a step at 180°C for 3 min followed by 45 min at 120°C.

3.3. Characterization

3.3.1. Structural properties

A combination of different analyses was used to characterize the structure and the degree of crystallinity of the PLLA films prepared in this work, such as X-ray diffraction (XRD), thermogravimetry (TG), differential thermal analysis (DTA) and differential scanning calorimetry (DSC).

X-ray diffraction (XRD) is a common technique used to study crystal structures and degree of atomic organization, to identify the presence phases and preferred orientation of crystals and crystalline materials [81].

XRD is the result of a constructive interference between monochromatic X-rays and crystalline samples. X-rays are produced by a cathode ray tube, filtered to become a monochromatic radiation, collimated and directed towards the sample. When an atom is bombarded with X-rays, electrons become sources of electromagnetic waves with the same wavelength as the incident radiation, producing constructive interference. It is then possible to determine the interatomic distances of the planes through William Bragg's law (Eq. 3):

$$2d\sin\theta = n\lambda \quad \text{Eq. 3}$$

where n is an integer, λ is the wavelength of the incident radiation, d is the interplanar spacing and θ is the angle between the incident beam and the diffraction planes from the crystal lattice. Moreover, the conversion of the diffraction peaks to d -spacings and their comparison with standard reference patterns allows the identification of the material because each material has its unique d -spacings [81-83].

In this study, to characterize the materials under study, a Rigaku Geigerflex XRD equipment was used. XRD was performed at room temperature, with a target source of X-ray of copper (Cu), in which the radiation wavelength was $K\alpha_1 = 1.54060 \text{ \AA}$ and $K\alpha_2 = 1.54443 \text{ \AA}$. The scan range was $5.0021^\circ < 2\theta < 99.9651^\circ$ with a step size of 0.0260° and a scanning step time of approx. 96.4 s.

Thermal behaviour of materials provides indirect information on the examined structure, since it is possible to determine the crystallinity degree, for example of a polymer. Generally, thermal analysis consists of two main techniques, thermogravimetry (TG) and differential thermal analysis (DTA) or differential scanning calorimetry (DSC).

TG measures the mass changes of a sample as a function of the temperature at which the sample is exposed over a period, and it is then possible to monitor physical and chemical changes of the sample. There are many different effects, which may lead to mass changes, loss or gain of mass, of the sample. Some of the effects are evaporation of volatile constituents, drying, adsorption and desorption of gases, moisture and other volatile substances, loss of water of crystallization, oxidation of metals, oxidative decomposition of organic substances, uptake or loss of water in a humidity controlled

experiments, thermal decomposition in an inert atmosphere, and heterogeneous chemical reaction [83].

DTA and DSC are similar, having as principle the comparison between the sample tested with an inert reference sample, usually alumina. These two techniques measure the heat flow from and to a sample and a reference material as a function of temperature as the sample is heated, cooled or maintained at a constant temperature. The signal is the energy absorbed or released by the sample (mV) [84]. The temperature of the sample becomes lower in endothermic processes, or higher in exothermic processes. DTA and DSC permit consequently to identify any chemical-physical transformation that occurs in the analysed material as a function of the temperature. The DTA and DSC curves obtained also allow the determination of the enthalpy, ΔH , the crystallization temperature, the melting temperature, among other more complex changes [83].

3.3.2. Morphology

Scanning Electron Microscopy (SEM) is one of the most widely used technique to characterize materials microstructure [83]. SEM is an electron beam technique in which the image topography of the sample surface is obtained by electron scattering, being possible to generate images with a few nanometers of spatial resolution. The electron beam penetrates through the sample surface, which has to be conductive or with some conductive coating previously applied. The emitted and reflected beam of electrons are collected and then displayed at the same scanning rate on a cathode ray tube, providing topographical information and composition on the sample surface structure [63,83].

Image formation in SEM depends on whether secondary electrons (SE) or backscattered electrons (BSE) are detected. SE mode is the most common used SEM imaging method, because these electrons can be easily collected due to their low energy (< 50 eV). SE are originated at the sample's surface and occur due to inelastic interactions between the primary electron beam and the sample. This mode is important to inspect the sample's surface topography. On the other hand, BSE are originated from a wide region within the interaction volume and occur due to elastic collisions of electrons with atoms, causing a change in the electrons trajectory. BSE is an important mode to provide a contrast between regions of different compositions and elements, because these electrons are dependent on the atomic number, this is, for larger atoms the scattering is stronger when compared to light atoms [83,85].

Energy dispersive X-ray spectroscopy (EDS), coupled to many Scanning Electron Microscopes (SEMs), provides a qualitative and semiquantitative analysis of the chemical composition of a localized surface area of the sample. In this method, the specific area under study is directly irradiated with the electron beam and the interaction of this beam with the sample releases a specific energy, after which the result of the X-rays emitted is observed. Since each element has a unique atomic structure, the energies of the X-rays emitted will be specific to each element and different from element to element. The use of this technique is important, especially when used in combination with SEM, because it provides elemental analysis combined with high resolution images of surface topography [83].

In this work, two SEMs equipment were selected, because materials with different nature were studied, organic (PLLA films) and inorganic (stainless steel substrates). Hitachi SU70 working under the electron acceleration field of 5 kV (to avoid the damaging of the films) was used for the observations of the PLLA films morphology. While Hitachi S4100 working under the electron acceleration field of 25 kV was the one selected to study the SS and SS 500C morphology. The chemical composition of the substrates was semi-quantified using EDS (Bruker, model QUANTAX 400). For samples already conductive, there was no conductive coating. However, for non-conductive samples (the ones with PLLA films), a carbon deposition was performed, to guarantee the necessary conductive pass of the sample surface.

To support the interpretation and understanding of the results of the adhesion tape test, an optical microscope, with the resolution up to the micrometer was operated together with Infinity Analyze software.

Nikon MICROPHOT with an infinity optical system, Infinity 1 and Leica EZ4HD magnifier with LAS 4.0 software was the selected optical microscope.

The relation between film adhesion and surface roughness is well known and of relevance in this work, hence it was selected a profilometer to study these characteristics. Profilometry is a non-contact technique to study the profile of a surface, as the roughness, defects and film thickness. This feat can be obtained through a physical probe or by using light. In case of an optical profilometer using light, the light is directed to the sample in such a way that it can detect the sample's surface in 3D. Profilometer equipment is composed by two parts: the detector, which regulates where the point on the sample is and the sample holder, which is where the sample is placed [86,87]. Optical profilometers can be used in a confocal mode, phase shift interferometer (PSI) or white-light vertical

scanning interferometer (VSI). Confocal mode permits to measure the surface height, apart from the surface roughness and it provides a high lateral resolution. On the other hand, PSI measures the surface of a smooth material with a sub-nanometer resolution. For last, VSI measures the surface of a smooth to moderately rough material [88].

Sensofar S neox was employed in this work in VSI mode and with a 10x objective to study the film profile and thickness.

Another relevant characteristic of films and substrate surface is their wettability since it affects the adhesion of a film on a substrate. Wetting occurs when a liquid contacts a solid surface. The wetting properties of a material are dependent of intermolecular interactions between the liquid and solid [89]. Contact angle (CA) is the most important parameter used to evaluate the wettability of a solid surface [89], as a consequence the surface energy. In addition it is an inexpensive technique [63,83]. Theoretically, CA describes the behaviour of a liquid drop on a solid surface in air, being defined as the angle between the tangent at the three phase point and the solid surface, as shown in Figure 15 and described by Young's equation (Eq. 4) [89]:

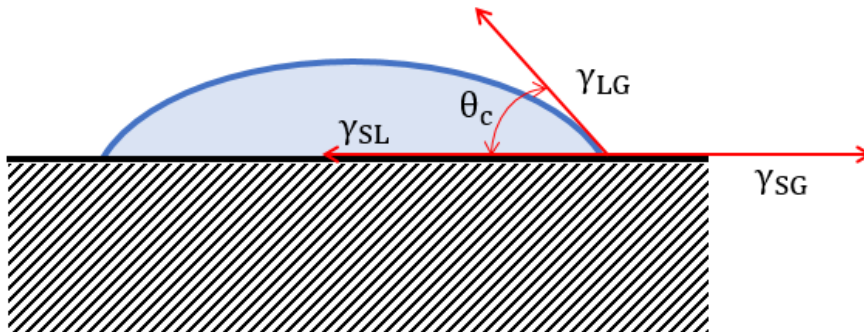


Figure 15 - Contact angle scheme. A liquid (in blue) contacts with a solid surface (in black). θ_c is the contact angle, γ_{SG} , γ_{SL} and γ_{LG} are the solid/gas, solid/liquid and liquid/gas interface tensions, respectively (based on [89]).

$$\gamma_{SG} - \gamma_{SL} - \gamma_{LG} \cos \theta_c = 0 \quad \text{Eq. 4}$$

where θ_c is the contact angle, γ_{SG} , γ_{SL} and γ_{LG} are the solid/gas, solid/liquid and liquid/gas interface tensions, respectively [89]. Smaller contact angles, $\theta_c < 90^\circ$, indicate a hydrophilic surface, that is, the surface is more wetting with a higher surface energy and consequently a greater work of adhesion. On the other hand, for higher contact angles,

$\theta_c > 90^\circ$, the surface is hydrophobic, that is, is less wetting with a lower surface energy and consequently a poor work of adhesion [63,89].

There are five ways to measure CA: the static or sessile drop method; the Wilhelmy balance technique; the captive air bubble method; the capillary rise method; and the tilting plate method developed by Adam and Jessop [83]. As the goal in this work was to characterize the wettability of the solid surfaces, a static CA measurement in air atmosphere was chosen.

For CA measurements there is no need for special sample preparation, however, the samples should be well clean and should not swell or dissolve in the test liquid [63,83]. There are certain aspects that can affect the accuracy of the results, including operator error, surface roughness, surface heterogeneity, contaminated fluids and sample geometry [83]. Generally, a certain volume of water is carefully dispensed onto the sample surface and the angle formed between the liquid and the surface is recorded.

In this work, a Data Physics OCA20 device was used. One drop of distilled water of 1 μL in volume was placed on the substrate, both in the border and in the middle, being the sessile drop used in ellipse mode. The CA was measured after approx. 3 to 5 seconds after droplet. For every sample, at least 10 measurements were performed, being then calculated an average value and its standard deviation. CA was measured for SS, SS 500C, and for different silanization times (30 sil, 60 sil, 90 sil, 120 sil and 180 sil).

3.3.3. *Chemical analysis*

Fourier Transformed Infrared Spectroscopy (FTIR) is a qualitative analysis and consists in the study of the interaction of infrared light with a material, analysing the vibration of the chemical bonds as a result of the absorption of energy. In this technique, infrared radiation passes through the sample and it can be absorbed by the material or transmitted. In order to obtain a frequency spectrum, which will facilitate an identification of the peaks, the measured signal is accomplished via Fourier transformation (FFT), which is performed by a computer. The resulting spectrum is unique for each molecule, being a representation of the absorption and transmission of this molecule. Each peak of FTIR spectra corresponds to the vibrational modes of the atoms constituting the material, being possible to identify a material. A scheme of FTIR apparatus is presented in Figure 16 [90], along with its main constituents: spectrometer that allows obtaining an

interferogram (or the raw data). This undergoes through a Fourier transformation to get the final FTIR spectrum.

Thermo Nicolet Nexus (670 FTIR, Thermo Scientific, USA) was used for conducting the chemical analysis of the samples after each step of surface modification. FTIR resolution was 4 cm^{-1} with 1024 scans collected to improve the signal to noise ratio.



Spectrum ← FFT (computer) ← Interferogram ← Spectrometer (source, interferometer, sample and detector)

Figure 16 - FTIR apparatus and the respective constituents: a spectrometer that allows obtaining an interferogram, that undergoes through a Fourier transformation to get the final FTIR spectrum.

X-ray photoelectron spectroscopy (XPS) is a relatively non-destructive technique and allows both qualitative and quantitative elemental information for all elements, except hydrogen (H) and helium (He) [51,68]. The X-ray photons derived from X-ray sources are in a range of energy between 100 to 2500 eV and after monochromation only one energy is used. This X-ray photons have limited penetrating power in a solid (around 1-10 μm) and they interact with atoms in this surface region by the photoelectric effect presented in Eq. 5, causing the emission of electrons. The kinetic energy of these electrons is then determined, using a hemispherical analyser and the corresponding electron binding energy calculated [63,91].

$$KE = h\nu - BE - \phi_s$$

Eq. 5

In Eq. 5 KE is the kinetic energy, $h\nu$ is the photon energy, BE is the binding energy of the atomic orbital which the electron originates and ϕ_s is the spectrometer work function [91].

The photoelectrons have unique energies for each element and are sensitive to their chemical states, providing a direct measurement of the elemental concentration by analysing the peak intensity in the photoelectron spectrum [83].

XPS is a surface sensitive analytical technique with a depth of analysis of the order of 5-10 nm. XPS instruments operate at high and ultrahigh-vacuum to minimize surface contamination. A schematic apparatus of XPS is presented in Figure 17 [92].

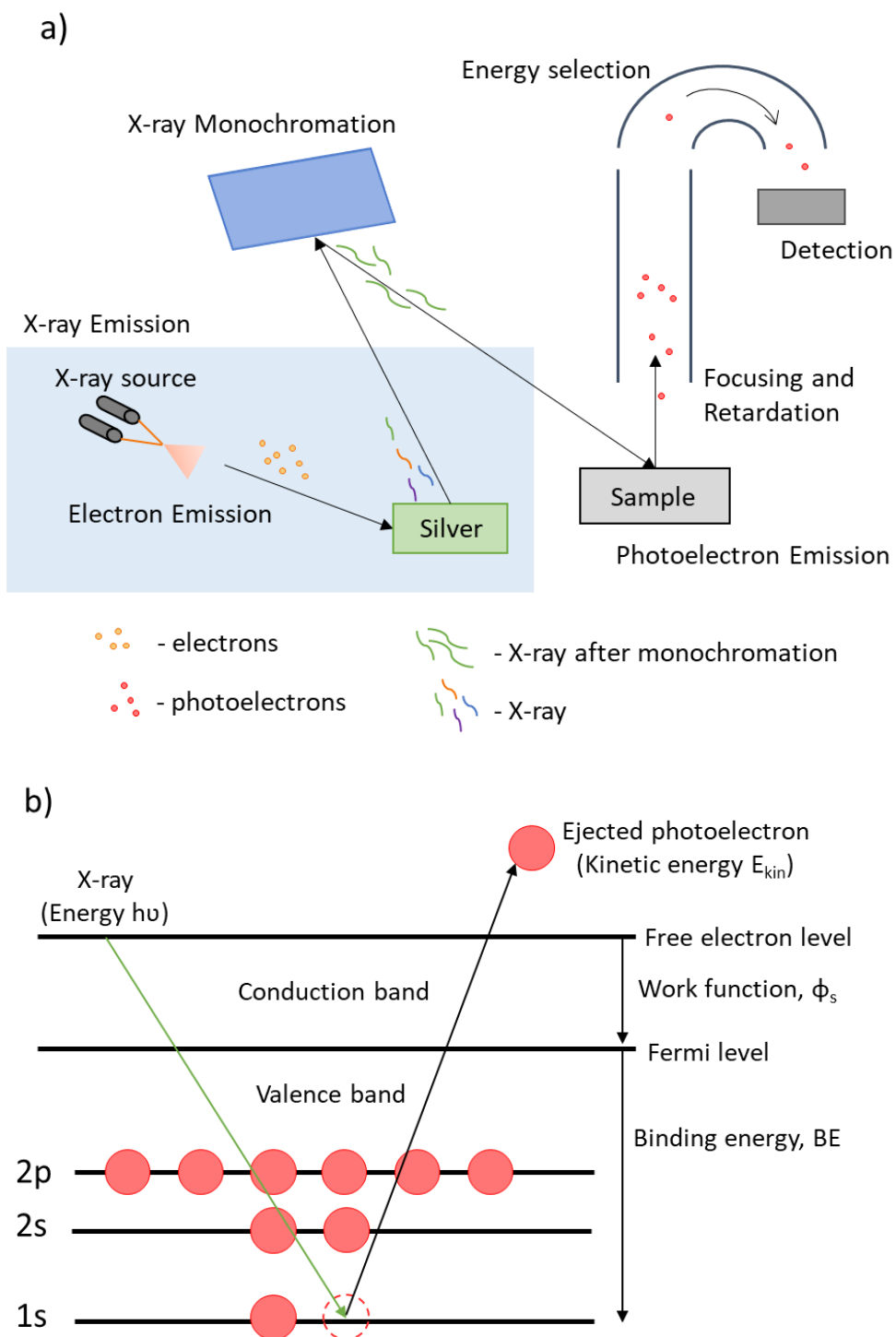


Figure 17 - a) XPS apparatus and b) photoelectric effect principle (based on [92]).

XPS was used to determine the chemical composition of the silane layer on the SS 500C substrate, as well as the differences between SS and SS 500C. In this work, XPS spectra were acquired in an Ultra High Vacuum (UHV) system with a base pressure of 2×10^{-10} mbar located at the Associated Laboratory TEMA, University of Aveiro. The

system is equipped with a hemispherical electron energy analyzer (SPECS Phoibos 150), a delay-line detector and a monochromatic Al K α (1486.74 eV) X-ray source. High resolution spectra were recorded at normal emission take-off angle and with a pass-energy of 20 eV, which provides an overall instrumental peak broadening of 0.5 eV.

The spectra recorded were: overview spectrum, C 1s, O 1s, N 1s, Fe 3s, Fe 2p, Mo 3p, S 2p, Si 2s and Si 2p. The binding energy scale was set by fixing the C 1s component at 284.5 eV. The peaks were decomposed using a linear, Shirley or Tougaard baseline, depending on the element and a component shape defined by the product of a Gauss and Lorentz function, using XPS PEAK41 software. An example of the decomposition of N 1s element for SS 500C 30 sil is present in Figure 18. Atomic percentage were calculated by the following expression (Eq. 6):

$$\text{Area}_{\text{normalized}} = \frac{\text{Area}}{T\sigma_{\text{element}}} \quad \text{Eq. 6}$$

where Area under the decomposed peak is according to the acquisition parameters, T is the transmission functions of the machine provided by the manufacturer and σ_{element} is the relative sensitivity factors, tabled and characteristic of each element (see Table VI) for 1486.6 eV energy [93].

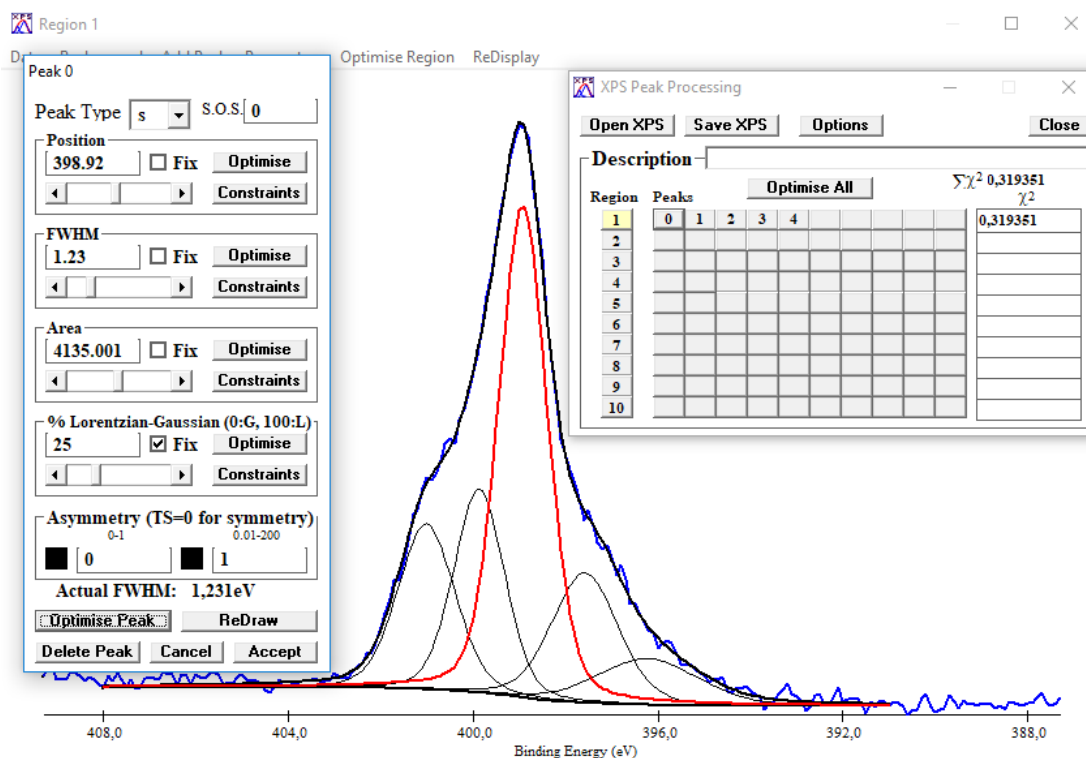


Figure 18 - XPS PEAK41 software: example of a decomposition in the different components regarding N 1s peak for SS 500C 30 sil.

Table VI - Relative sensitivity factor for different elements [93].

Element	C 1s	O 1s	N 1s	Si 2p
σ	0.014	0.04	0.025	0.011

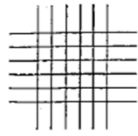
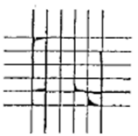
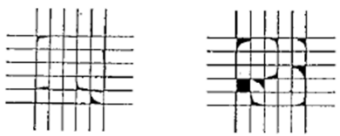
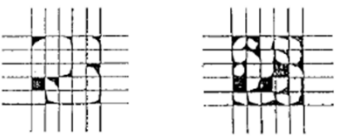
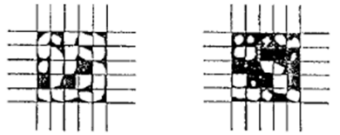
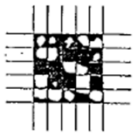
3.3.4. Adhesion measurements

Tape test method measures the adhesion of coating films to metallic substrates by applying and removing pressure-sensitive tape over cuts made in the film. This test only establishes whether the adhesion of a film to a metal substrate is at a generally adequate level and does not distinguish between different levels of adhesion.

In this work the adhesion test was performed according to the standard ASTM D3359. This standard mention two test methods, being the most suitable for this study the test method B, even though it was adapted. This test consists in creating a pattern in the film with five cuts in each direction (perpendicular) to the substrate. Afterwards, pressure-sensitive tape (Elcometer 99) is applied over the pattern and then removed in a 180°

direction and the adhesion is after evaluated by comparison with the indications in Table VII [67].

Table VII - Classification of tape test results according to standard ASTM D3359 (based on [67]).

CLASSIFICATION OF ADHESION TEST RESULTS		
CLASSIFICATION	PERCENT AREA REMOVED	SURFACE OF CROSS-CUT AREA FROM WHICH FLAKING HAS OCCURED FOR SIX PARALLEL CUTS AND ADHESION RANGE BY PERCENT
5B	0 % None	
4B	Less than 5 %	
3B	5 – 15 %	
2B	15 – 35 %	
1B	35 – 65 %	
0B	Greater than 65%	

A plastic piece was 3D printed (Figure 19 a)) to help the cuts so that they were always at the same distance and with the same angle between the two directions (90°). A x-acto

knife was used as the cutting tool. The cutting process is presented in Figure 19 b). To note that in this process there is an operator error that is not negligible, since the applied force cannot be precisely controlled, although in the current work it was minimized as much as possible.

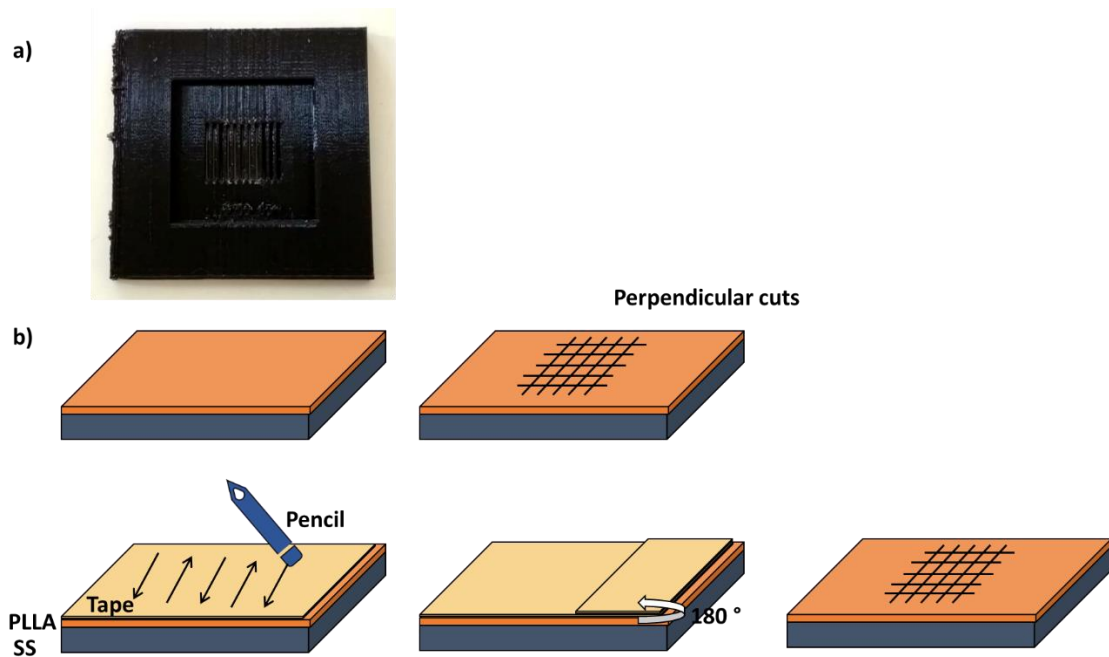


Figure 19 - a) 3D printed plastic accessory to help the cutting process and b) the cutting process.

3.3.5. Degradability tests in Phosphate buffered saline (PBS) solution

Phosphate buffered saline (PBS) solution of 0.01 M was used. The pH was set at 7.4 ± 0.1 , since it is approximately the human plasma pH.

Degradability tests were performed adapting the standard BS EN ISO 10993-13:1999 “Biological evaluation of medical devices — Part 13: Identification and quantification of degradation products from polymeric medical devices” [75].

The platforms were immersed in PBS in a ratio mass/volume of 1:10 (40 mL) inside a flask, which was firstly sterilized with UV light. The apparatus was kept at 50°C , which is higher than 37°C and lower than the PLLA glass transition temperature. The platforms were kept in these conditions for 2, 7 and 60 days. Flasks only with PBS were kept in the same conditions as well. Before the immersion and after each time, the solution pH was

measured. Platforms were taken from the bath at the time-points and were dried. Samples were also analysed by FITR. A scheme of this experimental test is presented in Figure 20.

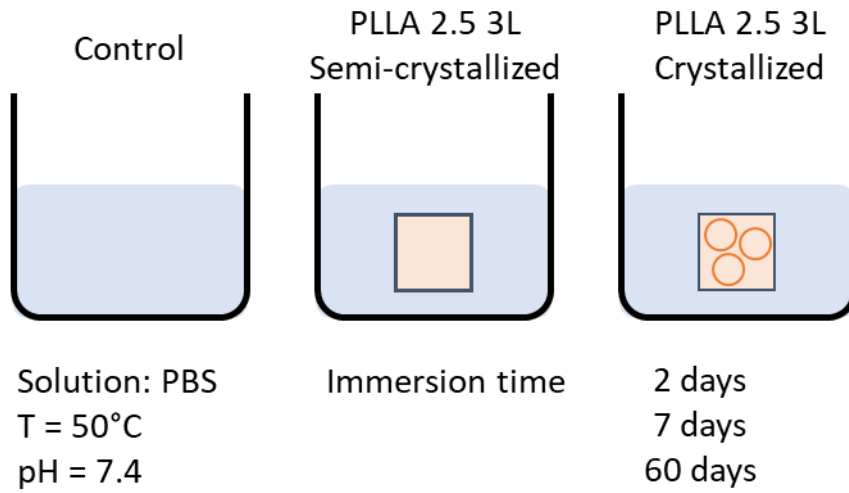


Figure 20 – Scheme of the degradability tests in PBS.

CHAPTER IV

RESULTS AND DISCUSSION

CHAPTER IV – RESULTS AND DISCUSSION

4.1. Stainless steel substrate characterization

In this section the results of all the processes to which SS was subjected, such as heat treatment and silanization are presented and their properly discussion. Firstly, it is made a characterization of SS before and after the thermal treatment, since this step is one of the most important to get SS silanized.

As mentioned in chapter 2.6.3., silanization is a chemical method, which consists in the adhesion of organosilanes to a surface to promote the formation of molecular bridges at the interface of organic and inorganic materials [68], aiming, for example, to promote cellular and protein adhesion (Table V).

In this work, silanes were used as an intermediate layer to promote the adhesion of a polymeric layer on a metallic substrate. To obtain the linkage between SS and silanes, it is important to promote the formation of a hydroxyl group layer on the SS surface and this can be achieved with a heat treatment or through chemical treatments such as acid etching or piranha solution [70]. Chemical treatments attack the surface at specific points, degrading the substrate, whilst the heat treatment favours the formation of the hydroxyl groups without degrading the surface. Hence, a systematic study of the thermal behaviour of the SS was conducted to optimize and understand the best silanization conditions. After the silanization process, a quantification of silanes on the SS surface was conducted using XPS analysis. Wettability assays were concomitantly performed to evaluate the surface changes.

The company supplier of 316 SS, Goodfellow Cambridge Limited supplied information about the thermal treatments used in the manufacture of these alloys. According to Goodfellow Cambridge Limited these alloys were subjected to an annealing treatment following the standard BS EN 10088-2 (1.4404), i.e., the heat treatment took place at around 1040°C and was held for a short period of time, being afterwards water-quenched in order to avoid carbide precipitation.

As described in the experimental section (chapter 3.2.1) 316 SS were heat treated at 500°C in air for 120 min. After the thermal treatment, a difference in the sample surface colour was noticed and thus, a deeper microstructural analysis was made, through OM and SEM micrographs images.

Figure 21 a) and b) shows the SS and SS 500C surfaces images, respectively. In contrast with the bright surface of SS, SS 500C presents a dark purple colour surface. These results are in accordance with what is referred in the literature when a steel is heated [94]. It is reported that a 304 SS alloy after a heat treatment at 450°C gets a dark purple colour, which can be related with the formation on a thin oxide layer [95]. Further results to support this information about the thin oxide layer will be presented after. It is possible to compare these two alloys (304 and 316) since the chemical composition is identical, as shown in Table VIII [8,58,59,96].

Table VIII - Chemical composition of 304 and 316 stainless steel alloys [8,58,59,96].

Component	304 (wt.% min.-max.)	316 (wt.% min.-max.)
C	0.08	0.08
Si	1.0	0.75
Mn	2.0	2.0
P	0.045	0.045
S	0.03	0.03
Cr	17.5-20.0	16.0-18.0
Ni	8.0-11.0	10.0-14.0
Mo	-	2.00-3.00
N	-	0.10
Fe	Balance	Balance

Analysing the OM images (Figure 21 c) and d)), the difference in the surface is clearer. The polishing marks on the SS are aligned (Figure 21 c)), whereas on the SS 500C these marks disappear and occurs a slight attack at the grain boundaries, which makes them more evident (Figure 21 d)). These differences in the surface are stronger when looking at the SEM micrographs presented in Figure 21 e), f) and g).

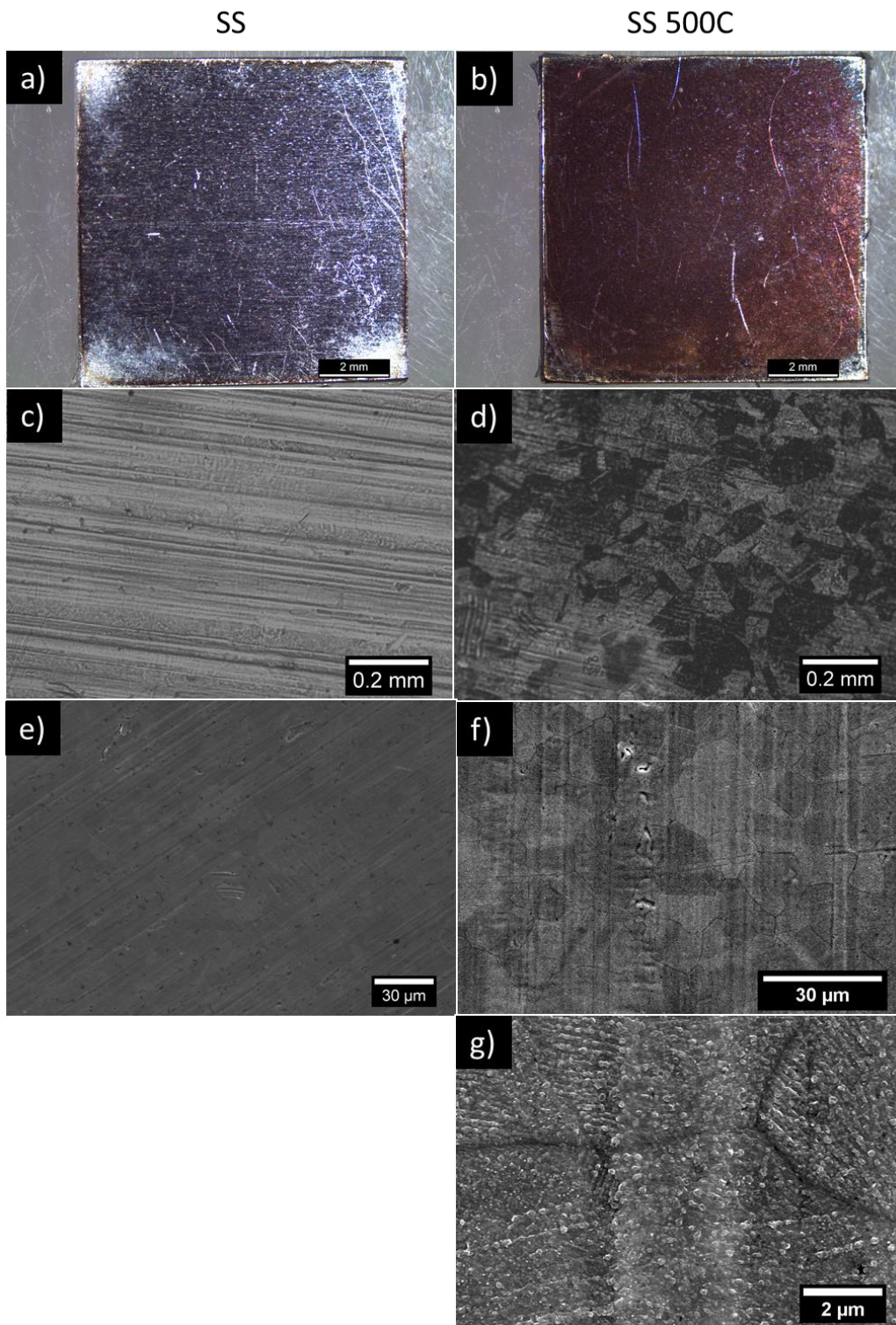


Figure 21 – SS substrates (left) and SS 500C (right) under different magnifications and using different equipment. Magnifier glass images (a) and b)), OM images (c) and d)) and SEM micrographs (e), f) and g)). Magnifier glass images display a clear difference in the surface colour while a higher magnification with SEM presents clearly grains and grain boundaries in the heat treated stainless steel substrate.

To systematically study the changes in SS 500C, a polishing to clean the thin oxide layer (purple colour) [95] of SS 500C substrates was performed, grinding the surface with a SiC paper #4000. SEM micrographs of SS, SS 500C and SS 500C after polishing cleaning are presented in Figure 22. The major differences between SS (Figure 22 a)) and SS 500C after polishing (Figure 22 c)) are in the polishing marks at the surface. In case of SS the surface has aligned polishing marks, while for SS 500C after polishing the substrates present random polishing marks. In addition, the grain boundaries disappear after the polishing (compare Figure 22 b) and c)), which indicate that these changes may be related to surface changes and not to changes in the bulk.

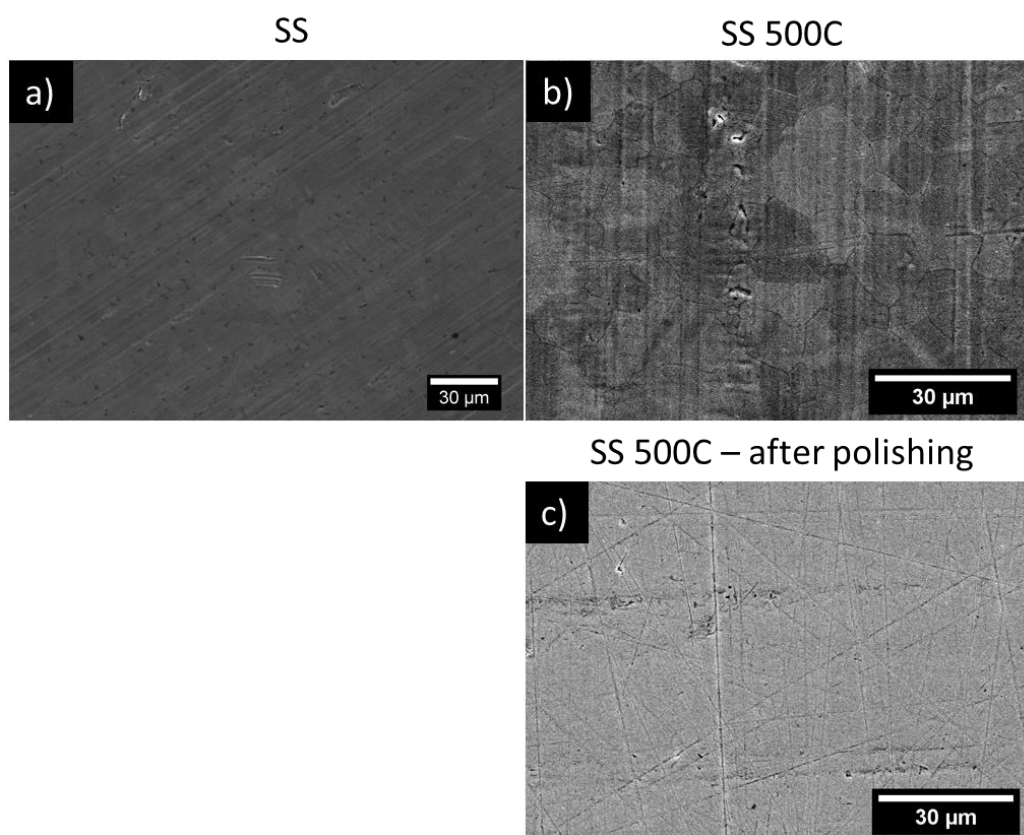


Figure 22 - SEM micrographs of a) SS, b) SS 500C and c) SS 500C after polishing in different magnification. A clear difference on the polishing marks is evident between SS and SS 500C after polishing and the grain boundaries disappear after the polishing.

To confirm the alloy composition of SS substrates a chemical EDS analysis was performed. In addition to the EDS of the as received SS substrates the composition of the substrates after the thermal treatment (SS 500C) and after the polishing cleaning (SS

500C after polishing) was examined as well to infer about possible chemical changes due to both processes. The determined chemical composition of SS substrates is presented in Table IX. SS substrates are an iron-chromium alloy rich in nickel, as typical austenitic alloy and in accordance to the typical chemical composition of SS (Table II). After the thermal treatment there is a slight increase of 0.5 wt.% for iron and chromium elements, consistent with XRD, XPS and FTIR results (later shown), which may suggest the formation of iron and chromium oxides. For SS 500C after polishing, comparing to SS 500C, the differences are insignificant (0.02 wt.% approximately).

Table IX - Chemical composition (wt.%) of SS, SS 500C and SS 500C after polishing. There are no significant differences among the samples chemical composition.

Component	Wt.% SS	Wt.% SS 500C	Wt.% SS 500C after polishing
Fe	73.13	73.62	73.64
Cr	16.43	16.91	16.95
Ni	9.20	9.14	8.99

To trace this chemical alteration of the substrates composition during the thermal treatments prior to silanization, *in-situ* XRD as a function of temperature was recorded and the XRD patterns of SS substrates under different temperatures (25, 400, 500, 600, 800, 1000 and 1200°C) are depicted in Figure 23, with the respective crystallographic compounds identified. The crystallographic plans and respective compounds are listed in Table X, based on JCPDS-PDF cards [97-100].

As expected, for SS at 25°C only austenitic phases (Fe) are identified. As the temperature increases, there is a shift of the diffraction peaks to the left associated to the lattice expansion and the formation of oxide phases starts after 800°C and is well noticed at 1000 and 1200°C. These phases, at higher temperatures, mostly consist of Fe₂O₃ and Cr_{0.25}Fe_{1.25}O₃ although, there is also a Fe₃O₄ phase.

In addition to the *in-situ* study, SS 500C was also analysed. A similar pattern to the *in-situ* at 500°C one (Figure 23 blue line) was obtained (not shown here). Hence, it is possible to conclude that there are no significant differences at the structural level in the steel substrates after the heat treatment, prior to the silanization.

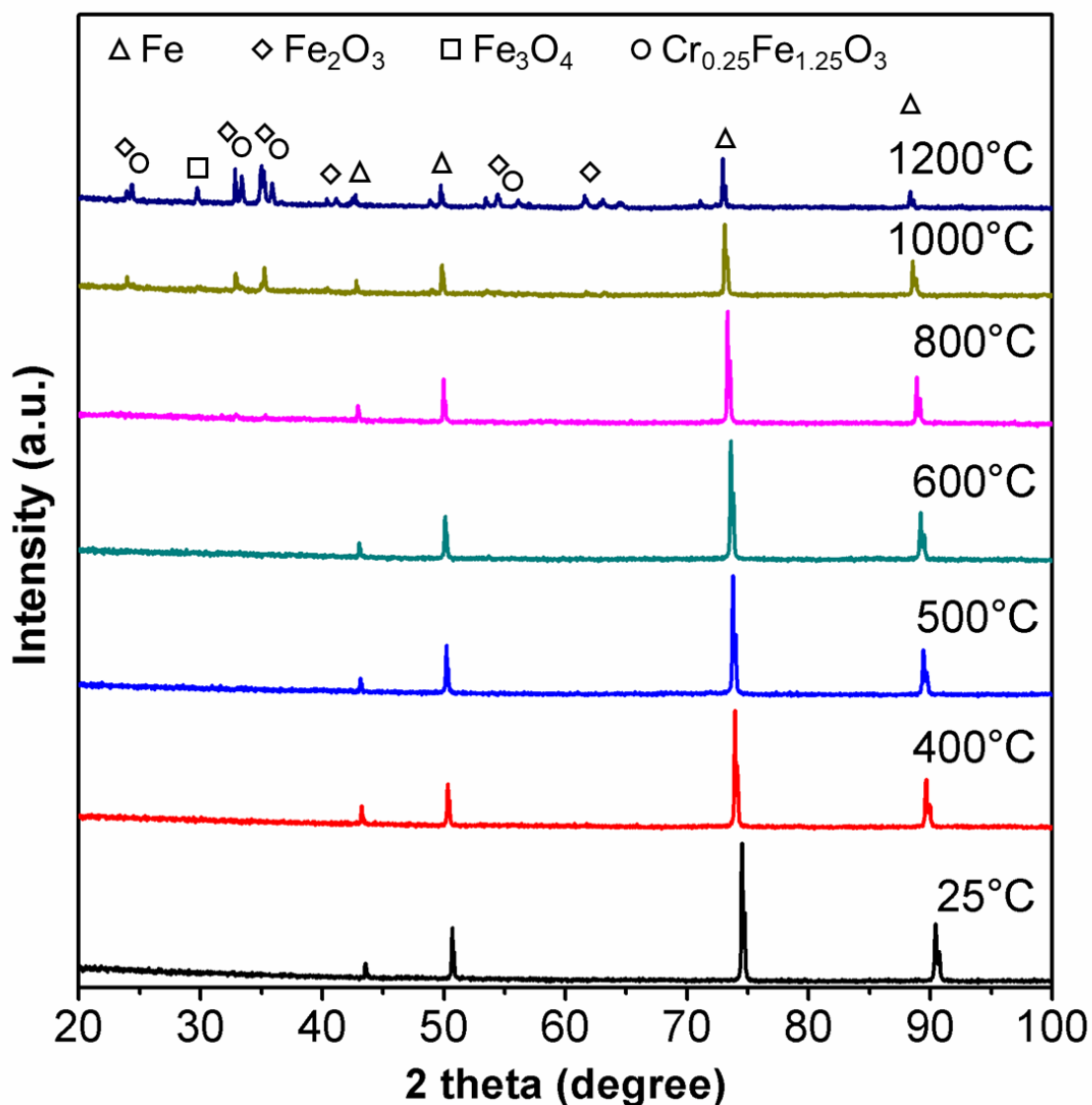


Figure 23 - *In-situ* XRD pattern of SS under different temperatures in air atmosphere. The crystallographic phases are identified based on JCPDS-PDF cards ([97-100]). For temperatures lower than 800°C only austenitic phases are identified, while for temperatures above 800°C the formation of iron and chromium oxides phases starts.

Table X - Crystallographic plans and respective compounds for SS under different temperatures in air atmosphere and *in situ* ([97-100]).

Diffraction angle, 2 theta (degree)	Crystallographic plans	Compound
23.9	(012)	Fe ₂ O ₃
24.4	(012)	Cr _{0.25} Fe _{1.25} O ₃
29.7	(220)	Fe ₃ O ₄
32.9	(104)	Fe ₂ O ₃
33.4	(104)	Cr _{0.25} Fe _{1.25} O ₃
35.1	(110)	Fe ₂ O ₃
35.9	(110)	Cr _{0.25} Fe _{1.25} O ₃
42.8	(202)	Fe ₂ O ₃
43.4	(111)	Fe
50.7	(200)	Fe
53.5	(116)	Fe ₂ O ₃
53.5	(116)	Fe ₂ O ₃
54.4	(116)	Cr _{0.25} Fe _{1.25} O ₃
61.7	(214)	Fe ₂ O ₃
74.5	(220)	Fe
90.5	(311)	Fe

According to Euroinox [94], 316L SS is resistant to corrosion due to the passive layer that forms naturally and instantly. The passive layer in 316L SS is caused by the presence of chromium and iron in the steel, which are very reactive with both oxygen and water presented in the air. The final product of this reaction is chromium and iron oxides and chromium and iron hydroxides. In addition to this natural process, there are other treatments that can increase the existing passive layer, as thermal and acid treatments.

A systematic study of the thermal behaviour of these alloys (316 SS) was performed from room temperature up to 1300°C, under different atmospheres (air, oxygen and

argon) under different heating rates (5, 10 and 20°C/min). Both the thermal gravimetric and differential analysis of SS are presented in Figure 24.

Considering the TG curves, it is possible to observe that the thermogravimetric behaviour of SS substrates is very dependent on the atmosphere. In air there is almost no weight variation up to 500°C (~ 0.38%). A slight weight gain is observed from 500 up to 1000°C (~ 1.0%). Above 1000°C there is a marked increase in the weight gain that is more intense and occurs for lower temperatures for the lower heating rate. The highest gain weight was observed in air atmosphere. Differently from this is the behaviour of SS substrates under argon. Gain weight starts for quite low temperatures; at 200°C there is already a gain weight of ~ 0.54%. The gain weight increases steadily up to almost 1000°C, reaching a value of ~ 2.76%. As the temperature keeps raising the weight gain increases with a high increasing rate, reaching a maximum of weight gain of ~ 5.24%. Under this atmosphere there is not a systematic dependence on the heating velocity being the lowest weight gains observed for the lowest heating rate. Thermogravimetry under oxygen presents an intermediate behaviour between air and argon atmospheres. Up to 1000°C the weight gain is small not exceeding ~ 1.0% increasing after up to ~ 5.44%. In this case the highest weight loss is observed for the highest heating rates.

Corroborating with the previous analysis the observed weight gain should be related with the formation of Fe₂O₃, Fe₃O₄ and Cr_{0.25}Fe_{1.25}O₃ oxides. Moreover, in air and oxygen there is almost zero weight changes from room temperature until 1000 - 1100°C, proving that this alloy is stable for low temperatures, which can be related with the protective role of its passive layer [94].

The different behaviour between air and oxygen needs to be related with the air atmosphere composition. In average dry air contains 78.09% nitrogen, 20.95% oxygen, 0.93% argon, 0.04% carbon dioxide, and small amounts of other gases [101]. Air also contains a variable amount of water vapour (~ 1%) [101]. Here we advocate that the presence of oxygen in the air approximates the thermogravimetric behaviour of SS substrates in air to the one observed in oxygen, for which the passivation layer of the substrates protects them from the oxidation.

The results indicate that the passive layer slows down the oxidation of steel and that argon will degrade the passive layer, promoting the oxide formation. Further studies on structural and morphological characterization should be taken into consideration to understand whether the percentage of weight gain is actually due to the formation of an oxide layer or to any other cause.

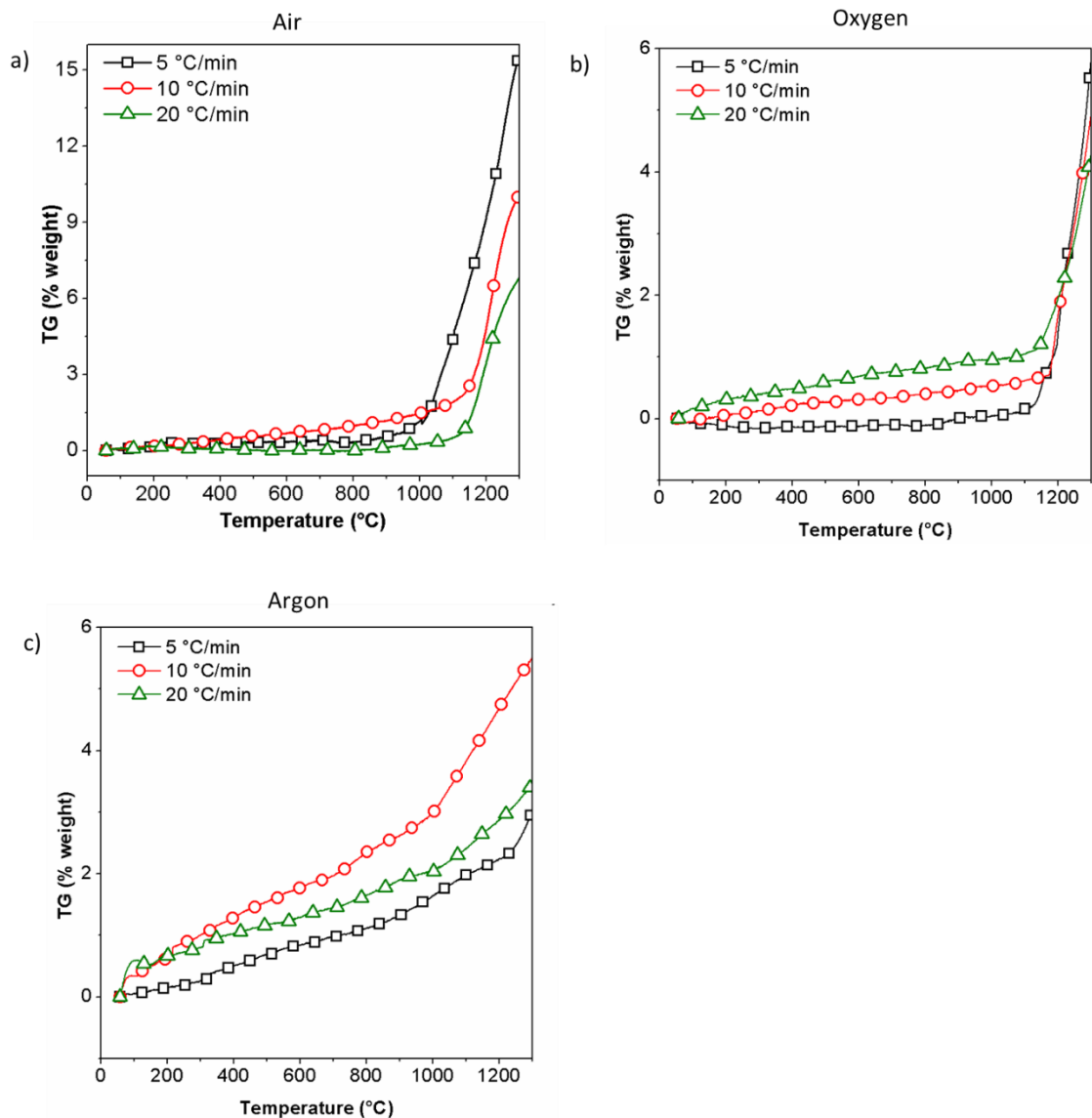


Figure 24 - Thermal analysis – TG (left) and DTA (right) of SS substrates conducted under three different atmospheres: a) air, b) oxygen and c) argon at three different heating rates: 5°C/min (black squares), 10°C/min (red circles) and 20°C/min (green up triangles). The weight gain under air is ~ 14.6%, under oxygen is ~ 5.44% and under argon is ~ 5.24%.

Schulz *et al.* [102,103] studied the formation of an oxide layer in X20CrMoV12-1, under different conditions. Firstly, at 600°C for 1000 h in H₂O-CO₂-O₂ and in air atmospheres, samples oxidation is lower for air atmosphere [102]. Secondly, the samples were subjected to a heat treatment from room temperature up to 650°C for 500 h. In this case, the authors suggest that an oxide layer was formed, which may be due to the

interaction between water vapour and oxygen present in the atmosphere by volatilisation of chromium oxide and iron oxide [102,103], as explained in Eq. 7.



Our results indicate that in air the oxidation of SS substrates is negligible up to 500°C. Thus, for the steel used in this work, it is suggested that 500°C for 2 h in air it is enough to promote the formation of –OH groups without significant oxidation that could cause degradation.

We have further analysed the results of the thermal treatment of SS substrates and looked at the surface constituents by XPS and the differences between SS and SS 500C components. An overview of XPS of SS and SS 500C is given in Figure 25. Further details on C 1s, O 1s, N 1s, Si 2p and Fe 3s compounds are shown in Figure 29, being explained afterwards together with silanization.

Metal components for the p spectra have two characteristic peaks regarding the two sub-levels: $1/2$ and $3/2$. For d spectra, for example, they are $3/2$ and $5/2$ and $5/2$ and $7/2$ for f spectra [104]. Thus, Fe 2p, Mn 2p and Cr 2p have two peaks one after another, being the $3/2$ more intense than the $1/2$.

SS overview (black line in Figure 25) shows peaks of the elements present in 316L alloy, as Fe, Mn, Mo, Cr, as well as some impurities as Ca [68,105].

The difference between the two substrates (SS and SS 500C) may be related with the formation of oxides, as:

- Iron oxides: FeO (709.6 eV, Fe $2p^{3/2}$ and 92.7 eV, Fe 3s) and Fe₂O₃ (55.5 eV, Fe $3p^{3/2}$). FeO appears only after the thermal treatment, whereas Fe₂O₃ is already present on SS and increases the peak intensity for SS 500C;
- Cr₂O₃ (577.3 eV, Cr $2p^{3/2}$) is also presented in both samples, before and after thermal treatment;
- MoO₃ (233.4 eV, Mo $3d^{3/2}$), which is formed after the thermal treatment.

Besides, the intensity peak for oxygen (528.6 eV, O 1s) increases appreciably after the thermal treatment [105,106].

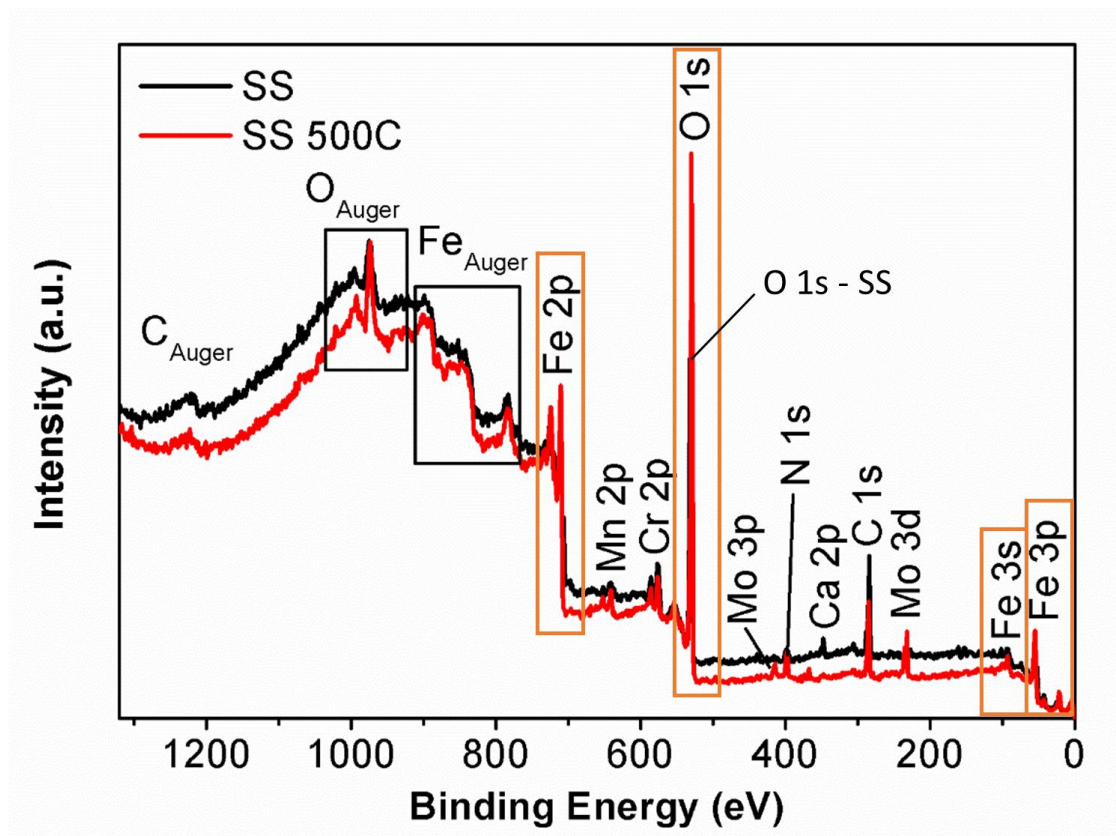


Figure 25 - XPS overview of SS (black line) and SS 500C (red line) with peaks identification. The major difference is the increase in iron and chromium elements related with the formation of oxides (inside the orange rectangles). Auger electrons are also detected by XPS, although not relevant for this discussion.

We went a bit further on the substrates characterization of the SS and conducted some FTIR spectroscopy analysis. FTIR allows to study the vibrational modes of the molecules present in a material and the results for SS and SS 500C FTIR spectra are shown in Figure 26. The base line fluctuation between $2400\text{-}2000\text{ cm}^{-1}$ is related with atmospheric CO_2 [107] and is presented in both substrates types. However, there is a peak at the vibrational mode of 659 cm^{-1} that appears only after the thermal treatment and is related with the formation of chromium oxide, Cr_2O_3 [107,108], which is consistent with previous XPS, XRD and EDS results.

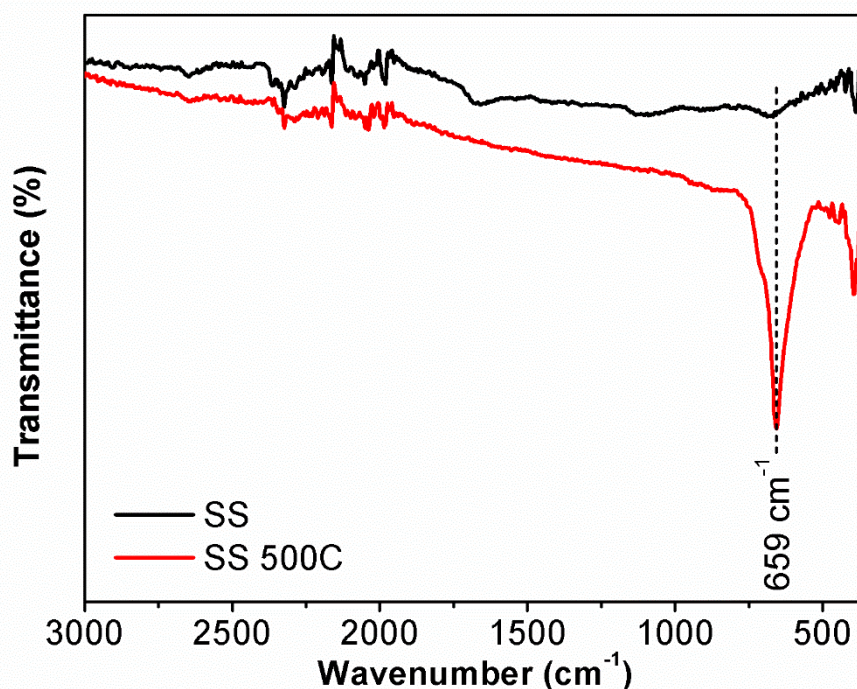


Figure 26 - FTIR spectra of SS (black line) and SS 500C (red line). The peak at 659 cm^{-1} for SS 500C is attributed to the presence of chromium oxide, Cr_2O_3 .

Herein, the results after the silanization process, the influence of the thermal treatment on the silanes adhesion as the quantification of silanes on the SS surface are presented.

Contact angle is a measurement that gives information on the surface wettability. A good wettability is considered for contact angles smaller than 90° and a poor wettability for contact angles greater than 90° , as previously mentioned (chapter 3.3.2).

The contact angles for SS and SS 500C as well as for the different times of silanization (30 sil, 60 sil and 90 sil) are presented in Figure 27. Table XI presents the average of contact angle measurements and respective associated errors. The differences between SS and SS 500C ($(73.1 \pm 5.8)^\circ$ and $(65.5 \pm 5.0)^\circ$, respectively) are not significant, if the error bars are considered, being only approximately 3° . These results are in accordance with the ones described before, in which the big difference between SS and SS 500C is at a chemical level and not at a physical level (roughness/surface).

Comparing SS and the different silanization times, there are no differences, which may be attributed to the absence of silanes on the surface of the SS substrates, due to

the lack of –OH groups. This will be further supported by the FTIR results. On the other hand, for SS 500C subjected to different times of silanization, there is an increase on the contact angle from 30 sil to 60 sil and then a decrease for 90 sil, even though these results are almost the same, considering the error bars. The presence of silanes on the surface creates more bonding sites what affects the substrate wettability making them more prone to be wet, i.e., more prone to attach to other molecules/materials.

The decrease of the contact angle for 90 sil can be associated to an overlapping of silanes molecules chains leading to a non-homogeneous layer. However, to better understand these results, in a future work, a study could be done through scanning tunnelling spectroscopy, for example. The wettability study for samples with 120 and 180 min of silanization time was also performed and the results were the same as for 90 sil sample (not presented here), suggesting the possibility of a non-homogeneous layer.

A review by Eustathopoulos *et al.* [109] stated that one of the factors influencing wettability is the amount of –OH groups on the material's surface. The presence of these groups provides larger contact angles, as 160-180° for silica, while the removal of the –OH groups causes a decrease in the contact angle values [109]. These results of this thesis work are not in agreement with the previous author, however the differences may be related to the material and the heat treatment used. In addition, if the error bars are considered, the contact angle values differences are not significant.

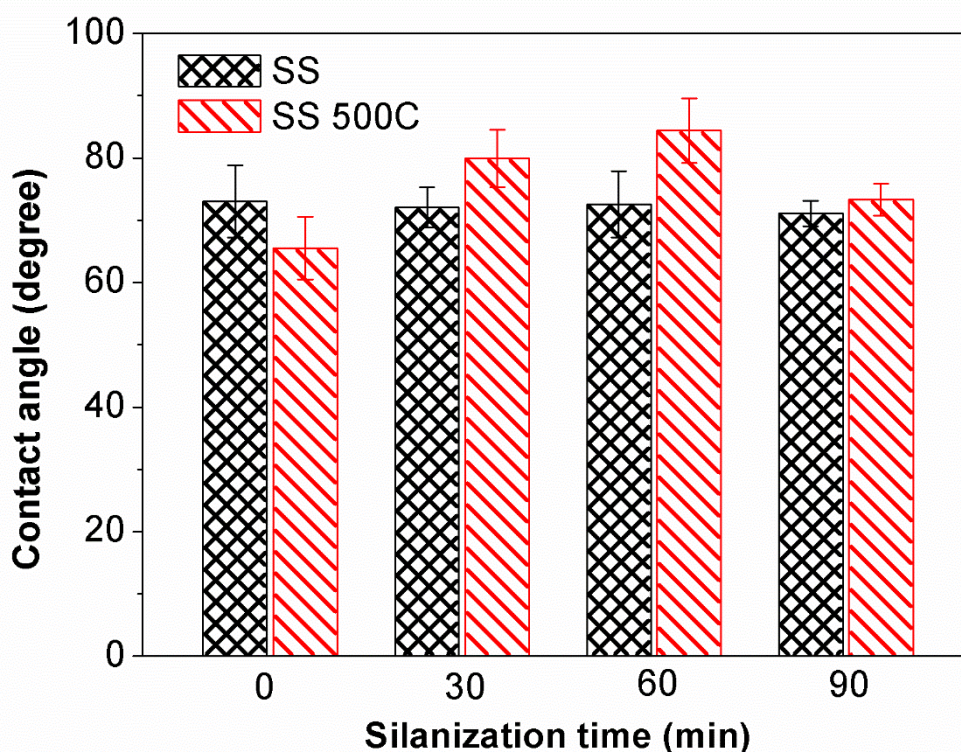


Figure 27 - Contact angle on SS and SS 500C for different silanization times. For different silanization time, there are no changes for the SS substrates, while for SS 500C substrates as the silanization time increases until 60 sil, so does the contact angle, decreasing to a longer silanization time (90 sil). If the error bars are considered, the contact angle values are almost the same.

Table XI - Contact angles of SS and SS 500C for different silanization times with the respective calculated errors.

Silanization time (min)	Contact angle (degree)	
	SS	SS 500C
0	73.1 ± 5.8	65.5 ± 5.0
30	72.1 ± 3.2	80.0 ± 4.6
60	72.6 ± 5.3	84.4 ± 5.2
90	71.1 ± 2.1	73.3 ± 2.6

FTIR spectroscopy was used in this part of the work to determine whether there are silane in the surface or not and the respective results are presented in Figure 28.

As previously seen (Figure 26), there is formation of chromium oxide, Cr_2O_3 , suggested by the vibrational mode of 659 cm^{-1} [107,108], after the heat treatment, and the base line fluctuation between $2400\text{-}2000\text{ cm}^{-1}$ is related with atmospheric CO_2 [107]. For SS (black line in Figure 28 a)) these Cr_2O_3 vibrations do not exist and no other vibrations are present for the different silanization times. On the other hand, when Cr_2O_3 vibrational mode is present (SS 500C, red line in Figure 28 b)), new peaks are formed for the wavelengths resumed in Table XII [61,110,111]. These vibration modes are related with silane vibration modes. As the silanization immersion time increases from 30 sil to 60 sil samples, the peak intensity of the respective silanes vibrational modes also increase. Comparing the 60 sil and 90 sil samples, the differences are not significant, being in accordance with the contact angle measurements, where it is believed that there is an agglomeration of the silane chains. The results corroborate, once again, that the heat treatment of SS promotes the formation of oxides compounds and -OH groups at the surface which influence the adhesion of silane [68].

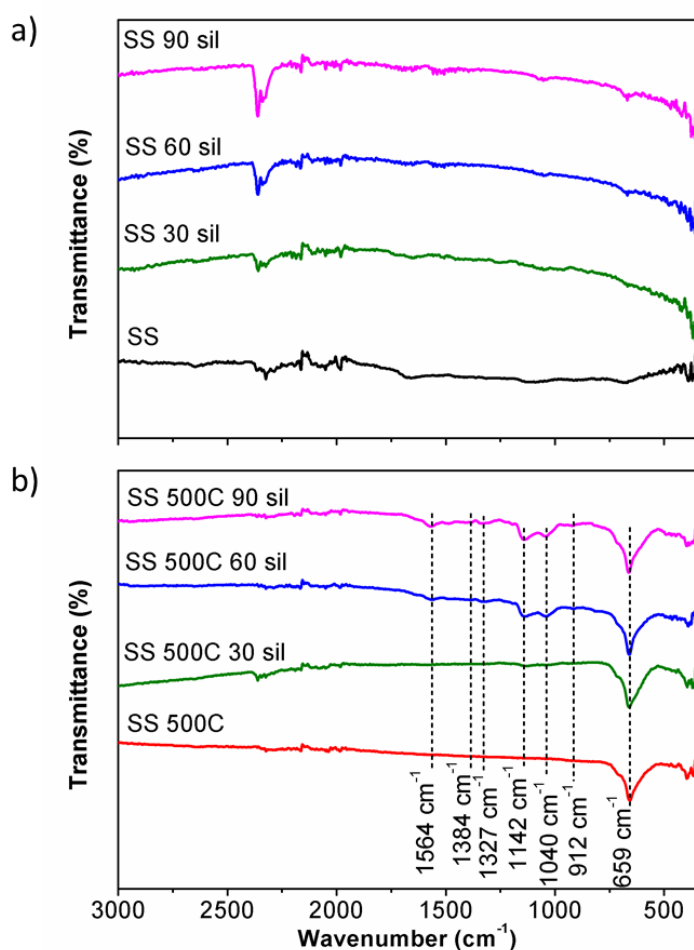


Figure 28 - FTIR spectroscopy results of a) SS (black line) and b) SS 500C (red line) for different silanization times: 30 sil (green line), 60 sil (blue line) and 90 sil (pink line). The presence of vibration modes corresponding to silanes only occur for the SS 500C.

Table XII - FTIR peak assignment for SS 500C after immersion in a silanized solution with APTES (1 vol.%) [61,110,111].

Wavenumber (cm ⁻¹)	Peak assignment
659	Cr ₂ O ₃
912	δ_s (O–H)/ ω (N–H)
1040	ν_{as} (Si–O–Si)
1080	ν_s (Si–O–C)
1140	ν_{as} (Si–O–Si)
1567	δ_s (N–H ₂)
2400-1900	Atmospheric CO ₂

ν_s – symmetric stretching vibration; ν_{as} – asymmetric stretching vibration; δ – bending; δ_s – symmetric bending; ω – wagging.

XPS representative O 1s, C 1s and Si 2p + Fe 3s peaks for SS before and after the heat treatment, as well as for the different silanization times are depicted in Figure 29 a), b) and c), respectively. First, the O 1s spectrum shows two peaks for SS (529.2 and 531.4 eV) and after the heat treatment only one peak is noted at the lower BE. Hryniewicz *et al.* [112], in their work studied the composition of the surface layer formed on 316L SS when subjected to different treatments. For that, the authors performed XPS studies, for which the results for the O 1s peak were relative to iron and chromium oxides and hydroxides for binding energies of 528.7, 531.3, 532.7, 529.4, 530.3 and 532.4 eV. However, the authors also studied the peak of Fe 2p and Cr 2p to determine which oxides and hydroxides were present [112]. The Fe 2p and Cr 2p compounds were not studied in this thesis, since one of the objectives was to quantify the silanes and not the oxides and hydroxides at the steel surface. In addition, the BE of 529.2 eV corresponds to a metal oxide M–O and the peak/shoulder at 531.4 eV corresponds to a surface hydroxyl oxygen in O–OH [113]. This suggests that the metal oxides increase after the heat treatment, while hydroxyl groups decrease. C 1s peak is also showed and it is also important to consider the presence of surface carbonates, around 288.3 eV [113]. This peak decreases for SS 500C and for the silanized substrates, indicative that carbonates are no longer on the substrate surface.

Regarding the different silanization times, in the O 1s peak, there is a formation of the component at 532.2 eV that increases as silanization time increases, and there is a decrease of the component at 529.2 eV. The first one may be related with the presence of C=O bonds, C–O bonds or even with Si–O bonds [113,114], and the decrease of the second component (M–O bonds) may be related with the coverage of the metal surface [115]. In the C 1s peak an increase of the component at 284.8 was observed as well as a shift of the BE to 285.2 eV as the silanization time increase. In the Si 2p and Fe 3s peak, a decrease on the component regarding the Fe 3s at 92.8 eV, due to the coverage of the metal surface. Along with this decrease, the component regarding Si 2p increases at 102.4 eV with the increase of silanization time.

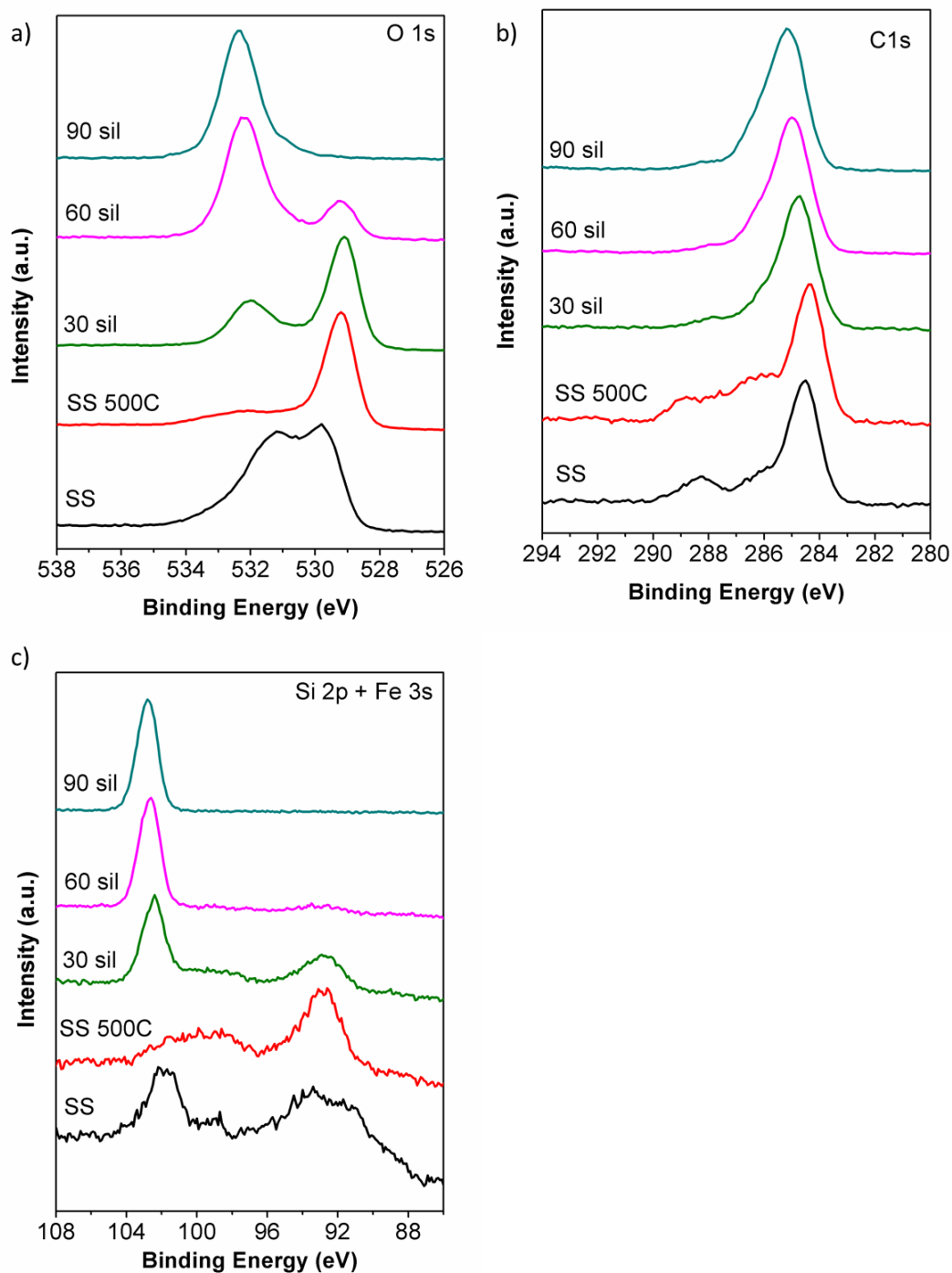


Figure 29 – XPS of a) O 1s, b) C 1s and c) Si 2p + Fe 3s peaks of SS (black), SS 500C (red) and for different silanization times: 30 sil (green), 60 sil (pink) and 90 sil (blue).

A decomposition of the XPS O 1s, N 1s, C 1s and Si 2p + Fe 3s peaks was made to acquire chemical information on the samples for the different silanization times. These data are shown in Figure 30 and Figure 31.

The O 1s peak (Figure 30) was decomposed in three components for 30 sil and 60 sil and in two components for 90 sil. The O 1s (1) component at 531.8 eV is related to single bonds between oxygen and carbon (C–O–H and C–O–C). The O 1s (2) component at 530.1 eV may be due to the double bond of carbon and oxygen (C=O), due to some contribution of metal hydroxides (M–O–H) and due to silicon and oxygen bond (Si–O). The O 1s (3) component is at 529.9 eV and is related to inorganic oxygen in metal oxides (M–O) [68][105][115]. For 90 minutes of silanization (90 sil), the O 1s (3) component (M–O) disappear which can be related with a full coverage of the metal surface.

The N 1s peak (Figure 30) has three components N 1s (1), N 1s (2) and N 1s (3) at 396.2, 397.6 and 399.9 eV, respectively, related to Mo 3p $3/2$ [115]. The component N 1s (4) at 399.8 eV is attributed to amine or amide (N–C) [105,115]. The last component N 1s (5) at 401.1 eV indicates the presence of protonated amines (N–H₃⁺) [114,115] and only appears for the silanized samples.

The C 1s peak (Figure 31) was fitted with three components. The C 1s (1) component at 287.7 eV is related to carbon making one double bond or two single bonds with oxygen (C=O, O–C–O). The C 1s (2) component at 285.7 eV is due to the bond between carbon and oxygen and/or nitrogen (C–O, C–N) in amine or amide. Lastly, the C 1s (3) component at 284.5 eV is due to the bond between carbon and carbon and/or hydrogen (C–H, C–C) [68,115].

The Si 2p peak (Figure 31) was fitted with three components. The Si 2p (1) component at 102.3 eV and the Si 2p (2) component at 98.9 eV, which are associated with non-oxidized silicon in the SS and with silicon of the silane, respectively. The peak at 92.6 eV is related with the Fe 3s peak [115]. As it is shown in Figure 31, the peak Si 2p (1) related with silicon from the silane increases as the silanization time increases and for 90 sil only this component is presented. Moreover, for the SS and SS 500C this component is absence (results not shown here). The components related with the SS substrate disappear with the increase of silanization time, as had already been reported for the components identified for N 1s peak.

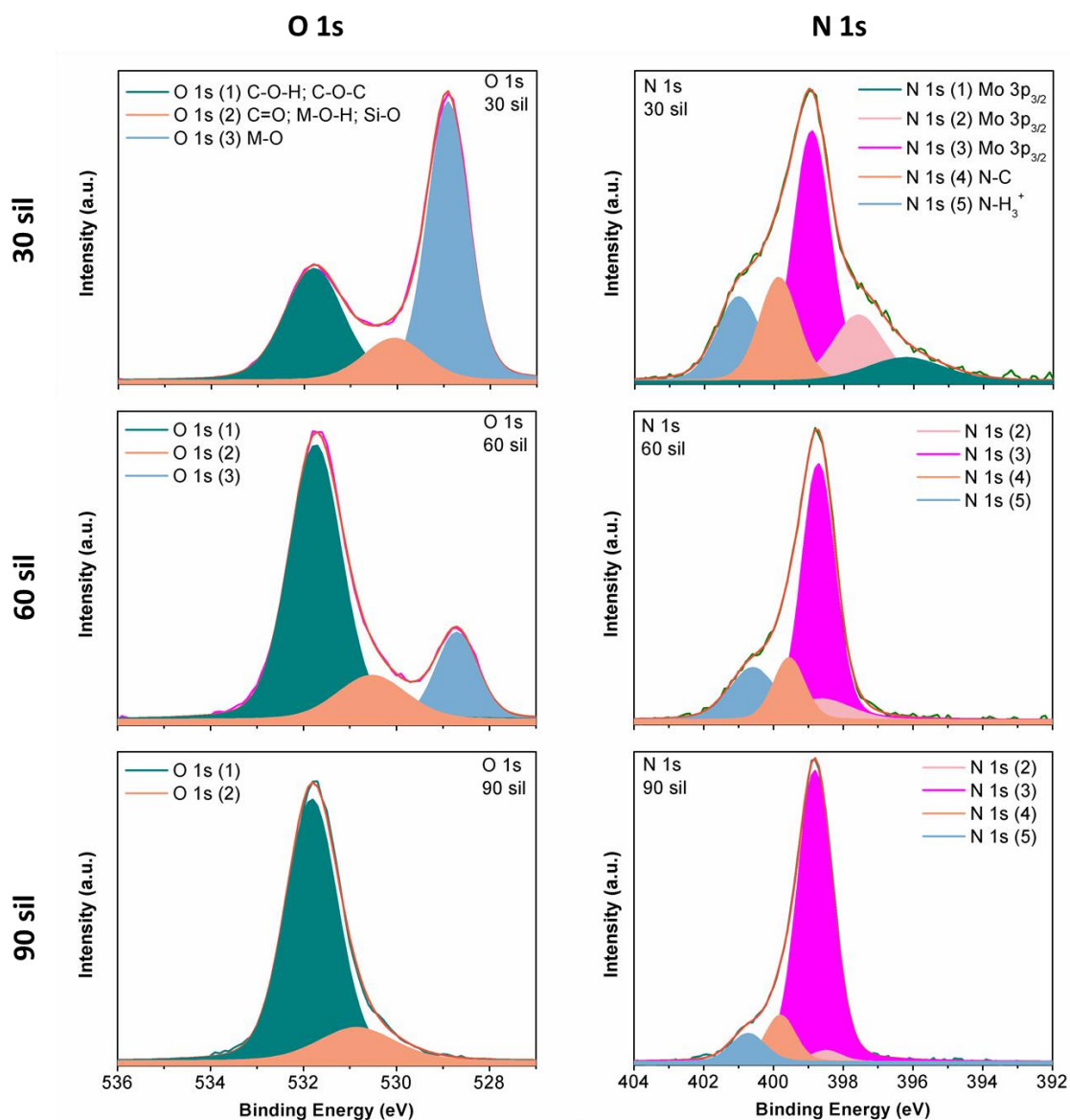


Figure 30 – XPS decomposition of O 1s and N 1s peaks recorded for different silanization times (30 sil, 60 sil and 90 sil). The N 1s peak is overlapped with a Mo 3p 2/3 contribution. The components are identified in the 30 sil plots.

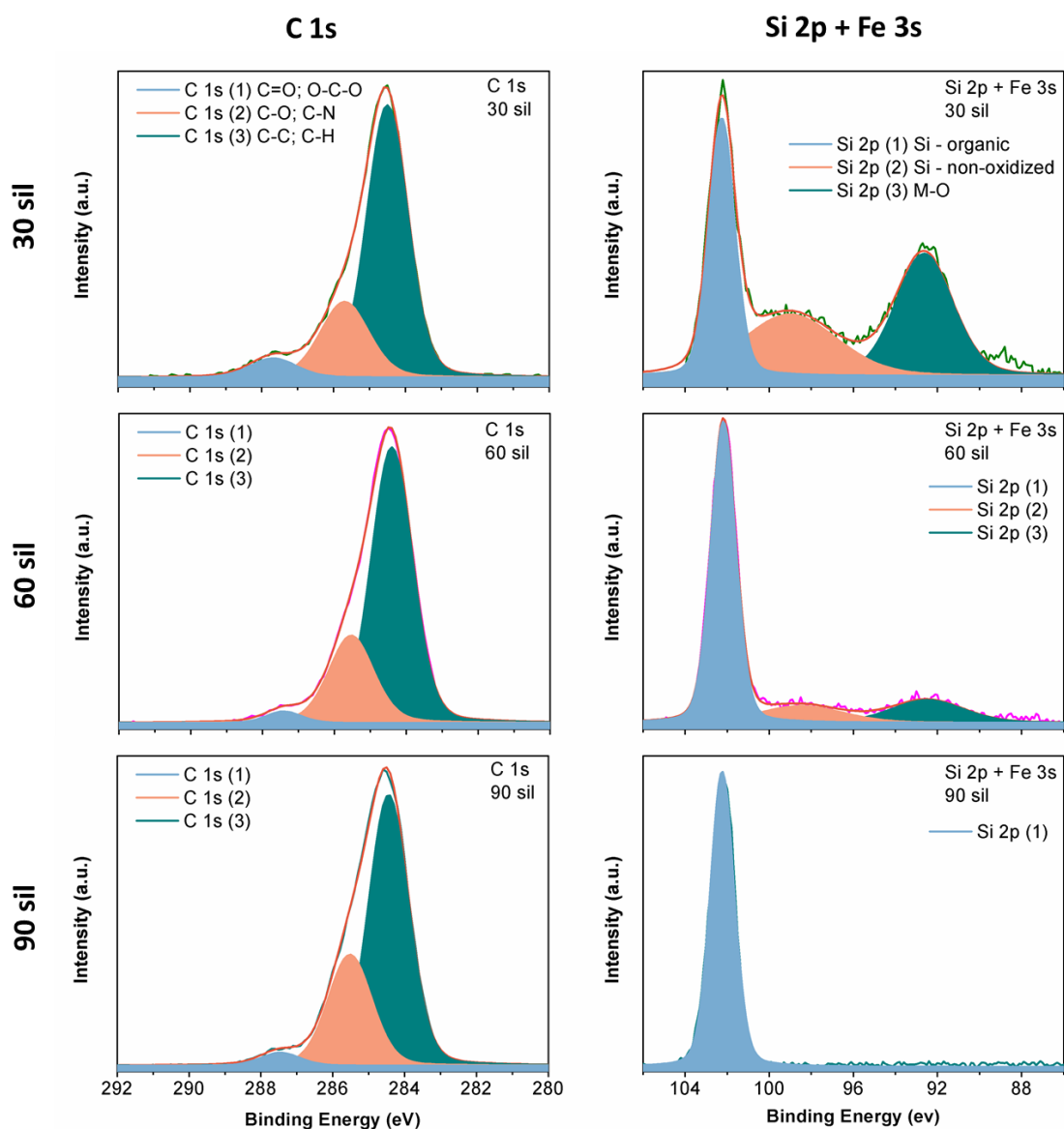


Figure 31 – XPS decomposition of C 1s, Si 2p and Fe 3s peaks recorded for different silanization times (30 sil, 60 sil and 90 sil). The components are identified in the 30 sil plots.

To determine the chemical composition and quantify the silane in the metal surface, the area under each component was measured. The surface concentrations (atomic %) of the chemical species related with the components of O 1s, N 1s, C 1s and Si 2p are presented in Table XIII. The results are consistent with the XPS spectrums, since the components present in silane, as Si organic and C–N, increase, whilst the components regarding to SS, as M–O, M–O–H and Si non-oxidized, decrease as the immersion time increase. Nevertheless, the concentration of C 1s components remains high which can suggest the presence of residual organics [115]. The C/Si (of silane) ratio decreased with

silanization time, due to the increase of Si concentration. Furthermore, the ratio of Si (of silanes) and the metal components (M–O and M–O–H) was calculated and also increased, suggesting not only that silanes increase, but also that the surface is being covered. These results are presented both in Table XIII and

Table XIII - Surface concentrations (atomic %) of the chemical species related with the components of O 1s, N 1s, C 1s and Si 2p, along with C/Si (from silane) ratio, for the different silanization times (30 sil, 60 sil and 90 sil), determined by XPS.

		Relative concentration (atomic %)		
		30 sil	60 sil	90 sil
O 1s	C–O–H; C–O–C	12.3	14.5	16.1
	C=O; M–O–H; Si–O	11.5	3.0	3.1
	M–O	20.5	3.6	0
N 1s	N–C	2.6	4.8	7.4
	N–H ₃ ⁺	1.0	1.4	0.7
C 1s	C=O; O–C–O	2.1	1.5	1.8
	C–H; C–C	25.9	40.1	37.9
	C–O; C–N	8.7	14.5	17.0
Si 2p	Si non-oxidized	5.5	2.3	0
	Si of silane	7.1	12.3	14.8
C/Si (of silane) ratio		5.20	4.54	3.83
Si (of silane)/M ratio		0.22	1.86	4.77

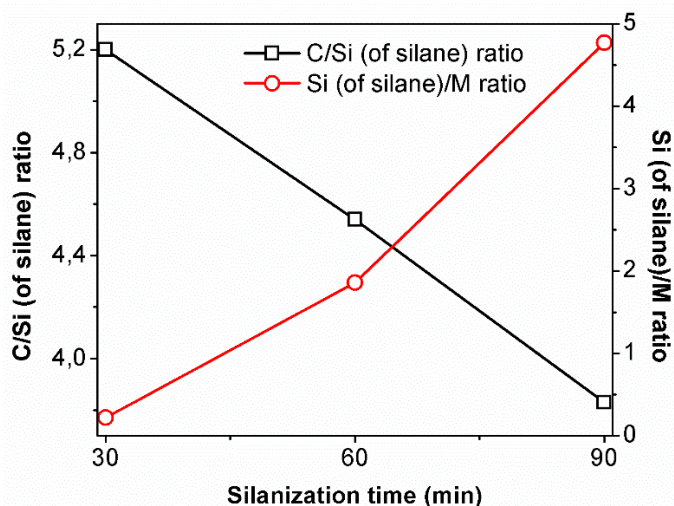


Figure 32 - C/Si (of silane) ratio (black squares) and Si (of silanes)/M ratio (red circles) for different silanization time. C/Si (of silane) ratio decreases due to the increase of Si concentration, while Si (of silanes)/M increased, suggesting not only that silanes increase, but also that the surface is being covered.

To sum up this part of the work about the silanization time and the importance of SS heat treatment, it is possible to say that the energy supplied to SS (500°C for 2 h) was not enough to change the substrate surface, being just enough to promote interface diffusion phenomena, promoting the formation of chromium and iron oxides and hydroxides. This may promote the formation of hydroxyl groups at the surface that are of high importance to promote silane coupling agents' adhesion. In addition, XPS results also confirmed that the increase of silanization time produces a consistent increase of the amount of silanes present in the samples and for higher silanization time the surface starts to get covered.

4.2. Poly(L-lactic acid) films and platforms characterization

In this section we will present and describe the full characterization of PLLA films and their adhesion to SS. Different thick PLLA films were produced, either changing the solution concentration (2.5 and 5.0 wt.%) or the number of deposited layers (1L, 2L and 3L). In addition, PLLA 2.5 and PLLA 5.0 films were submitted to two thermal process, one to obtain crystallized films (180°C for 3 min followed by 120°C for 45 min) and the other

one to obtain semi-crystallized ones (120°C for 60 min). The crystallo-chemical properties (XRD, DSC, TG and FTIR), the morphology (SEM, OM and profilometer), and the adhesion behaviour (tape test) of the different films was characterised. One of the most relevant studies refers to tape tests, since there is a need to understand the influence of silanization and the thickness of the films on adhesion. Lastly, the results for a preliminary degradation study of the films in PBS for 2 and 7 days will be presented.

The thermal analysis, both by DSC and TG, of PLLA 5.0 thick film without any thermal treatment is presented in Figure 33. The TG shows that the polymer loses 9% of the original weight from 66°C up to 185°C. Looking at DSC a peak related with the melting temperature (T_m) around 180°C is clearly visible. Similar DSC curves were obtained by Barroca *et al.* [45] in their study about composites of PLLA and bioglass, being T_m 184°C and the glass transition temperature (T_g) in the range of 60°C to 65°C [45].

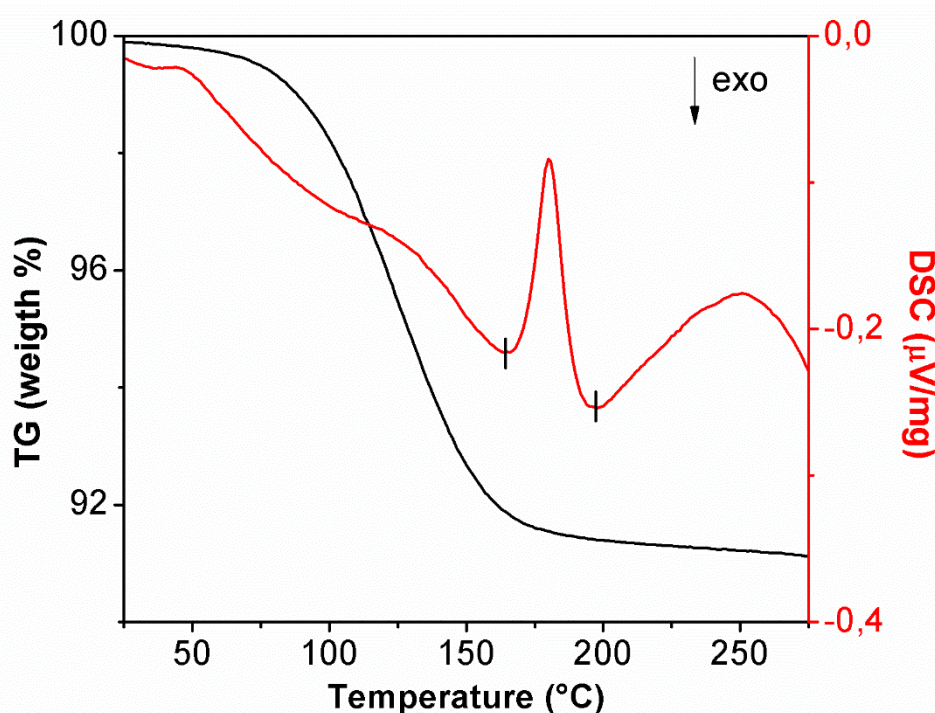


Figure 33 - Thermal analysis (TG in black and DSC in red) of PLLA 5.0 thick film conducted under air atmosphere from room temperature up to 250°C. T_m is around 180°C.

To further study the variation in crystallinity, XRD results of PLLA 2.5 and PLLA 5.0 films under the two different thermal treatments are shown in Figure 34. The plans corresponding to each of the four peaks presented in the XRD are depicted in Table XIV.

For the PLLA 5.0, all the four peaks are visible, which does not happen for the PLLA 2.5, in which only the peaks corresponding to the planes (110)/(200) and (203)/(113) appear. Righetti *et al.* [116], also studied the influence of temperature on the crystallization of PLLA, under different crystallization temperatures (T_c), 85, 95, 135 and 145°C. In their work they detected two different crystalline forms of PLLA, α and α' , and the α' -form only grew for $T_c = 85$ and 95°C, whereas crystallization at $T_c = 135$ and 145°C induced only α -form. Moreover, α -form is recognized by the (110)/(200), (203)/(113), (011) and (211) peaks at scattering angles 2 theta of 16.7, 19.0, 14.6 and 22.3 degree, respectively and α' -form is recognized by the (110)/(200) and (203)/(113) peaks at scattering angles 2 theta of 16.4 and 18.7 degree, respectively. That is, there is a shift of the angular values for (110)/(200) and (203)/(113) peaks. Based on Righetti *et al.* [116], it is likely that only the α -form is present in the PLLA films used in this work [45,116]. Another important aspect that should be considered is that the higher the crystallization temperature, the better the macromolecules mobility, which facilitates the organization of the polymers chains into ordered crystal structures [116], promoting the formation of spherulites (one of the forms of ordering the crystalline chains).

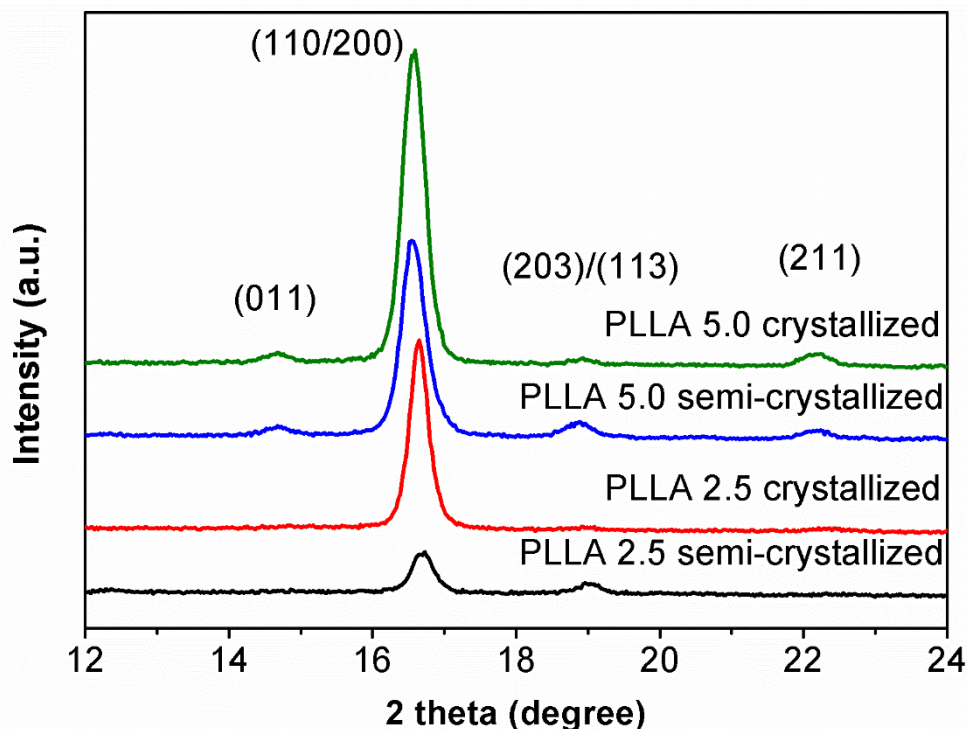


Figure 34 - XRD pattern of PLLA 2.5 and 5.0 films for two different crystallization processes: the semi-crystallized films were treated for 60 min at 120°C and the crystallized ones were treated for 3 min at 180°C and followed by 45 min at 120°C.

Table XIV - Crystallographic planes for PLLA and respective diffraction angle.

Diffraction angle, 2 theta (degree)	Crystallographic planes
14.7	(011)
16.6	(211)
18.9	(110)/ (200)
22.1	(203)/ (113)

The morphology of PLLA 2.5 and PLLA 5.0 films, for different number of deposited layers and for semi-crystalline and crystalline films are presented in Figure 35.

The semi-crystalline films morphology is homogeneous and smooth without any pores and there is no formation of spherulites because no sufficient energy (temperature and time) (temperature below T_m) was given for the formation of crystallite nuclei. In contrast, for the crystalline films, well developed and heterogeneous size spherulites are observed and the spherulite size increases along with the increase of the number of layers. For crystallized PLLA 2.5 1L films, these structures do not appear, and only small peaks are observed, probably related with nuclei or due to some detachment of the film from the substrate.

Spherulite size was obtained using ImageJ software, where about 30 spherulites were considered for each sample (crystallized PLLA 2.5 2L and PLLA 2.5 3L) through SEM micrographs, to further calculate the average area and the associated error. Comparing crystallized PLLA 2.5 2L and PLLA 2.5 3L samples, the spherulite average area size increases from approximately $864.4 \pm 91.6 \mu\text{m}^2$ to $1681.3 \pm 533.5 \mu\text{m}^2$. The observed results may be related to the mobility of the polymer chains, which is higher for a greater number of layers, since the polymers molecules move via diffusion [80]. However, there are other factors that affect the crystallization growth in films with lower thickness, as the surface energy at the interface and transporting process. When the film is too thin, the polymer cannot rotate freely in a one-dimensional confinement space, as the SS substrate surface [117], and this can justify the result for crystallized PLLA 2.5 1L.

A note on the statist validity of these results should be considered, since only 30 spherulites were measured and the ideal should be about 600. Given the small number of spherulites, the associated error is relatively high, and it is therefore necessary to validate these results in future work.

As mention in the state of the art, PLLA biodegradability and degradation is dependent on its crystallinity [80] and this may determine its final application. In order to form spherulites, three steps are important: induction period, primary crystallization and secondary crystallization. The first one is the time required to obtain stable nuclei; in the second one, spherulites are developed and eventually collide with each other; in the last step spherulites grows due to the continuation of spherulites colliding [80]. Furthermore, spherulites can have influence on how the cells interact with the polymer surface [118] and on how polymer electric polarization is affected [18]. The adhesion of fibroblasts cells in PLLA with different crystallinity gradients showed that the cells had a tendency to agglomerate near the spherulites with greater adhesion strength, whereas for the less crystalline regions the cells were more and with a more homogeneous distribution [118]. Polarization is another important factor that affects cells and proteins adhesion, and for polarized zones the protein adsorption is higher [17]. One way to control the decay of polarization is through the polymer crystallization degree. Barroca *et al.* [18], obtained a stable polarization of up to 10 days, period enough to occur cell proliferation and protein adsorption, to two crystalline forms of PLLA (α and α') when the poling occurred above glass transition, whereas for a poling at room temperature the polarization was lost only in minutes or hours [18]. Hence, it is important to obtain polymers with a high degree of crystallinity, not only to improve cell adhesion, but also to increase the time it can become polarized. In a future work, it would be interesting to study cell and protein adhesion, as well as polarization for crystallized PLLA 2.5 2L and PLLA 2.5 3L films, since these were the only ones for which spherulites were obtained.

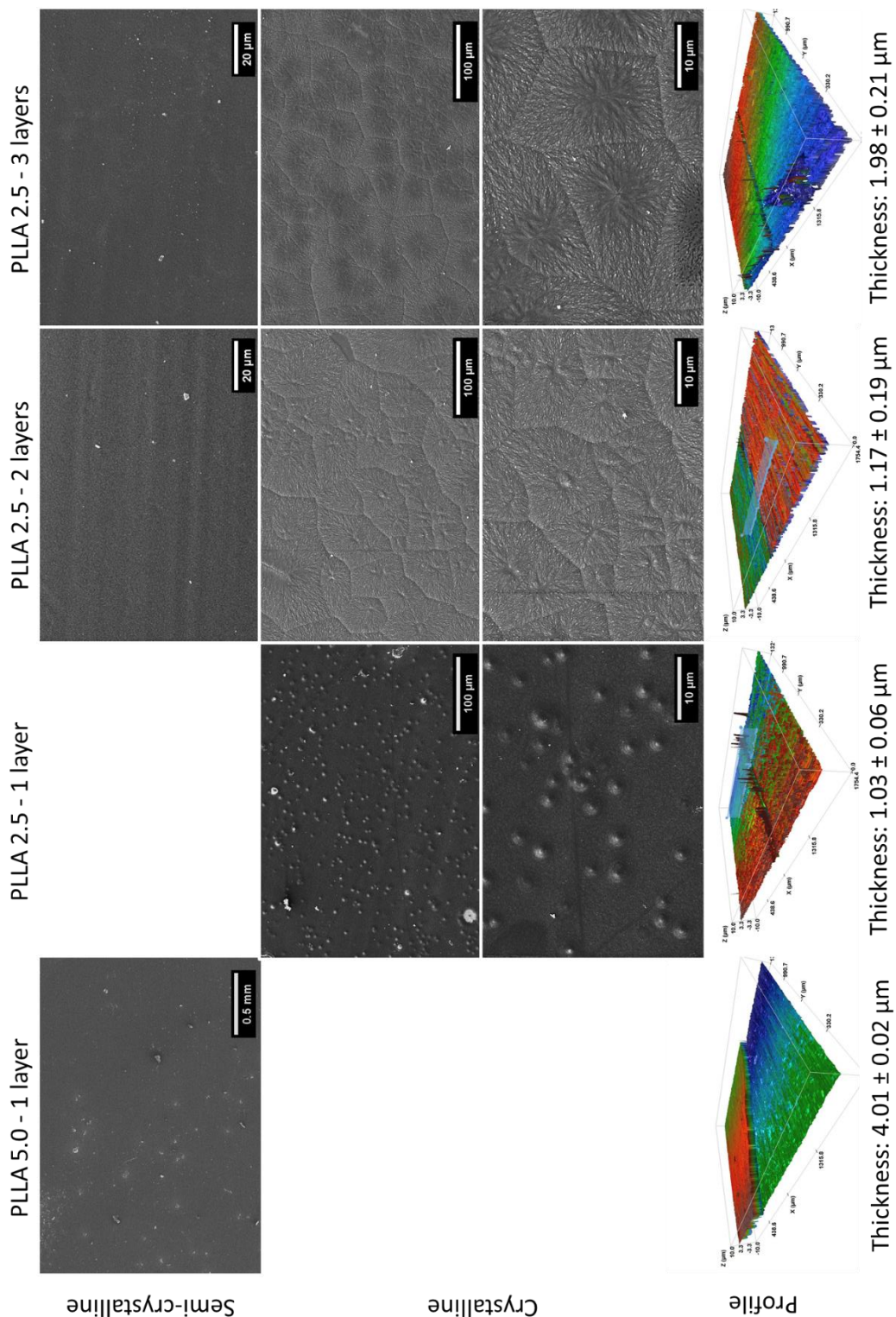


Figure 35 - SEM micrographs of PLLA 2.5 and PLLA 5.0 and with different number of deposited layers (1L, 2L and 3L), for semi-crystalline and crystalline films. For the semi-crystalline films there is no formation of spherulites, while for the crystalline ones the spherulites are not only formed, but also their size increase with the increase of the number of layers.

To fully study the polymer adhesion to metal in dry medium, a tape test following the ASTM D3359 standard [67] was performed and the results are presented in Table XV and in Figure 36. The tape test was performed for different substrates (SS and SS500C), different PLLA solution concentrations (2.5 and 5.0 wt.%), different number of deposited layers (1L, 2L and 3L), different types of crystallization films (semi-crystalline and crystalline) and for different silanization times (30 sil, 60 sil and 90 sil). The 0B result indicates that the film was completely removed, while the 5B is the best result for this test.

Table XV - Results of the tape test for different substrates, silanization times, crystallization and number of layers deposited of PLLA films with different concentrations.

Substrate	PLLA solution concentration (wt.%)	Number of layers	Crystallization	Silanization time	Tape test result
SS	5.0	1	Semi-crystalline	30 sil	0B
				60 sil	0B
				90 sil	0B
SS 500C	5.0	1	Semi-crystalline	30 sil	0B
				60 sil	0B
				90 sil	0B
SS 500C	2.5	1	Semi-crystalline	60 sil	5B
		2			3B
		3			0B
		3	Crystalline		5B

The results for the tape test in the case of PLLA 5.0 films were classified as 0B, meaning that films were completely removed from the metal surface. This can be related with the high thickness of the film (approx. 4 μm), that has behaved as a free-standing film (Figure 36).

All the follow tests were performed in SS 500C 60 sil substrates. For semi-crystalline PLLA 2.5 films, the results for the tape test were worse as the number of deposited layers (and thus its thickness) increased. Our results show that PLLA film thickness influences the adhesion to the substrate, and as thicker the film is, the worse the adhesion. For 1L the result is 5B, while for 2L and 3L, the results are 3B and 0B, respectively. However, a very interesting result was obtained for the crystalline PLLA 2.5 3L films, where the adhesion was improved, comparing with semi-crystalline PLLA 2.5 3L, from 0B to 5B. This

result indicates that besides the film thickness influence, crystallinity have also influence on the adhesion of the polymer to a silanized metal.

Nevertheless, it is necessary to systematically study the adhesion of PLLA 2.5 and PLLA 5.0 with higher crystallinity, since in this study only semi-crystalline PLLA 5.0 was studied and for PLLA 2.5 the influence of crystallinity was only studied for 3 deposited layers. To crystallize the PLLA film, a temperature of 180°C was used, although only for 3 min. However, this may have enhanced the interaction between the polymer and the intermediate silane layer and, consequently, improved adhesion.

Our observations are in agreement with results previously reported in the literature. Honkanen *et al.* [68] studied SS and thermoplastic urethane adhesion using silane coupling agents as an intermediate layer and a peel test to study the mechanical strength between the two materials. SS was also treated at 350°C for 100 min to improve the silane layer homogeneity and their results proved that this layer improved the plastic adhesion, as observed in the present work, although with a different polymer.

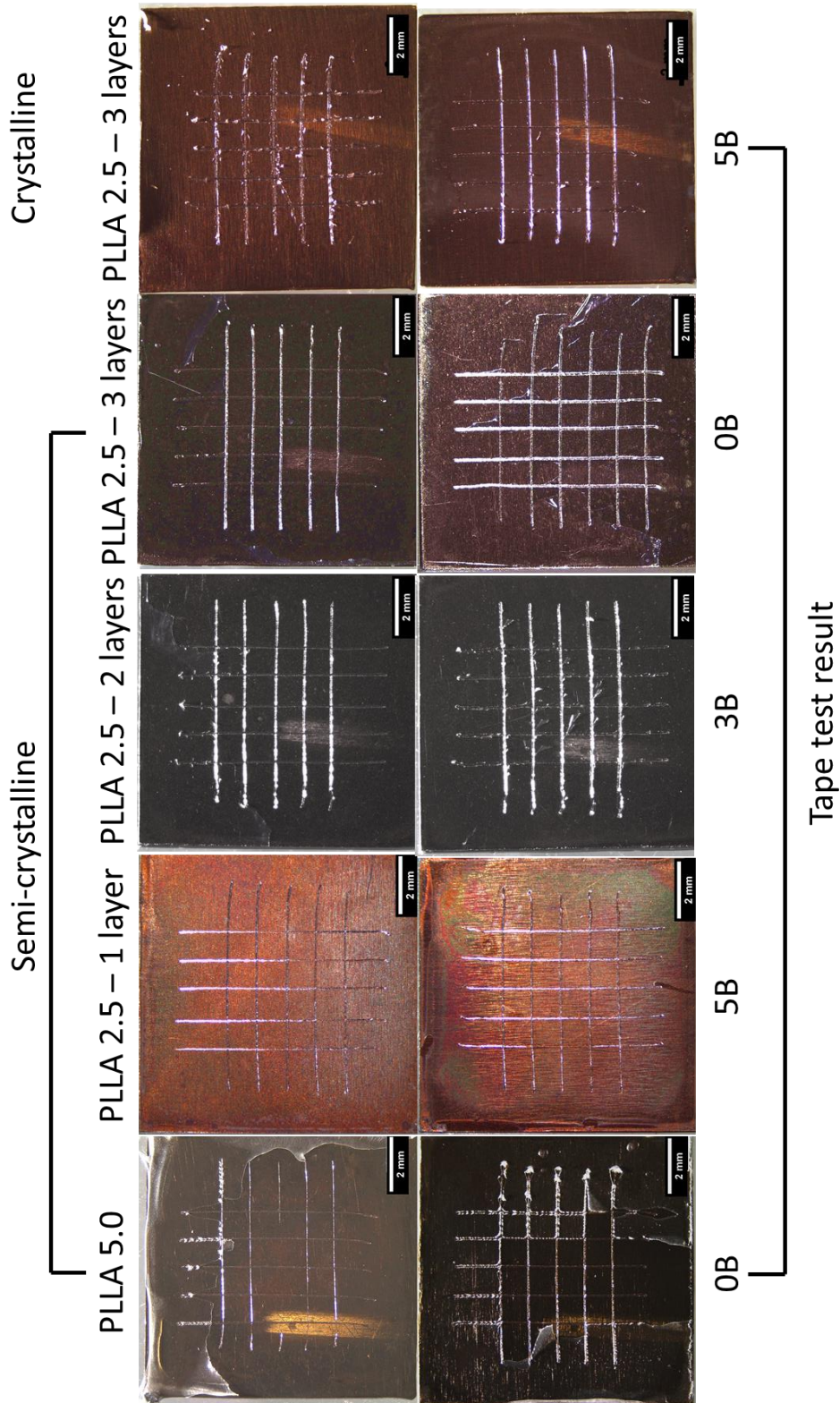


Figure 36 - Tape test results for PLLA 2.5 and 5.0 SS 500C 60 sil films with 1, 2 or 3 deposited layers and for semi-crystalline and crystalline films. The solution concentration, number of deposited layers and type of crystallinity influence the adhesion, as seen by the tape test results.

FTIR analysis, before and after tape test, for PLLA 2.5 1L films are presented in Figure 37 and for PLLA 2.5 1L and PLLA 5.0 films after tape test presented in Figure 38. These analyses were performed to support the results of the tape tests (Figure 36), i.e. to prove the presence of PLLA films on the substrate surface, after the tape tests, via the presence of modes related with PLLA bonding if the film stayed adhered, and vice versa. The peak assignments for the PLLA films are presented in Table XVI [119,120], along with the respective vibration modes. The peaks presented are typical of PLLA and the one at 923 cm^{-1} shows that the α crystalline form is present [119], being in agreement with XRD results.

For PLLA 2.5 1L SS 500C 60 sil before the tape test (Figure 37), the PLLA peaks are more intense, and although their intensity decreases after the tape test, the film stayed adhered. In contrast, for PLLA 5.0 after the tape test, the PLLA-related peaks disappear, indicating that the film detached from the substrate, and only the peaks referring to the silane and chromium oxide vibration bonds are present (Figure 28 and Table XII). These results are in agreement with the microscope observation of the surface of the films. In addition, these last results allow to understand that the tape just pulled-off the film and not the intermediate layer of silanes.

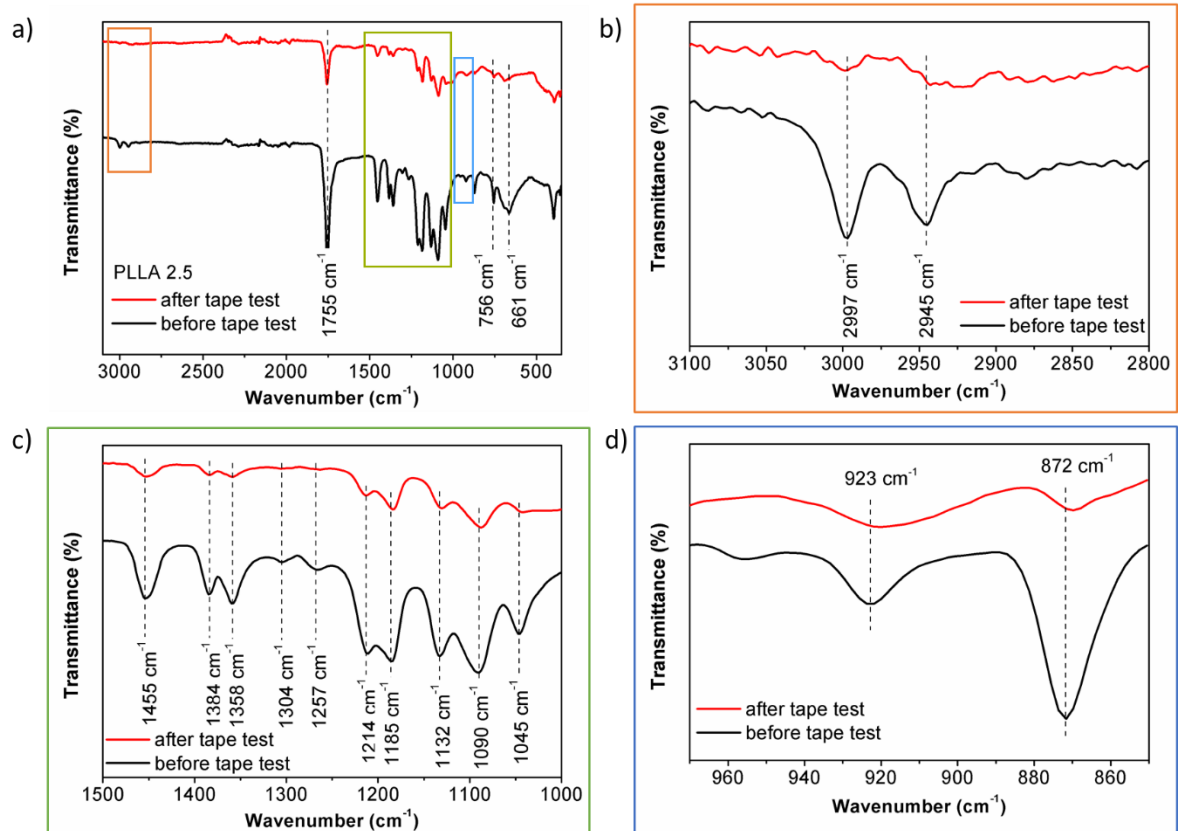


Figure 37 - a) FTIR spectra for PLLA 2.5 SS 500C 60 sil before (black line) and after (red line) the tape test, and b), c) and d) the respective zoom of the related bands (orange – 2800-3100 cm⁻¹; green – 1500-1000 cm⁻¹ and blue – 970-870 cm⁻¹). The peaks are identified in the graphics and are related to PLLA vibration bonds modes.

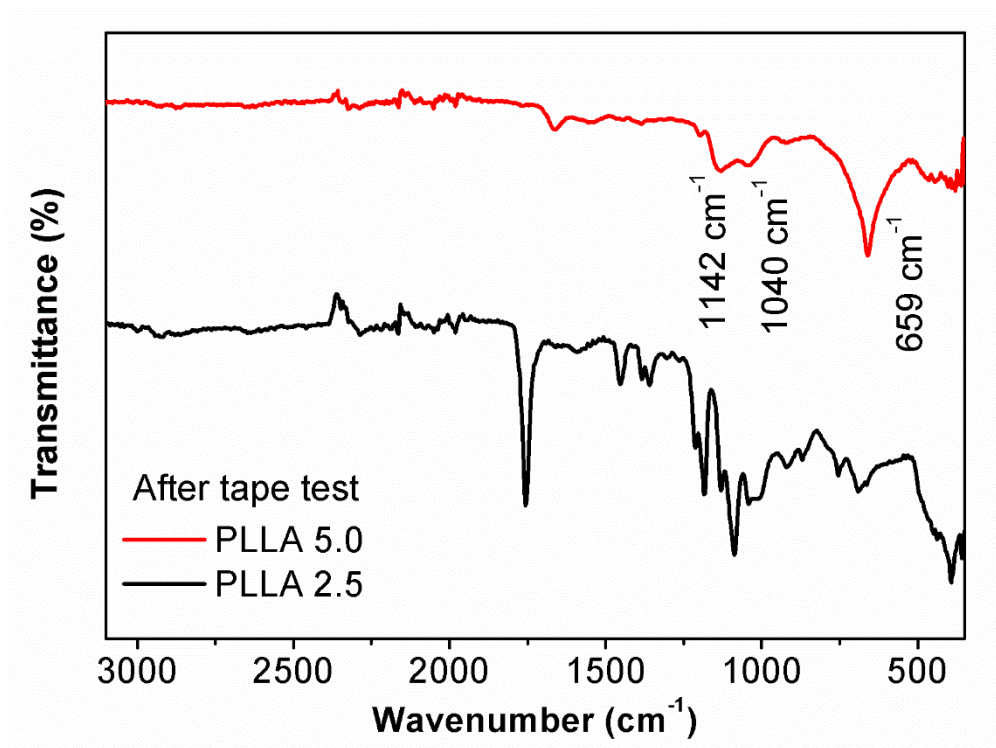


Figure 38 - FTIR spectra for PLLA 5.0 SS500C 60 sil (red line) and PLLA 2.5 SS 500C 60sil (black line) after the tape test. The peaks are identified in the graphic. PLLA peaks are visible after the tape test for PLLA 2.5, while for PLLA 5.0 only peaks regarding silane layer and substrate are present.

Table XVI - FTIR peak assignment of the vibration modes of PLLA films on SS 500C substrates prepared in this work [119,120].

Wave number (cm ⁻¹)	Peak assignment
756	ν_s (Si-C)
872	ν_s (C-C) + ρ (CH ₃)
923	ν_s (C-COO)
1132	ρ_s (CH ₃)
1214	ν_{as} (CCO-O) + ρ_{as} (CH ₃)
1257	δ (CH) + ν_s (C-O-C)
1358	δ_s (CH ₃) + δ (CH)
1384	δ_s (CH ₃)
1455	δ_{as} (CH ₃)
1755	ν_s (C=O)
2945	ν_s (CH ₃)
2997	ν_{as} (CH ₃)

ν_s – symmetric stretching vibration; ν_{as} – asymmetric stretching vibration; ρ – rocking; δ_s – symmetric bending; δ_{as} – asymmetric bending; ω – wagging.

From the results just presented, the crystalline PLLA 2.5 3L was one of the best results for the tape test and the semi-crystalline sample allows to compare the influence of the crystallization degree on the degradation and adhesion of the films when submitted to immersion in a solution. Thus, these two films were chosen.

To study the degradation and the adhesion of the semi-crystalline PLLA 2.5 3L and crystalline PLLA 2.5 3L films in SS 500C 60 sil in a solution, the PBS test was used for two immersion times (2 and 7 days) at 50°C, adapting the standard BS EN ISO 10993-13:1999 “Biological evaluation of medical devices — Part 13: Identification and quantification of degradation products from polymeric medical devices” [75].

The results of this study for both semi-crystalline and crystalline PLLA 2.5 3L SS 500C 60sil are presented in Figure 39 for two different immersion times in PBS (2 and 7 days). The red circles in the figure show removed parts, while the green circles show parts of the film attached.

As expected and due to the tape test result (0B), the semi-crystalline films were almost entirely detached from the substrate, staying only attached in the edges of the substrate. PBS solution probably infiltrated between the substrate and the semi-crystalline PLLA 2.5 3L film, since it was not completely adhered. In contrast, for the crystalline PLLA

2.5 3L films in SS 500C 60 sil, only some small parts of the films were removed for 2 immersion days (red parts in Figure 39), whereas for 7 immersion days, the film continued adhered in some parts of the substrate (green parts). The results for 60 immersion days are still running, and these results are essential to understand the adhesion behaviour of these films in the metal when immersed in a PBS solution.

FTIR analysis was also performed to understand if the film was only removed from the substrate or if it was also degraded. The respective spectra are presented in Figure 40, being compared to PLLA 2.5 1L films SS 500C 60 sil before immersion in PBS solution. FTIR results agree with the vibration modes of PLLA bonds (Table XVI). It is possible to state that the film is only detached from the substrate, as explained before, and there are no changes in the polymer chemical bonds. The present peaks in FTIR are related to PLLA vibration modes and there are no significant differences between the samples, which indicates that PLLA 2.5 film did not degrade with the immersion in PBS solution.

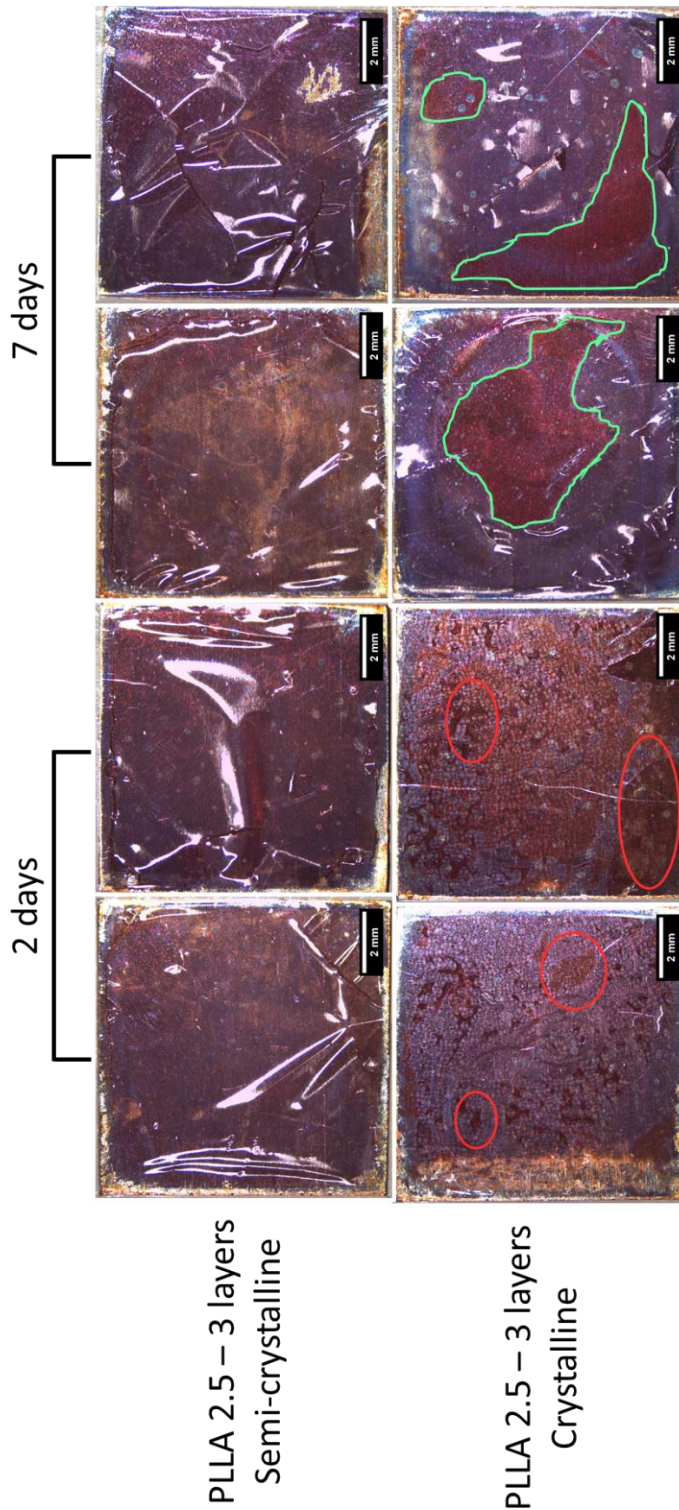


Figure 39 - PLLA 2.5 3L semi-crystalline and crystalline films in SS 500C 60 sil substrates, for two immersion times (2 and 7 days) in PBS. Semi-crystalline films were almost whole detached, whereas for crystalline films the major part of the film remains on the substrate (green parts), although some small parts of the film are removed (red parts) after 2 days or detached after 7 days.

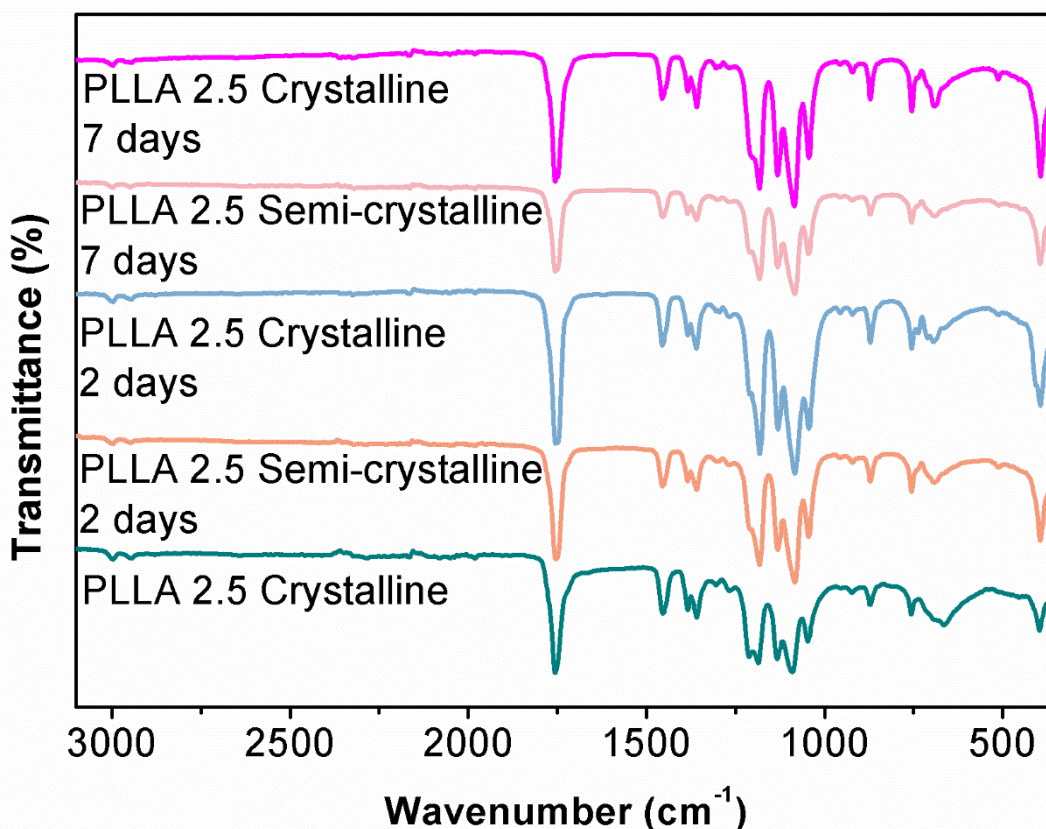


Figure 40 - FTIR results for PLLA 2.5 3L crystalline films in SS 500C 60 sil substrates before immersion PBS solution and for PLLA 2.5 3L semi-crystalline and crystalline films in SS 500C 60 sil substrates after immersion in PBS solution for 2 and 7 days. The present peaks are related to PLLA vibration modes and there are no significant differences between the samples, which indicates that PLLA 2.0 film did not degrade with the immersion in PBS solution.

4.3. Results in summary

To sum up, in this work a chemical approach, named silanization, was used to functionalize SS. This had as main aim to promote the adhesion of PLLA films with different thicknesses to SS. To functionalized SS, a pre heat treatment of the substrates was necessary. In the current work SS substrates were heat treated at 500°C for 2 h. The results showed that this step influenced more the surface chemistry and less the surface morphology: an increase of the –OH groups was observed by different studies and the film profile did not change significantly. Secondly, the amount of silanes increased as the

time of silanization increased, with 90 min of silanization time being considered a high period and the 60 min of silanization would be the best to proceed the studies. Regarding the adhesion of PLLA films to SS and SS 500C substrates, as thicker the film is, the easier is to be pulled-off when submitted to the tape test, since it behaves as a free-standing film. Moreover, silanes positively influence the adhesion of PLLA films to SS 500C substrates. Concerning to the PLLA crystallinity, adhesion is better for films with higher crystallinity. PBS solution tests demonstrate that PLLA 2.5 3L crystalline films in SS 500C 60 sil substrates with 1.98 μm is the ideal film, since there is no chemical and mechanical degradation of the films.

The results obtained in this work are the first prove of the mechanical and chemical feasibility of using SS coated with PLLA platforms as possible tissue regeneration platforms. These results open the possibilities for further exploitation of these platforms, namely to study the role of the electrical polarization of these PLLA films on hard tissue regeneration.

CHAPTER V

CONCLUSIONS AND FUTURE WORK

CHAPTER V – CONCLUSIONS AND FUTURE WORK

5.1. Conclusions

The aim of this study was to optimise the adhesion between an inorganic and an organic material, namely 316 SS and PLLA, for medical applications.

SS and PLLA were chosen for this work due to their properties, whereas SS has good mechanical properties and is currently used as medical implants, PLLA is biocompatible and has piezoelectric properties as the collagen in bone, which will benefit bone regeneration due to stresses and electric charges in vivo, as mentioned in the Chapter II – State of the Art.

To promote the adhesion between these two materials, a chemical route was used, in the sequence and complementary to the previous work by Marinho *et al.* [10] that studied a physical approach to enhance the adhesion of PLLA to 316L SS [10]. As a chemical route to functionalize the SS substrates, silanization was chosen. Silanes are used in medical application to promote protein and cell adhesion, however, in this work they were applied as an intermediate layer. To study and optimise the adhesion between SS and PLLA, different film thicknesses with varying solution concentration (2.5 and 5.0 wt.%), number of layers deposited (1, 2 and 3) and degree of crystallization were used.

Prior to the functionalization of SS substrates through silanization, a heat treatment of SS is necessary. A detailed study on the substrates changes during the thermal treatment was conducted through thermal, structural and morphological analysis. The substrates were then functionalized and the amount of silanes on the substrate surface quantified using XPS technique. After the functionalization of SS, PLLA films were deposited using a spin-coater. The PLLA solutions had two concentrations to obtain films with different thickness and the number of deposited layers were also different. In addition, PLLA films after deposition were submitted to two different thermal treatments (120°C for 60 min and 180°C for 3 min followed by 45 min at 120°C) to obtain films with different crystallinity degrees. Morphological, structural and chemical analyses were performed to fully characterize the different PLLA films. Finally, the adhesion between the functionalized SS substrate and the PLLA films was measured by tape tests, following the ASTM D3359 [67]. Since these platforms (SS+PLLA) are intended for medical applications, a study of degradation in PBS was also carried out for 2 and 7 days adapting the standard BS EN ISO 10993-13:1999 “Biological evaluation of medical devices — Part 13: Identification and

quantification of degradation products from polymeric medical devices” [75]. Morphological and chemical analysis of the samples after soaking in PBS were made.

In terms of SS functionalization, the main conclusions were regarding the changes on the chemistry of the steel, due to silanization and in the silane quantification. SEM micrographs revealed that after the heat treatment at 500°C for 2 h there were changes in the SS surface, as the grain boundaries contrast, however the bulk was not affected. XRD results indicated that the structure of SS was not significantly affected, and no new crystalline phases were detected for this heat treatment. Concomitantly by thermogravimetry no changes in the weight percentage for this temperature were observed. Chemically, there was a formation of chromium and iron oxides, as well as the formation of –OH groups, confirmed by FTIR and XPS. Thus, the main conclusion in this part is that the heat treatment (500°C for 2 h) is not enough to cause degradation of the steel surface but is sufficient to promote the formation of –OH groups, that are of high importance to promote silanes adhesion.

Regarding silanization, this is enhanced if –OH groups are present, as evidenced by FTIR results. In the case of SS without any heat treatment, the substrates did not show any silanes vibration bonds, while for SS 500C these were clearly present. XPS results also confirmed that the increase of silanization time produces a consistent increase of the amount of silanes present in the substrates.

As for the PLLA films, the thickness assessed by profilometer was influenced not only by the solution concentration, but also by the number of deposited layers. PLLA 5.0 films have a 4.0 μm thickness, while for PLLA 2.5 the thickness varied from 1.0 μm to 2.0 μm approximately, depending on the number of deposited layers (1 to 3).

Hereafter, the results are regarding toss 500C 60 sil substrates. For both PLLA 2.5 and PLLA 5.0 semi-crystalline films, their morphology was homogeneous and smooth without any pores, whereas for crystalline PLLA 2.5 samples the formation of spherulites was clear, since a temperature above T_m was used, promoting the formation of crystallite nuclei. Moreover, the spherulite size increased along with the increase of the number of layers, from $(864.4 \pm 91.6) \mu\text{m}^2$ in crystalline PLLA 2.5 2L to $(1681.3 \pm 533.5) \mu\text{m}^2$ in crystalline PLLA 2.5 3L. These results allowed to conclude that the mobility of polymer chains is higher for lower solution concentrations and for higher number of layers. However, the number of layers cannot be very high that the whole layer becomes so thick that it detaches from the substrate. The tape tests results gave better results for semi-crystalline PLLA 2.5 1L (5B) and semi-crystalline PLLA 2.5 2L (3B). The film crystallinity

also influences the adhesion, since for crystalline PLLA 2.5 3L films the result of tape test was 5B.

The tape test was confirmed by FTIR spectroscopy by showing that the typical peaks corresponding to the PLLA vibration bonds are still present after the tape tests and also indicate the presence of the α crystalline form of PLLA [119]. Moreover, FTIR results proved that the tape used in tape test only detached the PLLA film and not the silanes, confirming its good adhesion with the SS substrate.

PLLA 2.5 3L did not suffer any degradation in PBS, since the typical peaks of PLLA vibration bonds (FTIR spectroscopy) remained without any changes, independently of the immersion time. The semi-crystalline films were almost entirely detached from the substrate with rare attached parts in the edges of the substrate. This result was in agreement with those from the tape test. On the other hand, the crystalline PLLA 2.5 3L films were almost entirely attached, with only some small parts of the film removed. The crystallinity of PLLA films promotes the adhesion to the functionalised SS substrates and this was not affected when the platforms were immersed in PBS.

This study demonstrated the feasibility of manufacturing inorganic-organic platforms with promising adhesion between the metal substrate and the polymeric coating, using a chemical treatment, named silanization, to produce an intermediate layer. The observed stability of the PLLA coatings when immersed in PBS opens the way for the continuation of this work and the exploitation of the electrical polarization of PLLA films for enhanced tissue regeneration platforms and for the extension of this approach to the study of other platforms with potential for biomedical applications.

This study demonstrated the feasibility of manufacturing inorganic-organic platforms with promising adhesion between the metal substrate and the polymeric coating, using a chemical treatment, named silanization, to produce an intermediate layer. The observed stability of the PLLA coatings when immersed in PBS opens the way for the continuation of this work and for the extension of this approach to the study of other platforms with potential for biomedical applications.

5.2. Future work

PBS studies for 60 days of immersion time are currently running. Further studies on the crystallinity of PLLA films should be carried out, since in this work only crystalline PLLA 2.5 3L films were submitted to tape tests. Also, less number of film layers should be

tested by this method. As the polarization and piezoelectricity influence protein and cell adhesion, it is proposed that further research should be undertaken in these areas. In addition, and regarding to the main scope of this work, which consists of using these platforms for medical applications, future studies should focus on the protein and cell adhesion and proliferation.

BIBLIOGRAPHY

BIBLIOGRAPHY

- [1] A. R. Amini, C. T. Laurencin, and S. P. Nukavarapu, "Bone Tissue Engineering: Recent Advances and Challenges," *Crit. Rev. Biomed. Eng.*, vol. 40, no. 5, pp. 363–408, 2012.
- [2] R. Agarwal and A. J. García, "Biomaterial strategies for engineering implants for enhanced osseointegration and bone repair," *Advanced Drug Delivery Reviews*, vol. 94, pp. 53–62, 2015.
- [3] F. J. O. Brien, "Biomaterials & scaffolds for tissue engineering," *Mater. Today*, vol. 14, no. 3, pp. 88–95, 2011.
- [4] M. M. Stevens, "Biomaterials for bone tissue engineering," *Mater. Today*, vol. 11, no. 5, pp. 18–25, 2008.
- [5] G. Turnbull, J. Clarke, F. Picard, P. Riches, L. Jia, F. Han, B. Li, and W. Shu, "3D bioactive composite scaffolds for bone tissue engineering," *Bioact. Mater.*, 2017.
- [6] G. Ghersi, F. Carfi Pavia, G. Conoscenti, G. A. Mannella, S. Greco, S. Rigogliuso, V. La Carrubba, and V. Brucato, "PLLA Scaffold via TIPS for Bone Tissue Engineering," *Chem. Eng. Trans.*, vol. 49, pp. 301–306, 2016.
- [7] C. Ribeiro, V. Sencadas, D. M. Correia, and S. Lanceros-Méndez, "Piezoelectric polymers as biomaterials for tissue engineering applications," *Colloids and Surfaces B: Biointerfaces*, vol. 136, pp. 46–55, 2015.
- [8] I. Gotman, "Characteristics of Metals Used in Implants," *J. Endourol.*, vol. 11, no. 6, pp. 383–389, 1997.
- [9] M. Saini, "Implant biomaterials: A comprehensive review," *World J. Clin. Cases*, vol. 3, no. 1, p. 52, 2015.
- [10] M. da S. Marinho, M. H. V. Fernandes, and P. M. Vilarinho, "Biocompatible polymeric coatings for bone tissue regeneration," University of Aveiro, 2012.
- [11] W. Wang, Y. Ouyang, and C. K. Poh, "Orthopaedic implant technology: Biomaterials from past to future," *Annals of the Academy of Medicine Singapore*, vol. 40, no. 5, pp. 237–243, 2011.
- [12] S. B. Goodman, Z. Yao, M. Keeney, and F. Yang, "The future of biologic coatings for orthopaedic implants," *Biomaterials*, vol. 34, no. 13, pp. 3174–3183, 2013.
- [13] E. Fukada, "History and recent progress in piezoelectric polymers," *IEEE Trans. Ultrason. Ferroelectr. Freq. Control*, vol. 47, no. 6, pp. 1277–1290, 2000.
- [14] E. Fukada, "Piezoelectricity of biopolymers," *Biorheology*, vol. 32, no. 6, pp. 593–609, 1995.
- [15] N. S. Manam, W. S. W. Harun, D. N. A. Shri, S. A. C. Ghani, T. Kurniawan, M. H. Ismail, and M. H. I. Ibrahim, "Study of corrosion in biocompatible metals for implants: A review," *Journal of Alloys and Compounds*, vol. 701, pp. 698–715, 2017.
- [16] K. G. Marra, "Biodegradable Polymers and Microspheres in Tissue Engineering," in *Bone*

- Tissue Engineering*, J. O. Hollinger, T. A. Einhorn, B. A. Doll, and C. Sfeir, Eds. CRC Press LLC, 2005, pp. 150–162.
- [17] N. Barroca, P. M. Vilarinho, A. L. Daniel-Da-Silva, A. Wu, M. H. Fernandes, and A. Gruverman, "Protein adsorption on piezoelectric poly(L-lactic) acid thin films by scanning probe microscopy," *Appl. Phys. Lett.*, 2011.
- [18] N. Barroca, P. M. Vilarinho, M. H. V Fernandes, P. Sharma, and A. Gruverman, "Stability of electrically induced-polarization in poly (L-lactic) acid for bone regeneration," *Applied Physics Letters*, vol. 101, no. 2. pp. 1–4, 2012.
- [19] N. Barroca, A. Marote, S. I. Vieira, A. Almeida, M. H. V. Fernandes, P. M. Vilarinho, and O. A. B. da Cruz e Silva, "Electrically polarized PLLA nanofibers as neural tissue engineering scaffolds with improved neuritogenesis," *Colloids Surfaces B Biointerfaces*, vol. 167, pp. 93–103, 2018.
- [20] N. Barroca, M. H. V Fernandes, and P. M. Vilarinho, "Electromechanically active Poly (L-lactic) acid based structures for regenerative medicine," University of Aveiro, 2014.
- [21] E. N. Marieb, *Human Anatomy and Physiology*, 4th ed. Boston: Pearson, 1998.
- [22] B. Clarke, "Normal bone anatomy and physiology," *Clinical journal of the American Society of Nephrology : CJASN*, vol. 3. pp. 131–139, 2008.
- [23] E. Fukada and I. Yasuda, "On the Piezoelectric Effect of Bone," *Journal of the Physical Society of Japan*, vol. 12, no. 10. pp. 1158–1162, 1957.
- [24] D. J. Hadjidakis and I. I. Androulakis, "Bone remodeling," in *Annals of the New York Academy of Sciences*, 2006, vol. 1092, pp. 385–396.
- [25] <https://3c1703fe8d.site.internapcdn.net/newman/gfx/news/hires/2017/noncodingrna.jpg> [Accessed: 14-Dec-2017].
- [26] P. C. S. Melo, M. H. V Fernandes, and P. M. Vilarinho, "Electromechanical Poly(L-lactic acid) (PLLA) platforms for regenerative medicine," University of Aveiro, 2014.
- [27] O. M. Pearson and D. E. Lieberman, "The aging of Wolff's 'law': Ontogeny and responses to mechanical loading in cortical bone," *Yearbook of Physical Anthropology*, vol. 47. pp. 63–99, 2004.
- [28] https://cdn.shopify.com/s/files/1/1467/6660/products/RMQ-02_Femurs.jpg?v=1534883923. [Accessed: 20-Nov-2018].
- [29] https://static.cambridge.org/resource/id/urn:cambridge.org:id:binary-alt:20170810131619-26650-smallThumb-S0883769417000057_fig1t.jpg?pub-status=live. [Accessed: 20-Nov-2018].
- [30] <https://encrypted-tbn0.gstatic.com/images?q=tbn:ANd9GcSd-eCn04G9kfI9HH-uKc7xmtLKLaiD8TjP3Eyd2k9iaKFd0cM>. [Accessed: 20-Nov-2018].
- [31] P. M. Vilarinho, "Functional Materials: Properties, Processing and Applications," in *Scanning Probe Microscopy: Characterization, Nanofabrication and Device Application of Functional Materials*, P. M. Vilarinho, Y. Rosenwaks, and A. Kingon, Eds. Kluwer Academic Publishers, 2005, pp. 3–33.

- [32] M. Acosta, N. Novak, V. Rojas, S. Patel, R. Vaish, J. Koruza, G. A. Rossetti, and J. Rödel, "BaTiO₃-based piezoelectrics: Fundamentals, current status, and perspectives," *Appl. Phys. Rev.*, vol. 4, no. 041305, pp. 1–53, 2017.
- [33] "Direct and inverse piezoelectric effect." [Online]. Available: <https://wiki.metropolia.fi/download/attachments/103944429/piezoelectricity.gif?version=1&modificationDate=1396504790000&api=v2> (accessed on 2017-12-15). [Accessed: 15-Dec-2017].
- [34] <https://www.americanpiezo.com/knowledge-center/piezo-theory/piezoelectric-constants.html> [Accessed: 17-Dec-2018].
- [35] "bone piezoelectricity." [Online]. Available: <https://sciencing.com/piezoelectric-effect-bone-density-5969491.html>. [Accessed: 27-Dec-2017].
- [36] A. H. Rajabi, M. Jaffe, and T. L. Arinzeh, "Piezoelectric materials for tissue regeneration: A review," *Acta Biomaterialia*, vol. 24, pp. 12–23, 2015.
- [37] J. Jacob, N. More, K. Kalia, and G. Kapusetti, "Piezoelectric smart biomaterials for bone and cartilage tissue engineering," *Inflamm. Regen.*, vol. 38, no. 2, pp. 1–11, 2018.
- [38] J. J. Telega and R. Wojnar, "Piezoelectric effects in biological tissues," *Journal of Theoretical and Applied Mechanics*, vol. 40, no. 3, pp. 723–759, 2002.
- [39] "TE - definition." [Online]. Available: <https://www.nibib.nih.gov/science-education/glossary#g-42721>. [Accessed: 26-Nov-2018].
- [40] "te - definition 1." [Online]. Available: <https://www.nibib.nih.gov/science-education/science-topics/tissue-engineering-and-regenerative-medicine>. [Accessed: 26-Nov-2018].
- [41] "TE - definition 2." [Online]. Available: <https://www.britannica.com/science/tissue-engineering>. [Accessed: 26-Nov-2018].
- [42] E. M. Bueno and J. Glowacki, "Biologic Foundations for Skeletal Tissue Engineering," *Synth. Lect. Tissue Eng.*, vol. 3, no. 1, p. 95, 2011.
- [43] D. Zhang, X. Wu, J. Chen, and K. Lin, "The development of collagen based composite scaffolds for bone regeneration," *Bioact. Mater.*, vol. 3, no. 1, pp. 129–138, 2018.
- [44] S. Guo, X. Zhu, and X. J. Loh, "Controlling cell adhesion using layer-by-layer approaches for biomedical applications," *Mater. Sci. Eng. C*, vol. 70, pp. 1163–1175, 2016.
- [45] N. Barroca, A. L. Daniel-Da-Silva, P. M. Vilarinho, and M. H. V. Fernandes, "Tailoring the morphology of high molecular weight PLLA scaffolds through bioglass addition," *Acta Biomater.*, vol. 6, no. 9, pp. 3611–3620, 2010.
- [46] A. Marote, N. Barroca, R. Vitorino, R. M. Silva, M. H. V. Fernandes, P. M. Vilarinho, O. A. B. da Cruz e Silva, and S. I. Vieira, "A proteomic analysis of the interactions between poly(L-lactic acid) nanofiber s and SH-SY5Y neuronal-like cells," *AIMS Mol. Sci.*, vol. 3, no. 4, pp. 661–682, 2016.
- [47] C. Lee and S. Hong, "An Overview of the Synthesis and Synthetic Mechanism of Poly (Lactic acid)," *Mod. Chem. Appl.*, vol. 2, no. 4, pp. 1–5, 2014.
- [48] "PLA." [Online]. Available: <http://www.mdpi.com/materials/materials-09->

- 00435/article_deploy/html/images/materials-09-00435-g008.png. [Accessed: 14-Nov-2017].
- [49] "PLLA PDLA." [Online]. Available: [http://www.nptel.ac.in/courses/116102006/Flash/6.1/Figure 5.jpg](http://www.nptel.ac.in/courses/116102006/Flash/6.1/Figure%205.jpg). [Accessed: 14-Nov-2017].
- [50] L. S. Nair and C. T. Laurencin, "Biodegradable polymers as biomaterials," *Progress in Polymer Science (Oxford)*, vol. 32, no. 8–9, pp. 762–798, 2007.
- [51] P. A. Gunatillake, R. Adhikari, and N. Gadegaard, "Biodegradable synthetic polymers for tissue engineering," *European Cells and Materials*, vol. 5, pp. 1–16, 2003.
- [52] L. Xiao, B. Wang, G. Yang, and M. Gauthier, "Poly(Lactic Acid)-Based Biomaterials: Synthesis, Modification and Applications," in *Biomedical Science, Engineering and Technology*, D. N. Ghista, Ed. 2012, pp. 247–282.
- [53] Y. Ikada, Y. Shikinami, Y. Hara, M. Tagawa, and E. Fukada, "Enhancement of bone formation by drawn poly(L-lactide)," *J. Biomed. Mater. Res.*, vol. 30, no. 4, pp. 553–558, 1996.
- [54] E. Fukada, "History and recent progress in piezoelectric polymers," *IEEE Trans. Ultrason. Ferroelectr. Freq. Control*, vol. 47, no. 6, pp. 1277–1290, 2000.
- [55] A. K. Jaiswal, S. S. Kadam, V. P. Soni, and J. R. Bellare, "Improved functionalization of electrospun PLLA/gelatin scaffold by alternate soaking method for bone tissue engineering," *Appl. Surf. Sci.*, vol. 268, pp. 477–488, 2013.
- [56] D. Zhao, F. Witte, F. Lu, J. Wang, J. Li, and L. Qin, "Current status on clinical applications of magnesium-based orthopaedic implants: A review from clinical translational perspective," *Biomaterials*, vol. 112, pp. 287–302, 2017.
- [57] M. Prakasam, J. Locs, K. Salma-Ancane, D. Loca, A. Largeteau, and L. Berzina-Cimdina, "Biodegradable Materials and Metallic Implants—A Review," *J. Funct. Biomater.*, vol. 8, no. 44, pp. 1–15, 2017.
- [58] "chemical composition 316L." [Online]. Available: <https://www.bssa.org.uk/topics.php?article=183>. [Accessed: 29-Dec-2017].
- [59] M. Alonso Frank, C. Meltzer, B. Braunschweig, W. Peukert, A. R. Boccaccini, and S. Virtanen, "Functionalization of steel surfaces with organic acids: Influence on wetting and corrosion behavior," *Appl. Surf. Sci.*, vol. 404, pp. 326–333, 2017.
- [60] "stress shielding." [Online]. Available: <https://medical-dictionary.thefreedictionary.com/stress+shielding>. [Accessed: 29-Dec-2017].
- [61] G. Da Ponte, A. K. Ghosh, A. Kakaroglou, D. Van Hemelrijck, B. Van Mele, and B. Verheyde, "Adhesion Improvement between Epoxy and Stainless Steel Using a Silane Coupling Agent in an Atmospheric Plasma Process," *Plasma Process. Polym.*, vol. 12, pp. 347–361, 2015.
- [62] B. Escaig, "Binding metals to polymers. A short review of basic physical mechanisms," *Le J. Phys. IV*, vol. 3, no. C7, pp. 753–761, 1993.
- [63] F. Awaja, M. Gilbert, G. Kelly, B. Fox, and P. J. Pigram, "Adhesion of polymers," *Progress in Polymer Science (Oxford)*, vol. 34, no. 9, pp. 948–968, 2009.

- [64] E. Bertels, B. Goderis, and M. Smet, "Nano-Engineered Polymer-Steel Hybrids: Chemical and Physical Compatibilization," KU Leuven - Faculty of Science, 2015.
- [65] "Copyright © 2009 The Adhesive and Sealant Council, Inc. All Rights Reserved." .
- [66] A. Baldan, "Adhesively-bonded joints and repairs in metallic alloys, polymers and composite materials: Adhesives, adhesion theories and surface pretreatment," *Journal of Materials Science*. 2004.
- [67] "ASTM D3359, Standard test methods for rating adhesion by tape test." ASTM International, 2010.
- [68] M. Honkanen, M. Hoikkanen, M. Vippola, J. Vuorinen, T. Lepistö, P. Jussila, H. Ali-Löyty, M. Lampimäki, and M. Valden, "Characterization of silane layers on modified stainless steel surfaces and related stainless steel-plastic hybrids," *Appl. Surf. Sci.*, vol. 257, pp. 9335–9346, 2011.
- [69] "silanization into glass." [Online]. Available: <https://ars.els-cdn.com/content/image/1-s2.0-S0142961213014002-gr1.jpg>. [Accessed: 14-Nov-2017].
- [70] K. Rokosz, T. Hryniewicz, J. Lukeš, and J. Šepitka, "Nanoindentation studies and modeling of surface layers on austenitic stainless steels by extreme electrochemical treatments," *Surf. Interface Anal.*, vol. 47, pp. 643–647, 2015.
- [71] A. Foerster, I. Hołowacz, G. B. Sunil Kumar, S. Anandakumar, J. G. Wall, M. Wawrzyńska, M. Paprocka, A. Kantor, H. Kraskiewicz, S. Olsztyńska-Janus, S. J. Hinder, D. Bialy, H. Podbielska, and M. Kopaczyńska, "Stainless steel surface functionalization for immobilization of antibody fragments for cardiovascular applications," *J Biomed Mater Res Part A*, vol. 104, pp. 821–832, 2016.
- [72] M. Kheirkhah, M. Fathi, H. R. Salimijazi, and M. Razavi, "Surface modification of stainless steel implants using nanostructured forsterite (Mg₂SiO₄) coating for biomaterial applications," *Surf. Coatings Technol.*, vol. 276, pp. 580–586, 2015.
- [73] A. K. Padhi and A. Biswas, "Surface modification of 316L Stainless steel by Sol-Gel method," National Institute of Technology of Rourkela, 2014.
- [74] T. Yoshioka, K. Tsuru, S. Hayakawa, and A. Osaka, "Preparation of alginate layers on stainless-steel substrates for biomedical applications," *Biomaterials*, vol. 24, no. 17, pp. 2889–2894, 2003.
- [75] BSI, *Biological evaluation of medical devices Part 13: Identification and quantification of degradation products from polymeric medical devices (ISO 10993-13:2010)*. 2010.
- [76] J. P. Matinlinna, C. Y. K. Lung, and J. K. H. Tsoi, "Silane adhesion mechanism in dental applications and surface treatments: A review," *Dental Materials*, vol. 34, no. 1, pp. 13–28, 2018.
- [77] "silanization solvent." [Online]. Available: https://www.researchgate.net/post/What_difference_does_it_make_in_dissolving_APTES_in_ethanol_acetone_or_toluene. [Accessed: 21-Oct-2018].
- [78] "spin coating." [Online]. Available: <https://www.ossila.com/pages/spin-coating>. [Accessed:

- 14-Nov-2017].
- [79] M. D. Tyona, "A theoretical study on spin coating technique," *Adv. Mater. Res.*, vol. 2, no. 4, pp. 195–208, 2013.
- [80] S.-T. Hsu and Y. L. Yao, "Effect of Film Formation Method and Annealing on Morphology and Crystal Structure of Poly(L-Lactic Acid) Films," *J. Manuf. Sci. Eng.*, vol. 136, pp. 1–9, 2014.
- [81] "XRD." [Online]. Available: https://serc.carleton.edu/research_education/geochemsheets/techniques/XRD.html. [Accessed: 02-May-2018].
- [82] A. A. Bunaciu, E. G. Udriștioiu, and H. Y. Aboul-Enein, "X-Ray Diffraction: Instrumentation and Applications," *Crit. Rev. Anal. Chem.*, vol. 45, no. 4, 2015.
- [83] Ž. Mitić, A. Stolić, S. Stojanović, S. Najman, N. Ignjatović, G. Nikolić, and M. Trajanović, "Instrumental methods and techniques for structural and physicochemical characterization of biomaterials and bone tissue: A review," *Mater. Sci. Eng. C*, vol. 79, pp. 930–949, 2017.
- [84] M. Toledo, "Thermal Analysis of Polymers Selected Applications," *Mettler Toledo*, pp. 1–40, 2008.
- [85] L. Reimer, *Scanning Electron Microscopy: Physics of Image Formation and Microanalysis*. 1998.
- [86] "optical profilometer." [Online]. Available: <https://www.nanoscience.com/techniques/optical-profilometry/>. [Accessed: 25-Sep-2018].
- [87] "profilometer – 2." [Online]. Available: <https://www.zygo.com/?/met/profilers/opticalprofilersabout.htm>. [Accessed: 30-Sep-2018].
- [88] "Sensofar Metrology S neox 3D Optical Profiler Manual." .
- [89] T. Zhao and L. Jiang, "Contact angle measurement of natural materials," *Colloids Surfaces B Biointerfaces*, vol. 161, pp. 324–330, 2018.
- [90] T. N. Corporation, "Introduction to Fourier Transform Infrared Spectrometry." 2001.
- [91] J. F. Moulder, W. F. Stickle, P. E. Sobol, and K. D. Bomben, "X-ray Photoelectron Spectroscopy," in *Handbook of X-ray Photoelectron Spectroscopy*, vol. 3, no. 4, 1979, pp. 1–12.
- [92] "XPS." [Online]. Available: <https://xpssimplified.com/whatisxps.php>. [Accessed: 09-Jul-2018].
- [93] "sensitivity XPS." [Online]. Available: <https://vuo.elettra.eu/services/elements/WebElements.html>. [Accessed: 12-Jul-2018].
- [94] R. Crookes, "Pickling and Passivating Stainless Steel," in *Materials and Applications Series*, 2007, vol. 4.
- [95] "heat treatment colours." [Online]. Available: <https://www.bssa.org.uk/topics.php?article=140>. [Accessed: 03-Oct-2018].
- [96] "304 SS composition." [Online]. Available: <https://www.azom.com/article.aspx?ArticleID=965>. [Accessed: 03-Oct-2018].

- [97] "PDF Card - (Cr_{0.75} Fe_{1.25}) O₃ - 01-077-9861."
- [98] "PDF Card - Fe - 04-014-0264."
- [99] "PDF Card - Fe₂ O₃ - 01-088-2359."
- [100] "PDF Card - Fe₃ O₄ - 01-078-6086."
- [101] R. V. Rohli and A. J. Vega, "Atmospheric structure and composition," in *Climatology*, 3rd ed., Jones and Bartlett, Eds. 2013, p. 13.
- [102] W. Schulz, M. Nofz, M. Feigl, I. Dörfel, R. Saliwan Neumann, and A. Kranzmann, "Corrosion of uncoated and alumina coated steel X20CrMoV12-1 in H₂O-CO₂-O₂ and air at 600 °C," *Corros. Sci.*, vol. 68, pp. 44–50, 2013.
- [103] W. Schulz, M. Feigl, I. Dörfel, M. Nofz, and A. Kranzmann, "Influence of a sol-gel alumina coating on oxidation of X20CrMoV12-1 in air up to 650 °C," *Thin Solid Films*, vol. 539, pp. 29–34, 2013.
- [104] "spin-orbit." [Online]. Available: <http://www.xpsfitting.com/2012/08/spin-orbit-splitting.html>. [Accessed: 21-Aug-2018].
- [105] "NIST database." [Online]. Available: <https://srdata.nist.gov/xps/EnergyTypeValSrch.aspx>. [Accessed: 30-Jul-2018].
- [106] "xps simplified." [Online]. Available: <https://xpssimplified.com/periodictable.php>. [Accessed: 21-Aug-2018].
- [107] "NIST FTIR." [Online]. Available: <https://webbook.nist.gov/chemistry/vib-ser/>. [Accessed: 03-Sep-2018].
- [108] A. M. Oje and A. A. Ogwu, "Chromium oxide coatings with the potential for eliminating the risk of chromium ion release in orthopaedic implants," *R. Soc. Open Sci.*, vol. 4, no. 7, pp. 1–18, 2017.
- [109] N. Eustathopoulos, N. Sobczak, A. Passerone, and K. Nogi, "Measurement of contact angle and work of adhesion at high temperature," *J. Mater. Sci.*, vol. 40, no. 9–10, pp. 2271–2280, 2005.
- [110] N. S. K. Gunda, M. Singh, L. Norman, K. Kaur, and S. K. Mitra, "Optimization and characterization of biomolecule immobilization on silicon substrates using (3-aminopropyl)triethoxysilane (APTES) and glutaraldehyde linker," *Appl. Surf. Sci.*, vol. 305, pp. 522–530, 2014.
- [111] N. Majoul, S. Aouida, and B. Bessaïs, "Progress of porous silicon APTES-functionalization by FTIR investigations," *Appl. Surf. Sci.*, vol. 331, pp. 388–391, 2015.
- [112] T. Hryniewicz and K. Rokosz, "Analysis of XPS results of AISI 316L SS electropolished and magnetoelectropolished at varying conditions," *Surf. Coatings Technol.*, vol. 204, no. 16–17, pp. 2583–2592, 2010.
- [113] "O1s - xps." [Online]. Available: <http://sites.cardiff.ac.uk/xpsaccess/reference/oxygen/>. [Accessed: 09-Oct-2018].
- [114] Y. Y. Song, H. Hildebrand, and P. Schmuki, "Optimized monolayer grafting of 3-aminopropyltriethoxysilane onto amorphous, anatase and rutile TiO₂," *Surf. Sci.*, vol. 604,

- no. 3–4, pp. 346–353, 2010.
- [115] J. Landoulsi, M. J. Genet, K. El Kirat, C. Richard, S. Pulvin, and P. G. Rouxhet, “Silanization with APTES for Controlling the Interactions Between Stainless Steel and Biocomponents: Reality vs Expectation,” in *Biomaterials - Physics and Chemistry*, R. Pignatello, Ed. 2011, pp. 99–126.
- [116] M. C. Righetti, M. Gazzano, N. Delpouve, and A. Saiter, “Contribution of the rigid amorphous fraction to physical ageing of semi-crystalline PLLA,” *Polym. (United Kingdom)*, vol. 125, pp. 241–253, 2017.
- [117] C. Yu, Q. Xie, Y. Bao, G. Shan, and P. Pan, “Crystalline and Spherulitic Morphology of Polymers Crystallized in Confined Systems,” *Crystals*, vol. 7, no. 147, pp. 1–20, 2017.
- [118] V. Bernardo, G. M. Luz, N. M. Alves, and J. F. Mano, “Cell behaviour in new poly(l-lactic acid) films with crystallinity gradients,” *Mater. Lett.*, vol. 87, pp. 105–108, 2012.
- [119] A. Leroy, S. Ribeiro, C. Grossiord, A. Alves, R. H. Vestberg, V. Salles, C. Brunon, K. Gritsch, B. Grosgeat, and Y. Bayon, “FTIR microscopy contribution for comprehension of degradation mechanisms in PLA-based implantable medical devices,” *J. Mater. Sci. Mater. Med.*, vol. 28, no. 87, pp. 1–13, 2017.
- [120] B. Xue, L. Xie, and J. Zhang, “Detailed molecular movements during poly(l-lactic acid) cold-crystallization investigated by FTIR spectroscopy combined with two-dimensional correlation analysis,” *RSC Adv.*, vol. 7, pp. 47017–47028, 2017.